TECHNICAL NOTE 75-3

AN EVALUATION OF A HEMISPHERIC OPERATIONAL WAVE SPECTRAL MODEL

FLEET NUMERICAL WEATHER CENTRAL
MONTEREY, CALIFORNIA

JUNE 1975

(6) AN EVALUATION OF A HEMISPHERIC OPERATIONAL WAVE SPECTRAL MODEL.

(9) Final repts.

(12) 113

TECHNICAL NOTE NO. 75-3

(11) JUNE 1975

(14) FNWC-TN-75-3

By

(10) Sheldon M. Lazanoff
U.S. [redacted] Office

Norman M. Stevenson
Fleet Numerical Weather Central

138670

FOREWORD

This technical note describes the operational Spectral Ocean Wave Model (SOWM) and provides results of several evaluation studies. The SOWM, operational at Fleet Numerical Weather Central since December 1974, represents state of the science ocean wave analysis and forecasting techniques. It provides an improved specification of the sea surface wave energy and offers a challenge to both the environmentalist and the mariner to intelligently use the increased information available.

The SOWM is a result of joint efforts of the Naval Oceanographic Office and Fleet Numerical Weather Central.

Reviewed and approved 15 July 1975

C. R. WARD
Captain, U.S. Navy
Commanding Officer
Fleet Numerical Weather Central

TABLE OF CONTENTS

LIST OF FIGURES

TABLES

LIST OF SYMBOLS

$A[f,u(t,\vec{x})]$	Phillips resonance growth mechanism
$A(K)$	Tucker wave record characteristic
A_m	π
A_p	constant determined by Phillips
A^*	empirical term directly proportional to wave number and inversely proportional to water density and the square of gravity
$B[f,u(t,\vec{x})]$	Miles instability term
$B(\omega)$	Tucker wave recorder characteristic
C	phase velocity (escept where used to describe the Tucker wave recorder)
E_{Total}	total wave energy at a grid point
$F(\omega,\theta,U)$	directional spectra
H_r	wave height recorded by Tucker wave recorder
H_T	true wave height
$\overline{H}_{1_3}$	significant wave height
K	von Karman constant
$K(\theta_1)$	constant for given wind direction θ_1
L	wave length
$S(f,t,\vec{x})$	spectral density as a function of frequency, time and distance
$S_D(f_i, \theta_i)$	spectral component after dissipation
$S_o(f_i,\theta_i)$	spectral component before dissipation
U	wind speed
U^*	wind friction velocity
U'	mean wind profile slope
U''	mean wind profile curvature

W	used in calculation of A- term
Y	used in calculation of A term
Z	elevation
Z_m	matched layer where wind speed and phase are equal
Z_o	roughness parameter
c	constant (690 for ft^2)
r	used in calculation of A term
f	wave frequency
f_i	center frequency of spectral component
g	gravitational attraction of earth
k	wave number
t	time
$\vec{x}$	wave direction
u	wave velocity
Γ^2	constant
α	constant ($8.1 * 10^{-3}$)
β	constant (0.74)
ω	radian frequency
ω_o	directly proportional to g and inversely proportion to wind speed at 19.5 meters
ρ_a	density of air
ρ_w	density of water
π	pi
τ_o	surface stress
θ	angle between wind and wave direction
θ_i	center direction of spectral component
γ	constant

ABSTRACT

Through the cooperative efforts of the Naval Oceanographic Office (NAVOCEANO) and Fleet Numerical Weather Central (FNWC) personnel, the open ocean Icosahedral-Gnomonic wave spectral computer model developed by Professor Willard Pierson has been placed in real time operational use at FNWC under the title Spectral Ocean Wave Model (SOWM). The model computes semi-daily on-time analyses and forecasts to seventy-two hours. A gnomonic projection allows great circles to be represented by straight lines within the icosahedral triangles, thus minimizing propagation errors.

The growth of wave energy for a given wind velocity at grid points is accomplished by a modified Miles-Phillips techinque. Growth is limited by the Pierson-Moskowitz fully developed spectrum for the given wind speed. The wave energy direction is obtained through an equation derived by the Stereo Wave Observation Project (SWOP). The wave energy spectrum at each grid point is represented by a 15 frequency by 12 direction matrix.

High wave energy case studies were made for time periods during November-December 1969 and October 1973 for verification of the computer model. Measured wave spectra were obtained from Ocean Station PAPA (1973) and FLIP (1969) for comparison. The analyzed wave spectra are also compared to measured wave spectra from the National Data Buoy Office (NDBO) EB03 buoy for December 1974 but a detailed analysis was not made for this time period.

Comparison between the computed and measured wave spectra and analysis of FNWC computed wind fields indicate that the SOWM produces far superior results than the previous FNWC operational "singular" wave model.

AN EVALUATION OF A HEMISPHERIC OPERATIONAL WAVE SPECTRAL MODEL

I. INTRODUCTION

The capability of the U. S. Navy to analyze and forecast deep water wave conditions on a global scale has improved significantly during the past year. In the past, Fleet Numerical Weather Central (FNWC), the global forecasting arm of the U. S. Navy Weather Service, has relied on "singular" wave models (Hubert and Mendenhall, 1970; Schwartz and Hubert, 1973) to predict wind wave and swell heights and their corresponding directions and periods at points on Northern Hemispheric grid systems. The basic weakness of the "singular" models is that they do not accurately depict the complex wave propagation in the larger oceans such as the Pacific and Atlantic Oceans where several wave trains can coexist in one area at any given time.

In April 1972, through the cooperative efforts of the U. S. Naval Oceanographic Office (NAVOCEANO), FNWC and New York University (NYU cognizant personnel are now associated with the University Institute of Oceanography, City University of New York), an operational Mediterranean wave spectral model was placed into use at FNWC (Lazanoff, Stevenson and Cardone, 1972). The model computes twice daily on-time

analyses and forecasts out to thirty-six hours. Besides producing a far superior and more sophisticated product than the "singular" model, the performance of the Mediterranean wave spectral computer model demonstrated the practicability of running spectral models on an operational basis.

It was then decided to evaluate the NYU Icosahedral-Gnomonic (IG) wave spectral model as a real-time operational hemispheric wave spectral model. The NYU IG wave spectral model, modified for operational use, commenced operational evaluation in July 1973 and in December 1974 was designated the operational FNWC hemispheric open ocean wave model under the title Spectral Ocean Wave Model (SOWM).

II. THE ICOSAHEDRAL-GNOMONIC WAVE SPECTRAL MODEL

The IG wave model was designed by Professor Willard J. Pierson for global use; however, since the global model program requires a large amount of computer storage and computation time, it was decided that it would be impractical to use the full global model on the present FNWC computers. The SOWM is limited to the Northern Hemisphere.

The origins of this particular wave spectral model can be traced back to the original NYU Atlantic wave model (Baer, 1962), and, as with the previous NYU wave models, can be divided into two independent parts: (a) growth at each grid point and (b) propagation from grid point to grid point.

A. Wave Energy Growth

The growth technique is essentially the same as the one used in the Mediterranean wave model and was originally developed by Inoue (1967). Inoue combined the Miles instability theory with the Phillips resonance theory such that when the sea begins to grow from calm conditions, the resonance mechanism predominates and later, as the wind velocity begins to increase, the instability mechanism becomes more dominant. The Phillips theory essentially states that a resonance between the air-sea system could occur when a component of the surface pressure distribution moved at the same speed as a free surface wave of the same wave number (where the wave number, K, is equal

to $2\pi/L$, and L is the wave length). The Miles instability theory states that the mean rate of energy transferred from the parallel sheer flow to the surface wave is proportional to the curvature of the wind profile at the height where the mean wind velocity is the same as the phase speed of the wave component.

The wave spectra which are computed for the given wind velocity at each time step are not allowed to exceed the Pierson-Moskowitz fully developed spectrum for the same wind velocity. The directional spectra are computed by an equation developed from Stereo Wave Observation Project (SWOP) data. The energy spectrum at each grid point is divided into a 15 frequency by 12 direction (30° increments) matrix. The delineation of the frequency bands is shown in Table 1. The highest frequency, in practice, is limited from 0.164 to 0.40 HZ and the wave energy within this frequency range is not propagated.

One significant change has recently been made to the growth portion of the wave spectral program. Professor Vincent Cardone, CUNY, has modified the Phillips' resonance mechanism or initial growth portion of the model (personal communication, 1974). For lower wind speeds (less than or equal to 30 knots) the wave energy will grow at a faster rate during the initial six hours using the Cardone modification than it did under the old scheme. The reverse is true for wind speeds greater than 30 knots. After six hours the new growth rate is always slower

than the old growth rate. Comparisons between the two growth schemes are shown in Figures 1-7 for the 35 knot case.

Wave energy dissipation in this wave spectral model is a function of the wind-wave interaction (Inoue, 1967) and the land sea boundary delineation. Energy dissipation as a function of wave-wave interactions and breaking waves is not included; however, there are plans to consider these parameters at a later date. Although not used within the model as an energy dissipation mechanism, a whitecap percentage for each grid point is calculated. Whitecaps are a manifestation of wave breaking and are considered to be closely related to the energy transferred to the fully developed portion of the spectrum (Cardone, 1969). The calculations are made on the assumption that the fetch length is uniform. It now appears that the computation of whitecap percentages should also be based on the interaction between wind waves and swell and the variability of fetch length (Shemdin, 1973; Ross and Cardone, 1974). Phenomena such as foam and streaks are not considered in the calculation of whitecap percentages but may also prove to be useful tools in accounting for energy dissipation. Knowledge of the percentage of whitecaps, foam and streaks in a geographical area has significance in other meteorological and oceanographic studies and will be discussed in more detail in a later paper.

Appendix A contains a list of the most significant equations used in the wave spectral model.

B. Wave Energy Propagation

The most significant difference between the previous wave spectral models developed by the Pierson oceanography group and the SOWM wave spectral model is the method used to propagate wave energy. A number of papers (Lockheed, 1965, 1966, 1967; Pierson, Tick and Baer, 1966; Adamo, Baer and Hosmer, 1968; Salfi, 1974, among others) have been written, thoroughly describing the reasons for selecting this particular grid system and propagation scheme. Only a brief discourse on the subject will be presented in this paper.

Since deep water wave energy propagates along great circles at group velocity, it is highly desirable for modeling work to represent great circles as straight lines. The gnomonic projection is the only plane projection which has this unique feature. Unfortunately, if this projection was to be used over large areas such as the North Pacific Ocean, there would be great areal distortion. An icosahedron is used to depict the shape of the globe to minimize the areal distortion. An icosahedron is a twenty sided polygon with equilateral triangles for it's faces. Each face of the icosahedron is a separate gnomonic projection. The icosahedral-gnomonic projection is shown in Figure 8. The mathematical properties of the gnomonic projection on an icosahedral triangle are shown in Table 2. Note that areal distortion is within reasonable limits throughout most of the triangle. The distortion becomes a maximum near the vertices. This is

demonstrated in Figure 9. The triangles are oriented in a manner such that as many vertices as possible are located on land; as many edges as possible are along shore lines; and as few faces as possible are used for ocean areas.

The SOWM uses seven triangles for the North Pacific Ocean, six triangles for the North Atlantic Ocean, and one triangle for the Indian Ocean. Each triangle has 325 grid points with a spacing of approximately 350 km. at the point of tangency and 194 km at the vertices. All points south of the equator are treated as land points at this time. A time step of three hours is used in this model.

The propagation of the wave energy is done by a modified velocity gradient technique. For a given wave direction along a great circle, the energy as a function of frequency is assumed to be propagated at group velocity in accordance with linear theory--i.e. the multiplication of the linear product of energy computed from adjacent grid points by the group velocity. It has been shown (Lockheed, 1965) that propagation by this linear velocity gradient technique is inadequate if the wave component fields are not continuous to the first order. Since obvious discontinuities exist, an additional field is computed and updated at each time step to account for this problem. Salfi (1971) indicates several criteria under which discontinuities can exist in the energy fields: (a) any local maximum or minimum, (b) any land point adjacent to a sea point,

and (c) any point where the change in value between that point and the down-stream grid point exceeds 20% (an arbitrarily set value) of the arithmetic average of the two points. This discontinuity field ranges in value from zero to one where "one" indicates that no discontinuity exists. Values less than one indicate the fractional distance that a specified directional-frequency energy component has moved towards the adjacent downstream grid point. Wave energy in the highest frequency band is considered fully arisen and is not propagated. Wave energy in this frequency band takes between twelve to twenty hours to reach the adjacent grid point and thus, it is not practical to propagate this energy.

Wave energy as a function of direction cannot always be propagated directly from grid point to grid point within the triangles. In order to make full use of the icosahedral-gnomonic projection, as described in the second paragraph of this section, the selected grid system is based on a 60° co-ordinate system. Remembering that the wave energy spectra are divided into twelve direction bands and great circles are represented by straight lines within the icosahedral triangles, it can be seen that two different propagation situations exist when wave energy is propagated as a function of direction. There are six primary geometrical directions (o°, 60°, 120°, 180°, 240°, 300°) and six secondary directions (30°, 90°, 150°, 210°, 270°, 330°). Wave energy is propagated directly from grid point to grid point along the six primary directions and

by zig-zag method along the six secondary directions. The zig-zag method is illustrated in Figure 10. Wave energy from location 3 is propagated on alternate time steps via locations one and two in the example. The same method is used for all secondary directions. The zig-zag method is modified near land points so that wave energy propagation near coast lines can be accurately depicted. Near the coast both upstream grid points and discontinuity values must be checked at all time steps.

A significant problem arises when wave energy is propagated across triangle interfaces. While the great circles are depicted by straight lines within triangles, they refract, as can be seen in Figure 8, when crossing from one triangle to another ie., there is a discontinuity between triangles. Propagation across these interfaces is accomplished by designing triangles so that adjacent triangles have a common row of grid points. When computing the wave energy propagation along this common row of points, the angle of refraction and the conversion from one set of geometrical coordinates to another must be accounted for because of the difference in orientation between the triangles. An example of this type of propagation is shown in Figure 11.

When the geometrical directions are converted to geographical directions, the display of the geographical directions will differ from triangle to triangle for points located at the same position within the triangles since the triangles are not all oriented in the same direction.

III. WIND VELOCITY INPUT

It cannot be stressed too strongly that no matter how sophisticated and scientifically correct a wave prediction model may be, the accuracy of the wave model is still limited by the accuracy of the wind velocity input to the model. The methods of calculating wind velocities at FNWC vary depending on whether the program is in an analysis or prognosis mode. At analysis time the previous (six hour old) sea level pressure (SLP) field is kinematically extracted as a first guess. The SLP fields are retained on a hemispheric 125*125 grid system. Observed data are added to the SLP, by the Fields by Information Blending (FIB) technique (Holl and Mendenhall, 1971). The FIB technique is a method which assigns weights to observed data depending on the age of the data, the accuracy of the observations as compared to adjacent observations or, in data spare areas, climatology, and the source of observations. Above 20°N and below 20°S fourth order geostrophic winds in u and v components are computed from the analyzed SLP (Hubert and Mendenhall, 1970). The geostrophic wind velocities are corrected for cuvature and stability as a function of sea surface temperature advection. A correction in proportion to the sea surface temperature advection serves as an empirical correction for latitude. Persistence (six hour old wind velocity analysis) is used between 20°S and 20°N. The wind analyses are then modified by observed wind data. The observations must pass gross error and lateral

reject checks. A numerical variation analyses (NVA) scheme uses the equations of motion to couple the wind and pressure analyses within reasonable dynamical constraints (lewis and Grayson, 1972). The NVA provides a method of extrapolating observations from data-rich areas to data-deficient areas. LT Roger Langland, FNWC meteorologist, has determined that the overall root mean square error (RMSE) between the observed data and the final analyses is on the order of 2.75 meters/ seconds. The RMSE does appear to vary depending on the amount and quality of observed data in the area and the location of the area; however, FNWC has not broken the errors down into finer detail at the present time. SLP and wind field analyses are calculated every six hours on an operational basis at FNWC.

The SLP prognoses are computed by the FNWC primitive equation (PE) model. The operational PE model computes SLP prognoses every six hours out to 72 hours on a twice-daily basis. Modified geostrophic wind velocity prognoses are then computed by the method described above. There are no statistics available for determining the accuracy of the wind velocity prognoses. It is known that the PE model moves typical weather systems at approximately 82% of the actual speed of the systems because of truncation errors in the second order differencing scheme used in the PE model. In the near future a fourth order differencing scheme used in the PE model and it is expected that the movement of the prediction weather systems will

closer approximate the actual movement of the weather systems.

Frictional wind velocities (U_*) are computed from the analyzed or forecasted wind speeds and are the actual input to the wave spectral model growth equations. For a given wind speed, U_* can vary considerable depending on whether stable, neutral or unstable conditions exist. An unstable condition occurs when the underlying sea surface temperatures is warmer than the above air temperature. The wave energy growth rate is the highest under unstable conditions (Cardone, 1969). The importance of determining which condition exists is shown in Figure 12. As an example, if winds were measured at 20 meters, a wind speed of about 24 knots would be needed under stable conditions to produce the effective wave generating ability of a wind speed of only about 19 knots during neutral conditions and 17 knots under unstable conditions (Cardone, 1969). The present operational wave spectral model only calculates U_* for neutral conditions (Salfi, 1974); thus, growth rate errors can exist if stable or unstable conditions actually exist. The greatest errors would occur under stable conditions. Note that the above example was based on wind measured at 20 meters above the sea surface. The vertical change in wind speed in the marine boundary is considered to have a logarithmic profile from the sea surface to the top of the layer. Stable conditions produce the more significant deviations from the purely logarithmic profile than equivalent unstable conditions do.

The initial growth equation, Phillips Resonance Theory, (Appendix A, Equations 3 and 4) was derived from winds measured at 6.1 meters while the remander of the growth equation and the Pierson-Moskowitz fully developed spectra were derived from winds measured at 19.5 meters. When Pierson and his group use the wave spectral model, they put a great deal of effort into converting the wind input from various sources to the proper height for use in the growth portion of the model. This is not presently being done in the operational version of the IG model. The FNWC surface wind fields are not based on any specific height nor is any attempt made to correct for any height deviation from 19.5 meters or 6.1 meters. This omission may cause significant errors under certain meteorological conditions. The calculation of U_* based on stability considerations and the adjustment of wind speed for height are among the highest priority areas of work that will be done in the near future and should make significant contributions in improving the accuracy of the model.

IV. COMPUTER RESOURCES REQUIRED FOR PRESENT OPERATIONAL HEMISPHERIC WAVE MODEL

The following CDC 6500 computer resources are required to run the SOWM on an operational basis to produce an analysis and forecast to 72 hours. Each time step requires 20 seconds of Central Processing Unit time per subprojection.

A. North Pacific Ocean (7 Subprojections)

1. Computer Time 56 minutes
2. Central Memory 145000_8
3. Extended Core Storage 740_8K

B. North Atlantic Ocean (6 subprojections)

1. Computer Time 48 minutes
2. Central Memory 142000_8
3. Extended Core Storage 640_8K

C. Indian Ocean (1 subprojection-North of Equator)

1. Computer Time 8 minutes
2. Central Memory 110000_8
3. Extended Core Storage 212_8K

V. VERIFICATION OF THE WAVE SPECTRAL MODEL

In order to have some degree of confidence in any operational computer model, the results of the model need to be verified with measured data. Under normal circumstances, routine shipboard visual observations are not adequate for verification of a wave spectral model because of the complexity of the model output, ship observers' biases, and the peculiarities of the World Meteorological Organization coding system used to routinely report wave parameters. Data from calibrated wave measuring instruments such as Tucker Shipboard Wave Recorders and wave buoys are considered more desirable. Since the Icosahedral-Gnomonic wave spectral model was first used in an operational-evaluation mode in the North Pacific Ocean at FNWC, the initial verification studies have been concentrated in this area. Four case studies are presented. The first case, 30 November - 2 December 1969, demonstrates the ability of the SOWM wave spectral model to propagate low frequency wave energy. The second case, 26 October - 28 October 1973, compares results of the wave spectral model to measured data from a Tucker Shipboard Wave Recorder. The third case, December 1974 - January 1975, compares the results of the wave spectral model to data from the NOAA Data Buoy Office (NDBO) EB-03 wave buoy. The fourth case demonstrates an application of the wave spectral model. A Ship Routing group compared output of the spectral model to wave observations from a large (950 feet) container ship. The

container ship logged wave observations and these observations were compared to the SOWM analysis.

A. Case Study for 29 November-2 December 1969

An extratropical storm with a center located at approximately 40°N, 165°E began to intensify at 0600Z, 29 November 1969. According to the original FNWC wind analysis the maximum wind speed attained was 65 knots; however, the wind fields have been reanalysed and from 1200Z, 29 November 60 0600, 1 December the highest velocities were over 70 knots, with a maximum wind speed of 91 knots reached at 1800Z, 30 November. The storm moved in a southeasterly direction and the wind directions associated with the highest speeds ranged from 250° to 340°. The wind field analysis for 18Z, 30 November is shown in Figure 13. Only every other grid point is plotted; therefore, the highest speed may not be shown. The highest wind velocities, their location, and associated significant wave heights (the average height of the highest one-third waves--see Appendix A Equation 12) computed by the SOWM for every six hours are shown in Table 3.

Using the original wind data as input, the FNWC singular wave model, which was the operational wave model in 1969, computed a maximum significant wind wave height of 40 feet (Hubert and Mendenhall, 1970). This wave height is much less than the significant wave heights computed by the wave spectral model (Table 3). Even if a wind speed of 91 knots had been used as

input to the singular wave model, the highest significant wind wave height computed by the model still would not have exceeded 41 feet. These figures demonstrate one of the limitations of the FNWC singular model.

During this time period the manned spar buoy FLIP was operating in a vertical mode in the vicinity of 27°30'N, 157°45'W. The singular wave model indicated that the swell or low frequency wave energy which propagated from the above-mentioned storm area to the area in which FLIP was located had an average height of 12-15 feet. The maximum significant height computed by the singular model for any grid point during this time period never exceeded 25 feet. Because FLIP was operating in a vertical mode, scientists aboard FLIP were able to accurately measure the wave heights against various points on the buoy. In addition, 16mm movies were taken of FLIP from it's tow ship and the data from the movies were correlated with the FLIP observations (Rudnick and Hasse, 1971). FLIP's log indicated that the seas were constantly building for approximately 35 hours preceding 2300Z, 1 December. The period of maximum wave intensity existed from approximately 2300Z, 1 December to 0400Z, 2 December. During this time period the wave measurements shown in Table 4 were obtained. It is obvious that when these data are compared to the singular wave model calculations, the singular model did not properly propagate the swell.

The SOWM wave spectral model was run in the hindcast mode for the time period of 16 November - 3 December 1969. The model was initialized on 16 November to ensure that steady state conditions would be reached by 29 November. Plots of one-dimensional wave spectral (spectral density vs. frequency) for the closest grid point, 27.16°N, 156.6°W, to FLIP's position are shown in Figure 14. The wave spectra were plotted every six hours for the time period of 12Z, 01 December to 06Z, 2 December. Analyzed wind velocities are also indicated. The logs of near-by ships indicated that the winds for this time period were generally from the west and had speeds on the order of 20-30 knots (Rudnick, et al). Other ship logs from this area (McConathy, 1974) do show that the wind speeds started to decrease no later than 0930Z, 2 December. Thus, there appears to be good agreement between the reported and analyzed wind velocities in the vicinity of FLIP.

The computer wave spectra for 18Z, 30 November and 0Z, 6Z, 1 December consist primarily of high frequency wave energy which was a function of the local wind. The 12Z and 18Z, 1 December wave spectral contained both high and low frequency wave energy. The last two wave spectra, 0Z and 6Z, 2 December, of this time sequence were dominated by low frequency wave energy whose significant frequency bands were centered at 0.044HZ (22.7 seconds) and 0,05HZ (20 seconds). As shown in Table 4, the observed significant frequency bands as computed from the movies which were taken approximately 23Z 1 December 1969, range from 0.05HZ

to 0.062 HZ (20 to 16 seconds). The entire film was shot during a five minute interval and divided into five sequencies of 8, 57, 45, 20 and 28 seconds. Only in three of these sequences would there have been enough time to observe wave frequencies of less than 0.05 seconds and even these time sequences were rather short. It is not unreasonable to assume that sometime during the five hour period from 23Z, 1 December to 04Z, 2 December, significant wave frequencies of less than 0.05 HZ could have existed.

Several discrepancies were revealed when comparing the analyzed wave data to the measured wave data. The computed wave energy shown in Figure 14 peaked at 06Z, 2 December which was at least two hours after the observed wave conditions actually reached their greatest intensity. In addition, the computer model calculated a maximum significant wave height of 49 feet. Several questions arise: (a) are these discrepancies solely a function of the wave spectral model or are there other reasons for the errors.

In this case the SOWM analysis were far superior to the singular model analysis. Had the SOWM been operational in 1969, (even with discrepancies described above) FLIP could have been better prepared for the intense low frequency wave energy which propagated through it's operating area. It is interesting to note that FLIP was able to withstand wave heights up to 80 feet with a minimum of damage; however, as shown in Figure 15 (Kerr, 1964), FLIP was probably in more danger because the significant

frequency of the propagating wave energy was approaching the resonant frequency of FLIP. If the significant frequency of the wave energy had equaled the resonance frequency while FLIP was in the vertical position, FLIP would become unstable and probably capsized. The SOWM did accurately depict the range of the significant frequency bands of the low frequency wave energy.

The wave spectral model propagated a larger portion of the low frequency wave energy to the north of the FLIP. This may have been caused by errors in the analyzed wind fields used as input to the model. If the storm's geographical position was not analyzed correctly or the wind directions within the storm area were incorrect, the low frequency energy would not propagate in the right direction. The low frequency wave energy in the area of FLIP seemed to be concentrated in a rather narrow direction band as can be seen in Figures 16 and 17. Prior to 06Z, 2 December almost all the low frequency wave energy was concentrated in the 308° direction band and at 06Z, 2 December the wave energy was primarily located in the 308° and 338° direction bands. The grid points to the north of FLIP also had significant wave energy in the 278° and 248° bands as seen in Figure 18. The significant wave height for the grid point (39°N, 161°W) shown in this figure was comparable to that measured by FLIP. Since there was no measured data available from the storm area, it is possible that the analysis incorrectly positioned the storm or miscalculated the wind direction.

This case study does point out the type of errors that can occur in the wave spectral model if the wind fields are incorrect. An error of 15° in the wind direction can be significant to the wave spectral model since the wave energy is divided into 30° direction bands. If the wave energy is misplaced by one direction band, and this wave energy is allowed to propagate with minimum interference, the ensuing can cause the wave energy to be misplaced by several grid points over a 1000 mile track. This could have occurred in this case study.

In addition to improving the wind analysis, the above problem might have been partially alleviated by increasing the number of direction bands used to define the wave energy spectra. Professor Pierson divides the spectra into 15° increments for hindcast studies. Of course, the number of parameters to be calculated at each grid point increases from 180 to 360, requiring additional computer memory and computation time to run the model, currently impractical on the FNWC computer system.

B. Case Study - 26 October - 28 October 1973

Until December 1974 wave spectra computed from wave recorders on a routine, synoptic time basis were not available. Wave recorders usually were installed for specific projects and after the projects were completed, the recorders were removed from their moorings. To the best of our knowledge there has only been one deep-water wave recorder being operated in a semi-permanent basis in the North Pacific Ocean. The Canadians

keep a weather ship at 50°N, 145°W, Ocean Station Vessel (OSV) PAPA, as seen in Figure 19 and the ships which maintain this station have wave recorders mounted in their bow.

On 26 and 28 October 1973 the Canadian weather ship, CCG&S VANCOUVER , made special wave measurements in conjunction with a NAVOCEANO wave project at OSV PAPA. Both sets of measurements began at approximately 20Z and lasted for about one hour. These measurements were made in addition to the normal wave measurements made every three hours at OSV PAPA and were probably of better quality than the routine measurements since the ship was oriented in the best position to record the waves.

The Tucker shipboard wave recorders used by the Canadian weather ships have been described by Tucker (1956) and only significant points will be discussed in this paper. The Pierson-Moskowitz fully developed spectra were derived from Tucker wave data. The pressure transducer measures the high frequency wave energy up to 0.15HZ. This upper limitation is due to the attentuation of the wave pressure with depth (Briscoe, 1971). The wave recorders are mounted approximately 13 feet below the mean water-line on the Canadian weather ships. The vertical accelerometer measures the low frequency energy down to 0.04HZ and at that frequency, errors in the electronic double integration of the accelerometer signal used to cancel ship's heave becomes significant. Since the frequency boundaries are essentially 0.16HZ and 0.039HZ in the wave spectral model, the

frequency range of the Tucker recorder is quite adequate. The ship must be in a hove-to position, preferably headed into the waves, in order to accurately measure the wave heights. The data from the Tucker recorder are currently recorded as analog traces by a strip chart recorder at a speed of either one inch or 2 inches per minute for approximately 15 to 20 minutes every three hours. The analog traces were digitized every 0.01 inches which is equivalent to 0.6 or 0.3 seconds, depending on the analog chart speed, at FNWC. Before wave spectral could be computed from the digitized wave data, a correction factor was applied to the wave data. Several versions of the correction factor have been cited in the literature (M. Darbyshire, 1960; J. Darbyshire, 1963; D. Cartwright, 1963 Ewing, 1969; Holland, 1972); however, the most common correction is shown to be:

$$\frac{H_T}{H_r} = C \cdot B(\omega)\ A(K) \qquad (1)$$

and C is a constant (0.83)

$B(\omega)$ is due to the characteristics of the internal electrical circuits of the instrument and is equal to $[1 + (8.8\ \omega)^{-2}]^{3/2}$ where $\omega = 2\pi/T_m$, T_m is the near crossing period (i.e., the number of positive zero crossing divided by the total time and 8.8 represents the time constant of three filters used in the instrument.

A(K) represents the relation between the height of water above a fixed point on the ship's hull and the pressure measured

at this point. A(K) is also affected by the ship's heaving response and is equal to $e^{2.5d\omega^2/g}$ where d is the depth of the recorder below the mean water line (13 feet) and g is the acceleration of gravity. The ratio of the true wave height (H_T) to the measure wave height (H_r) can be written:

$$\frac{H_T}{H_r} = 0.83\ [1 + (8.8\ \omega)^{-2}]^{3/2}\ e^{-2.5\ \omega^2\ d/g} \qquad (2)$$

Note that the correction factor is a function of frequency and the higher the frequency the larger the correction factor. Table 5 shows the ratios that can be applied depending on the mean cross frequency (period). Dr. Briscoe (1971) suggested that no correction factor be applied to the wave records. He arrived at this decision based on information supplied to him by the National Institute of Oceanography. Briscoe believes that it is difficult to select one correction factor which is dependent on all frequencies in the spectrum and there is less overall error when no correction factor is applied than when an incorrect factor is used.

The Canadians alternate two weather ships at OSV PAPA. Dr. J. R. Wilson of the Canadian Marine Environmental Data Service, who graciously allowed us to use the original analog wave records, did some comparison between corrected data from the Tucker recorders used aboard the CCG & S QUADRA and from a Datawell Wave rider (personal communication, 1974). The two sets of data compared rather well. Data from the CCG & S VANCOUVER

have not been compared to data from other instruments; however, there is a possibility, based on hand analyses, that the corrected wave heights from this recorder may be too high.

Table 6 contains the observed wind velocities from OSV PAPA and the analyzed wind velocities from the two closest grid points to OSV PAPA for the time period of 06Z, 26 October - 0Z, 29 October. The analyzed wind fields were computed every six hours while the observed winds were obtained every three hours. Generally speaking, the analyzed winds compared rather well with the measured winds. In some cases such as 18Z, 26 October the wind velocities for one grid point may compare better with the observed wind velocities than the wind velocities from the adjacent grid point. These differences will be reflected in the computation of the wave spectra.

At 06Z, 24 October there was a low pressure center located at 50°N, 178W, approximately 1000 nautical miles from OSV PAPA. Initially, the highest wind speeds around the low pressure center were on the order of 30-35 knots, but as the low pressure center moved in a northeasterly direction, the pressure gradients became less intense and the highest wind speeds decreased to 20-25 knots. A plot of the 12Z, 25 October wind field is shown in Figure 19. It can be seen from this figure that the wave energy propagated from this low pressure area towards OSV PAPA came from approximately 200°-250°. At 12Z, 26 October the analyzed low pressure center was to the northwest of OSV PAPA and the pressure gradients around the center were intensifying.

The analyzed wind field for 12Z, 26 October is shown in Figure 20.

Comparisons between non directional wave spectral computed from OSV PAPA data and the 2 grid points of the SOWM are shown in Figures 21-28 for 18Z, 20Z, 26 October and 00Z, 27 October. The wave spectral model computes wave spectra in terms of variance (ft^2); however, since the fifteen band widths are unequal, it was decided the wave spectra would be better represented by variance density (ft^2/HZ) which is obtained by multiplying the variance by the frequency band widths. There are some instances such as an example which will be shown later where this process may obscure spectral peaks. Even when the wave spectra are converted to variance density, there are instances when the curves are not completely smoothed. For example, the double peaks in Figures 22, 24, 25 and 28 are probably a function of the frequency band widths and do not really exist.

The OSV PAPA wave spectra were computed by the Blackman-Tukey method (1959). Thirty degrees of freedom was selected for the computation of all the spectra. This means that the number of lags varied for each spectrum, depending on the length of wave record that was digitized.

Generally speaking, the computed wave spectra, including significant wave heights and dominant frequencies, compared favorably with the measured wave spectra. In some case such as shown in Figures 24 and 25 the comparison was better for one grid point (in this case, 48.5°N, 142.5°W) than for the adjacent grid point (50.9°N, 145.6°W). In this instance the

discrepancy can be accounted for by the differences in the analyzed and observed wind speeds. The significance of accurate wind velocity input can be seen in Figure 25 where the computed wave spectrum for 0Z, 26 October is compared to the measured wave spectrum for 20Z, 26 October and Figure 27 where the same computed wave spectrum is compared to the measured spectrum for 0Z, 27 October. The comparison is better than in Figure 27 because a higher wind speed existed in OSV PAPA for at least three more hours than was analyzed at the grid point. The low frequency energy of the computer wave spectra for 48.5°N, 140.5°W compares better to the low frequency energy that was measured at OSV PAPA (Figures 24 and 28). This also can be seen in Figures 29 and 30 which contain the computed two dimensional wave spectra. More low frequency energy exists at 48.5°N, 152.5°W than at 50.9°N, 145.6°W which is closer to OSV PAPA. Note that at 18Z, 26 October (Figure 29) the predominant low frequency energy has shifted to 200° at both grid points. Thus it appears that, in this case, given correct analyzed winds, the computer model is propagating the low frequency energy correctly.

A rather poor comparison at 06Z, 27 October is shown for 48.5°N, 142.5°W in Figure 31. The comparison for the adjacent grid point is similar. The computed spectrum compares favorably to the measured spectrum in the low frequency range but does not compare at all in the high frequency range. An investigation of the computed two dimensional wave spectrum which is calculated

in terms of variance indicates that an energy peak existed at 0.092HZ. The energy peak was obscured when the spectrum was converted to variance density by multiplying by the uneven bandwidths. The measured energy peak which was significantly larger in magnitude was at 0.105HZ. A similar situation occurred between 18Z, 28 October and OZ, 29 October and will be discussed in a later section. Some possible causes of these discrepancies will also be discussed.

This case indicates the importance of being aware of which physical units, i.e., variance or variance density, are being used to display the model wave spectra. Since the frequency bandwidths are unequal, two differently shaped curves can be obtained from the same set of data. For example, if only the variance density wave spectra were available for this case, the high frequency energy peak would have been obscured by the low frequency energy; however, a review of the variance wave spectra indicates that there was significant high frequency wave energy at the grid point.

After 00Z, 27 October the low pressure center mentioned earlier continued to move northeastward. The 12Z, 27 October analysis places the low pressure center directly to the north of OSV PAPA (Figure 32). At 18Z, 27 October a new low pressure center formed southwest of OSV PAPA (Figure 33). The wind system which generated the wave energy that propagated towards OSV PAPA had speeds of 30-40 knots from the south (Figure 34). Thus, between 18Z, 28 October and OZ, 29 October two distinct

wave trains existed at OSV PAPA which were confirmed by photographs taken by a NAVOCEANO airplane between 20-21Z, 28 October.

There were no wave spectra from OSV PAPA available for comparison between 00Z, 28 October and 20Z, 28 October. The 18Z, 28 October and 00Z, 29 October computer wave model wave spectra for the grid point at 50.9°N, 145.6°W are compared to the 20Z and 21Z wave spectra from OSV PAPA in Figures 35-37. The OSV PAPA wave spectra were computed from twenty minute records for each hour. The OSV PAPA spectra in Figures 35-36 indicate that the wave energy was growing rapidly as a function of the local wind velocity. The high frequency wave energy shifted towards the low frequency end of the scale. Data obtained by a NAVOCEANO airplane during the same time period agreed with the OSV PAPA spectra. The computer model wave spectrum also had two peaks expected, but as in the 06Z, 27 October case, the high frequency energy peak is located at a lower frequency than the OSV PAPA high frequency energy peaks even though the OSV PAPA wave spectrum in Figure 36 was measured three hours after the model wave spectrum was computed. Unfortunately, the weather ship was underway at 0Z, 29 October and the measured wave spectrum obtained at that time was considered unreliable. The analyzed wave spectrum as shown in Figure 37 no longer has bi-modal peaks and the wave energy is concentrated in the lower frequency range.

A review of the analyzed and observed wind velocities listed in Table 6 for both 06Z, 27 October and 18Z October-0Z, 29 October

seems to indicate that the two sets of winds were in good agreement. In the majority of the comparisons the analyzed wind speeds were lower than the observed wind speeds. The one significant difference between the observed and analyzed wind velocities is that the observed winds show change every three hours while the analyzed winds which are computed every six hours, or two wave model time steps. Thus, the 12Z, 28 October wind speed of 21.8 knots was used as input at 09Z and 12Z and the 18Z, 28 October wind speed of 34.3 knots was used at 15Z and 18Z. The differences between the observed and analyzed wind speeds at 09Z and 15Z were approximately 8 knots for each case. This means that there were two time steps over a twelve hour period where the computed wave energy was being grown as a function of a significantly higher wind velocity than what actually existed at that time; however, this argument can not be used for the 06Z, 27 October case when the analyzed wind speeds at 50.9°N, 145.6°W were always less than the observed wind speeds.

The wind directions in both cases were such that if the energy dissipation equation (Appendix A, equation 11) in the computer model is correct, energy dissipation due to wind velocity should be a minimum during this time period. An investigation of the wind directions do point out one possible explanation as to what may have caused the discrepancies in the high frequency range. In both the 06Z, 27 October and 18Z, 28 October-00Z, 29 October cases, the wind was primarily from the south to southwest for at least six hours prior to and at

analysis time. A southerly wind should increase the air temperature. If the air temperature was significantly higher than the underlying sea surface temperature, then stable atmospheric conditions would exist. Cardone has used the air-sea temperature difference of 0.9°C as the cut-off point. As mentioned in Section III, the wind velocities, which are derived from the wind fields and used as input to the growth portion of the wave spectral model, are calculated for neutral stability. If stable conditions existed, the wave energy growth rate in the model may have been excessive. A review of ship observations for the area during both time periods could neither confirm or disprove this hypothesis as temperature data from several ships in the area varied considerable.

Another possibility is the growth equations and/or the Pierson-Moskowitz (P/M) wave spectra used in the computer model do not always represent the existing sea conditions. A similar hypothesis has been suggested by W. E. Cummins (1974) of the Naval Ship Research and Development Center. Cummins compared P/M response curves to wave spectral from OSV INDIA (60°N, 20°W) while investigating ship responses in various sea conditions. OSV PAPA and OSV INDIA have several points in common. Since extratropical storms propagate primarily from west to east, OSV INDIA which is located in the northeastern Atlantic is able to measure wave energy across a broad frequency range, as does OSV PAPA in the northeastern Pacific Ocean.

Extratropical storms in the Pacific Ocean, generally speaking, are probably more intense and cover a larger area than storms in the

Atlantic and wave spectra in the Pacific probably cover a larger frequency range and contain more wave energy. Both OSV PAPA and OSV INDIA use Tucker shipboard recorders to measure waves and the P/M curves were derived from Tucker wave recorder data; thus, all of these spectra should have the same basic characteristics. Cummins believed that since P/M spectra essentially represent a theoretical sea; i.e., generated by a steady wind blowing for an infinite time over an infinite fetch, uncontaminated by swell, these spectral will fall to one side of the OSV INDIA spectra because the measured spectra reflect the total energy--variable locally generated wave energy and energy propagated from distant generating areas--at the weather station. Cummins cited three sea conditions where the P/M curves had major discrepancies: in low significant wave height situations where the swell dominated the P/M spectra were too low ;in the intermediate wave heights cases the P/M spectra were significantly larger than the OSV INDIA spectra which, Cummins claimed, meant that these seas were rarely fully developed; in the highest in wave height conditions the P/M spectra were low, sometimes by a factor of two, which Cummins suggest meant these very high seas had much shorter wave lengths than the P/M spectra would imply. This could arise from very strong winds blowing for short periods (not defined), with the result that high frequency steep seas would be generated but would never become fully developed.

Since, as mentioned in Section IIA, the icosahedral gnomonic wave spectral model uses the P/M spectra as upper limits to its' growth curves and only in the fully developed state would the model spectra resemble the P/M spectra, the first two situations described by Cummins may not occur; however, the last situation is similar to the two cases cited above. In those cases there seem to be two distinct wave trains--one consisting of low frequency wave energy propagated from adjacent points and the other containing energy locally generated. This can be seen in the OSV PAPA wave spectra (Figures 31, 35-37) which have two distinct energy peaks. The model spectra only have low frequency peaks. If Cummins' conclusions are correct, then it is possible that under certain wind conditions the P/M curves are restricting the growth rate of the wave energy in the high frequency range and forcing the wave energy to shift toward the low frequency range sooner than it should. Certainly in the two cases under discussion this explanation seems plausible.

More data are needed for investigation of the two above hypotheses. It is hoped that data from the NDBO wave buoys will provide some of the answers.

C. Case Study - December 1974 - January 1975

A NOAA Data Buoy Office (NDBO) wave buoy (EBO3) was deployed in the northeastern Pacific Ocean (Gulf of Alaska) at 56.0°N, 147.9°W in 3 December 1974 in a location where severe extratropical storms transit during the winter season. Since most of the storms develop in the northwest Pacific Ocean,

this buoy is ideally located to monitor the propagation of wave energy over great distances as well as every growth for local high wind velocity cases. The buoy is configured to provide wave spectral and wind information in real time to a shore station.

The buoy itself is a large discus (40 feet in diameter) which NDBO claims exhibits a near unity response amplitude ratio over a broad frequency band below a high frequency cutoff (Michelena, Steele, Niedermann and Hindman, 1974). Assuming this to be true, monitoring the buoy motion will give a response equivalent to the sea surface motion. The wave sensing instrument is a servo-type accelerometer whose axis is fixed to the vertical center line of the buoy. Since the gyro-stabilized platforms which NDBO had used previously to maintain the axis of the linear accelerometer vertical relative to the mean surface have proved to be unreliable, NDBO realized that by fixing the axis of the accelerometer, an error would be introduced and that the determination of the error magnitude would be diffcult because of the interactions of the buoy hull and the sea surface. NDBO made the assumptions that the sea was an unidirectional simple swell wave of one frequency and the buoy was a perfect surface-follower that moves as a particle would--in a circle. Based on highly idealized sea conditions and buoy motion, NDBO found the error in wave heights to be on the order of 2%. An assumption was made that the error would not be significantly larger under more complex conditions.

The analog wave data are digitized every 0.5 seconds over a fifteen minute period (1800 points) every three hours. Wave spectra are computed from the acceleration data and are converted to displacement spectral densities by multiplying by ω^4 (circular frequency). The spectra are considered accurate within a frequency range of 0.01HZ to 0.5HZ. Significant wave height, average wave period and spectral width are obtained from moments of the displacement spectrum.

The wave buoy was calibrated in the laboratory comparisons were made between data obtained at sea by the wave buoy and from nearby a Datawell Wave Buoy a highly reliable and accurate wave sensor. The comparison between the wave spectra from the wave sensors was excellent. A report has been written by Ocean Data Systems, Inc. (ODSI) for NDBO Comparing wave spectral from the wave buoy to wave spectra from the SOWM (1975). One of the conclusions of this report was that the significant wave heights computed from the SOWM were generally higher than the significant wave heights computed from the buoy data. ODSI concluded that the computer model wave spectra had 20% excess energy and suggested that the cause was lack of strong decay coefficients in the low frequency range. Another conclusion was that the SOWM in some cases seemed to anticipate the arrival of the low frequency wave energy. Although significant if true, these conclusions were apparently made by only comparing significant wave heights, average wave periods, and wave spectra, and without regard to the meteorological conditions either upstream or at the grid point. Without further analysis, it

is difficult to ascertain whether the errors are a function of the wind input or the wave spectral model itself. Some of the comparative spectra, along with the local analyzed and observed wind velocities, are shown in Figures 38-42. Most of the comparisons are good and many of the differences seem to be caused by differences in the local wind velocities. In one case (Figure 42) where there was low velocity winds there was significant wave energy in the frequency bands centered at approximately 0.08HZ of both spectra that was either propagated from other areas or had been generated before the local wind had subsided. In several of the wave spectra not presented in this paper there does seem to be differences which can't be accounted for by local wind velocity differences. Since the wave spectral data from EBO3 are being transmitted routinely to FNWC, continuing analysis and comparison of the data are being made.

D. Case Study - Application of Wave Spectral Data to Optimum Track Ship Routing

One of the principal applications of wave spectral data is Optimum Track Ship Routing (OTSR). There are two U.S. Navy OTSR groups--one of which is located at FNWC and responsible for U.S. Navy ships and ships under military contract that transit the Pacific and Indian Oceans and the other, located at FWC, Norfolk is responsible for ships that transit the Atlantic Ocean. It has been demonstrated that the OTSR groups save the U.S. Navy at least 4.5 million dollars per year by minimizing fuel consumption during transit, minimizing

ship damage in storm areas, and increased reliability of ship's schedules.

A container ship's log containing positions, wave period, height and direction observations, and ship's speed made while the ship transitted the Pacific Ocean has been obtained. Although visual observations are usually considered unreliable, observations from this ship have proved to be highly reliable in the past and in this case were made by the Master in reponse to a request for carefully observed data. The ship is 950 feet in length and capable of speeds in excess of 30 knots. Excerpts of the ship's log compared to output of the computer wave spectral model are shown in Table 7. The actual ship's track along with the significant wave height analysis for 00Z, 7 February 1975 are shown in Figure 43. Considering that the analyzed wave information in Table 7 were only available on twelve hour increments, the analyzed wave heights and directions compared very well to the observed data. The wave directions shown in parentheses are the secondary directions. The most interesting comparisons occurred between 22Z, 6 February and 05Z, 7 February. Prior to this time the ship had maintained speeds on the order of 26-27 knots. At 22Z, 6 February the ship's speed began to decrease and for several hours (there was no notation in the log from 05Z-21Z, 7 February) the ship was unable to maintain a speed greater than 8 knots because of high wave conditions. At 00Z, 7 February the ship's observations was 50 feet while the SOWM had calculated a wave

height of 42 feet. The wave directions also compared well. It can be seen from Figure 35 that the model did compute significant wave heights up to 55 feet. These waves were approximately 300 nautical miles northwest of the ship's position. Based on the distance the ship travelled from 05Z-21Z, it appears that the ship could not average more than 14 knots during this time period. In order to make up the lost time the ship had to maintain speeds of 30-32 knots for the remainder of the journey which required greater fuel consumption and thus, greater operating costs for the transit.

It is interesting to note that, based on the ship's log, the ship could maintain normal operating speeds in wave heights up to 25 feet.

Prior to the advent of the SOWM, OTSR used hand analyzed wave charts and the output of the singular wave model was used to route ships. The FNWC singular wave model had a limiter which kept it from building wave heights greater than about 44 feet and since the constraint conditions for OTSR routes and diversions were wave heights of 20 feet or less the OTSR were frequently not carefully analized in the areas where sea heights were extremely high. The wave product users have not heretofore been used to seeing analyzed significant wave heights of 45 or greater. It has been demonstrated that the SOWM is doing a better job of representing the total range of energy in the ocean than the singular model or hand analysis procedures did.

VI. CONCLUSION

The operational Icosahedral-Gnomonic wave spectral computer model (SOWM), produces a far superior wave product than the FNWC singular wave model, the previous operational model. The singular wave model was limited from growing waves greater than 44 feet and could not adequately describe complex wave conditions. The SOWM considers the total wave energy in a 15 frequency band by 12 direction bands matrix in a grid point and propagates the energy throughout the grid system as a function of frequency and direction. The case studies in Section V demonstrated the ability of the wave model to accurately propagate low frequency energy (Study A), to cope with more than one wave train at any given time (Study B), to correlate well with observations from an operational spectral observing station (Study C), and to grow high waves for high wind conditions (Study D).

Since this is the first time that a hemispheric wave spectral model has been used routinely on an operational basis, it is expected that some modifications will have to be made to improve the model. Other wave spectral models such as the Gelci spectroangular model (Gelci, Chavz and Devillaz, 1963) and the Barnet model (Barnett, 1968) are also being tested and evaluated to determine which model would provide the best results. It may be that a hybrid model containing the best features of each model may evolve. For example, the Barnett model has a wave-wave interaction term which may improve the

dissipation of wave energy. If it does, such a term will be included in the operational model.

The initial thrust to improve the present operational model will be slanted towards improving the wind input. Wind fields will be derived every three hours rather than the present six hours so that the wind input can coincide with the basic time step of the wave spectral model. Investigations are being made to determine if the Cardone Planetary Boundary Layer Model modified by Dr. Jack Kaitala, FNWC meteorologist, will produce wind fields better suited for use as input to the spectral model than the existing FNWC wind analyses and prognosis. It is believed that some significant improvement should occur since the wind velocities will be computed for some known height above the sea surface (preferable 19.5 meters) and frictional wind velocities (U_*) will be a function of atmospheric stability.

One modification that would probably significantly improve the wave spectral model is to increase the number of direction bands used to define the directional spectra from the present twelve bands (30° increments) to twenty-four bands (15° increments). This would better define the travel path of the wave energy over long distances. Unfortunately, doubling the number of direction bands would also double the amount of computer storage and computation time needed to operate the computer model. Thus, for operational purposes, this modification is not practical on the present FNWC computers and

must be held in abeyance until a larger computer system becomes available.

A similar problem exists in defining the frequency spectra. It has been suggested that for certain applications of the output of the wave spectral model, the highest frequency should be better defined. Essentially, the highest frequency band extends from 0.164HZ to 0.4HZ which could be subdivided into two or three smaller bands; however, the same problem as was discussed with the direction bands would exist. The size of the two dimensional wave energy matrices would increase and strain the present FNWC computer resources. One short-term solution would be to delete the lowest frequency band (0.039HZ) and divide the highest frequency into two smaller bands. This would not increase the size of the arrays in the computer model. Before this modification can be made, a determination must be made as to whether the deletion of the lowest frequency band will significantly alter the computer wave spectra.

The NDBO Buoy wave spectra along with the corresponding meteorological data will be closely monitored to determine if the errors, such as described in Case Studies B and C in the computed spectra have a definite trend or are random. Measured wave spectra from other sources such as OSV PAPA, airplane lasers and satellites will also be monitored for verification purposes.

In addition to being more accurate than the output of the singular model, the output of the wave spectral model has a wider range of applications for U.S. Navy use. Investigations are now underway to determine the feasibility of applying the wave spectra to such projects as ship motion studies, acoustical ambient noise problems, and shallow water wave refraction studies.

A considerable amount of effort was expended by a number of people in order for the SOWM to reach the status it has today. Consderably more effort will be required to improve the computer model and to make full use of its potential.

References

Adamo, L. C., L. Baer, and J. P. Hosmer, Icosahedral-Gnomonic projection and grid of the world ocean for wave studies, Journal of Geophysical Research, 73 (16), pp. 5125-5132, 1968.

Baer, L., An experiment in numerical forecasting of deep water ocean waves, Ph. D. Dissertation, New York University Department of Meteorology and Oceanography, 1962.

Barnett, T. P., On the generation, dissipation, and prediction of ocean wind waves, Journal of Geophysical Research, 73 (2), pp 513-529, 1968.

Blackman, R. B. and J. W. Tukey, The Measurement of Power Spectra, Dover Publications, 190 pp, 1958.

Briscoe, M. G., A FORTRAN computer program for the analysis of some simple characteristics of Sea-surface waves, SACLANT ASW Research Centre Technical Memorandum No. 163, 19 pp, 1971.

Cardone, V. J., Specification of the wind distribution in the marine boundary layer for wave forecasting, New York University Department of Meteorology and Oceanography TR 69-1, 131 pp., 1969.

Cardone, V. J., personal communication, 1974.

Cartwright, D. E., The use of directional spectra in studying the output of a wave recorder on a moving ship, Ocean Wave Spectra, Prentice-Hall Inc., pp 203-218, 1963.

Cummins, W. E., Prediction of seakeeping performance, Seventeenth American Towing Tank Conference, California Institute of Technology, June 1974.

Darbyshire, J., The one-dimentional wave spectrum in the Atlantic Ocean and in coastal waters, Ocean Wave Spectra, Prentice-Hall Inc., pp. 27-30, 1963.

Darbyshire, M., Waves in the North Sea, The Dock and Harbour Authority, November, pp. 225-228, 1960.

Ewing, J. A., Personal Communication to Lionel Moskowitz, May 1969.

Gelci, R., P. Chavy, and E. Devillaz, Numerical Treatment of the state of the sea, Cahiers Oceanographiques, 15(3), pp 153-160, 1963.

Holl, M. M. and B. R. Mendenhall, the FIB methodology and application, Meteorology International Inc., Project M-167 Final Report for Fleet Numerical Weather Central, 1971.

Holland, G. L., Personal communication, May 1972.

Hubert, W. E. and B. R. Mendenhall, the FNWC singular sea/swell model, Fleet Numerical Weather Central Technical Note 59, 66 pp, 1970.

Inoue, T., On the growth of the spectrum of a wind generated sea according to a modified Miles-Phillips mechanism and its application to wave forecasting, New York University Department of Meteorology and Oceanography, TR 67-5, 74 pp, 1967.

Kerr, K. P. Stability characteristics of various buoy configurations, Buoy Technology, Transactions of 1964 Marine Technology Society Symposium, pp 5-16, 1964.

Lazanoff, S. M., N. M. Stevenson and V. J. Cardone, A Mediterranean Sea wave spectral model, Fleet Numerical Weather Central Technical Note 73-1, 82 pp, 1973.

Lewis, J. M. and T. H. Grayson, The adjustment of surface wind and pressure by Sasaki's variational matching technique, Fleet Numerical Weather Central Technical Note 72-1, 49 pp, 1972.

Lockheed California Company, Pacific Wave Study, Lockheed Report 19354, 36 pp, 1965.

Lockheed Ocean Sciences Department, The Icosahedral-Gnomonic projection and grid of the world ocean for wave studies, Lockheed Report 20157, 24 pp, 1966.

Lockheed Ocean Sciences Department, Pacific Ocean wave forecasting study, Lockheed Report 20850, 76 pp, 1967.

McConathy, D., personal communication, 1974.

Michelena, E. D., K. E. Steele, C. S. Neederman and J. H. Hinchman, A reliable wave measurement system for NOAA data buoys, Procedings from Marine Technology Society Meeting, September, 1974.

Ocean Data Systems, Synoptic comparison of EBO3 and spectral wave data, ODSI Technical Report 2, 27 pp, 1975.

Pierson, W. J., L. J. Tick and L. Baer, Computer based procedures for preparing global wave forecasts and wind field analyses capable of using wave data obtained by a spacecraft, Proceedings of the Sixth Naval Hydrodynamics Symposium, 1966.

Ross, D. V. and V. Cardone, Observations of oceanic whitecaps and their relation to remote measurements of wind speed, Journal of Geophysical Research, 79(3), pp 444-452, 1974.

Rudnick, P. and R. W. Hasse, Extreme Pacific waves, December 1969, Journal of Geophysical Research, 76(3), pp 742-744, 1971.

Salfi, R. E., Operational computer based spectral wave specification and forecasting models, University Institute of Oceanography of the City University of New York Technical Report, 130 pp., 1974.

Schwartz, E. and W. E. Hubert, The FNWC singular advective wind wave/swell analysis and forecast model, Fleet Numerical Weather Central Technical Note No. 73-2, 1973.

Shemdin, O. H., R. J. Lai, A. Reece and G. Tober, Laboratory investigations of whitecaps, spray and capillary waves, University of Florida Coastal and Oceanographic Engineering Laboratory Technical Report No. 11, 101 pp, 1972.

Tucker, M. J., A shipborne wave recorder, Transactions of Institute of Naval Architects, XCVIII, pp 236-250, 1956.

APPENDIX A

EQUATIONS USED TO GROW AND DISSIPATE WAVE ENERGY

Comprehensive derivations of most of the following equations can be found in Inoue (1967) and Cardone (1969).

FNWC analyzed and forecasted surface wind speeds are used essentially as a first guess in the following equation to obtain frictional wind felocities (U_*) and surface roughness parameters (Z_o). Equation (1) is

$$U_* = \frac{KU}{\log(Z/Z_o)} \qquad (1)$$

where K is Von Karman's constant and has a value of 0.4,

U is the wind velocity,

Z is the elevation at which the wind velocity is measured or, in this case, calculated,

Z_o is the surface roughness parameter and in this program is defined as

$\alpha/U_* + \beta U_*^2 + \gamma$ and α, β and γ are constants.

The growth equations in the wave spectral model are designed to use 6.1 meter and 19.5 meter wind velocities. If the winds input is based on some other height than those above-mentioned, then the wind speeds should be recalculated for either 6.1 meters or 19.5 meters, depending on which equation is being used. The FNWC wind fields are only considered surface winds without any

regard to height. The operational wave model does not make any attempt to correct the FNWC winds for elevation.

Since there are two unknowns (U_*, Z_o) in equation (1), the equation is solved by reiterative means. Once U_* and Z_o have been calculated equation (1) is used to obtain the 6.1 meter and 19.5 meter wind speeds.

Neglecting non-linear effects, the spectral components can be initially expressed as

$$\frac{d}{dt} S(f,t,\vec{x}) = A[f,U(t,\vec{x})] + B(f,U(t,\vec{x})]\ S(f,t,\vec{x}) \qquad (2)$$

where $A[f,U(t,\vec{x})$ is the resonance growth mechanism,

$B(f,U(t,\vec{x})]\ S(f,t,\vec{x})$ is the Miles instability term,

$S(f,t,\vec{x})$ is the spectral density, and

f is the wave frequency, t is time, $\vec{x}$ is wave direction.

Based on Cardone's recent work, A(f,U) can be defined in one of two ways depending on the magnitude of $(2\pi f/U_{6.1})$. If the value of $(2\pi f/U_{6.1})$ is less than 0.02, then $A(F,U_{6.1})$ is defined as

$$0.675*10^{-12} \left[\int_{-\pi_2}^{\pi_2} \frac{0.02^{2.28}\ \omega^4\ U_{6.1}^3}{W + Y} \right] d\theta \qquad (3)$$

where $W = [0.270r^2 + \{k \sin\theta\}]$, and

$Y = [\frac{1}{9} \{0.02^{1.28}\}^{2.5} + \{k \cos(\theta - r)\}^2]$

where $\omega = 2\pi f$,

g is the gravitational acceleration,

$U_{6.1}$ is the wind speed at 6.1 meters,

$k = \omega^2/g$, and

$r = \omega^2/U_{6.1}$

If the value of $(2\pi/U_{6.1})$ is greater than 0.02 then $A(f,U)$ is defined as

$$0.675 \cdot 10^{12} \left\{ \int_{\pi^2}^{\pi^2} \frac{\omega^{5.25} \, U_{6.1}^{1.75}}{0.2704\, r^2 + [K \sin\theta]^2 \left[\frac{1}{9}\left(\frac{\omega}{g}\right)^{2.25} + \cos(\theta - r)\right]^2} \right\} d\theta \qquad (4)$$

The instability growth term is described as follows:

$$B/F = \frac{\rho_a}{\rho_\omega} \frac{2\pi}{C^2 K} \left\{ \frac{A_m \Gamma^2 k^4}{\cos^2\theta} \left(\frac{U''}{U'} \right)_{Z_m} \left(\int_{Z_m}^{\alpha} [U \cos\alpha - C] \, e^{-kZ} dZ \right)^2 \right. \qquad (5)$$

$$\left. + A_p \int_0^{\alpha} \Gamma^2 \, (-U'') \cos\theta \, |U \cos\theta - C| \, e^{-2kZ} dZ \right\}$$

Where ρ_ω is the density of water,

U'' is the mean wind profile curvature,

U' is the mean wind profile slope,

θ is the directional difference between the wind and wave,

A_m is a constant and equal to π,

A_p is a constant determined by experiment and ascertained by Phillips to be 1.6×10^{-2} with an uncertainty of 30%, Γ^2 is +1 above the matched layer and less than +1 below the matched layer.

The first term on the right hand side is Miles' solution and the second term is a later contribution by Phillips. B/f is a dimensionaless quantity. A relationship exists between B/f and U_*/C (where C is the phase velocity of the wave energy) and a number of investigators have examined this relationship on a theoretical basis or in field experiments. Inoue's solution which is used in the wave spectral model is

$$B(f,U_*) = \{1.29 * 10^{-3}\ell^{-7000}[U_*/C - 3.1 * 10^{-2}]^2 + \quad (6)$$

$$+ 0.725(U_*/C)^2\ell^{-4} * 10^{-4}(C/U_*)^2\}f$$

If the wave growth equation was used in the computer model without any constraints, the wave energy could have unlimited growth. Since this does not occur in nature, the concept of a fully developed sea was introduced in order to approximate the real world. The essence of this concept is that if a wind with the same magnitude blows in the same direction over a given fetch for enough time, the wave spectrum will become fully developed and no matter how much longer the same wind velocity exists, the spectrun will no longer continue to grow. The Pierson/Moskowitz (P/M) fully developed spectrun is used to limit wave growth and has the form

$$S_\infty(\omega) = \frac{\alpha g^5}{\omega^5} e^{-\beta(\omega_0/\omega)^4} \qquad (7)$$

where $\alpha = 8.1*10^{-3}$

$\beta = 0.74$, and

$\omega_0 = g/U$

The wave spectrum at each grid point is compared to the P/M spectrun for the given wind speed. The P/M spectrun is inserted in equation (2) by

$$\frac{ds}{dt} = [A\{1 - \frac{S}{S_\infty}\}^2\}^{1/2} + BS] [1 - (\frac{S}{S_\infty})^2] \qquad (8)$$

The solution for zero initial conditions is

$$S(f,t) = A\{\frac{\ell^{Bt} - 1}{B}\} [1 + \{\frac{A\ell^{Bt} - 1}{B\ S}\}^2]^{-1/2} \qquad (9)$$

Since equations (8) and (9) only provide one dimensional spectra, an equation developed by the Stereo-Wave Observation Project (SWOP) is used to obtain the directional spectra. This equation is

$$F(\omega,\theta,U) = \tau[1+(0.5 = 0.82\ \ell^{-1/2}(\omega U/g)^4 \cos 2\theta \qquad (10)$$

$$+ \theta.32\ell^{-1/2}(\omega U/g)^4 \cos 4\theta]$$

for $-\pi/2 < \theta < \pi/2$ and θ is the angle between the wind and wave directions. $F(\omega,\theta,U)$ is equal to θ everywhere else.

The directional spectra are computed for 30° increments. As an example, if the wind direction were 180°, the distribution of wave energy would be as follows: 37.5% of the energy would be placed in the 180° direction band; 25% would be placed in the 150° and 210° bands; and 6.25% of the energy would be placed in the 120° and 240° direction bands. If the wind direction were 190° rather than 180°, then the energy distribution would be more biased in the 210° and 240° direction bands, than in the 120° and 150° bands.

Wave energy is only dissipated when the waves encounter land or interact with the wind. Inoue developed a formula to account for the wave dissipation if the angle between the wind and wave directions is greater than 75°. The formula is:

$$S_o(f_i,\theta_i) = S_o(f_i,\theta_i)\ [e^{-C\sqrt{S_\omega}\ f_i^4}]^{k(\theta_1)} \qquad (11)$$

where $S_o(f_i,\theta_i)$ is spectral component after dissipation,

$S_o(f_i,\theta_i)$ is spectral component before dissipation,

f_i,θ_i is the center frequency and direction of the component,

C is a constant 690 for ft^2/sec and 169.2 for m^2/sec),

$S_\omega = \Sigma^1\Sigma^1 S_\omega(f_i,\theta_i)$

and $K(\theta_1)$ is 0 for $\theta_1 \leq 75°$

$K(\theta_1)$ is 1.5 for $75° \leq \theta \leq 105°$

$K(\theta_1)$ is 3.0 for $105° < \theta_1 \leq 135°$

$K(\theta_1)$ is 4.5 for $135° < \theta_1 \leq 165°$, and

$K(\theta_1)$ is 6.0 for $165° < \theta_1 \leq 180°$.

Significant wave height ($\overline{H}_{1/3}$) which is defined as the average height of the highest one-third waves is obtained by

$$\overline{H}_{1/3} = 4\sqrt{E_{TOT}} \tag{12}$$

where E_{TOT} is the total two-dimensional wave energy at a grid point.

TABLE 1

Central Frequency (H_z)	Central Period (Seconds)	Frequency Bandwidth (H_z)
0.164	6.1	.164 - ∞
0.153	6.5	.142 - .164
0.133	7.5	.125 - .142
0.117	8.6	.108 - .125
0.103	9.7	.097 - .108
0.092	10.9	.086 - .097
0.083	12.0	.080 - .086
0.078	12.9	.075 - .080
0.072	13.8	.069 - .075
0.067	15.0	.064 - .069
0.061	16.4	.058 - .064
0.056	18.0	.053 - .058
0.050	20.0	.047 - .053
0.044	22.5	.042 - .047
0.039	25.7	.036 - .042

TABLE 2

PROPERTIES OF THE GNOMONIC PROJECTION ON A FACE OF AN ICOSAHEDRON[1]

Area, 1/20th of the Earth's surface		7.45×10^6 sq n mi
On the Earth:		
Length of side	or	$63^\circ 26.1'$
		3806. n mi
Length of altitude	or	$58^\circ 16.9'$
		3497. n mi
Vertex angle (spherical)		72°
On the Plane:		
Length of side		4552. n mi
Length of altitude		3942. n mi
Vertex angle		60°
Distortion relative to 1.00 at the tangent point:		
Radial - maximum (at vertices)		1.58
- midpoint of sides		1.15
Transverse - maximum		1.26
- midpoint of sides		1.07
Areal - maximum		1.99
- midpoint of sides		1.23
Distortion relative to 1.00 at the location of mean distortion:		
Radial - maximum (at vertices)		1.40
- minimum (at tangent point)		.88
Transverse - maximum		1.19
- minimum		.94
Areal - maximum		1.65
- minimum		.82

[1]Assumes spherical Earth of radius 3440.19 n mi

(Lockheed, 1966)

TABLE 3

DTG	LOCATION	WIND SPEED(K+5)	WIND DIRECTION	SIGNIFICANT WAVE HEIGHT(F
YYMMDDHH				
69112906	48°N,165°E	58	320	30
69112912	45°N,170°E	69-70	260-270	32-33
69112918	45°N,170°E	68	290-300	45
6911300	40°N,175°E	72-73	240	50-52
69113006	45°N,178°E	66-68	290-300	52
69113012	40°N,176°W	73-74	250-260	55-62
69113018	40-45°N,180°W	87-91	320-340	74
69120100	40°N,165°W	78	250-270	69-72
69120106	42°N,170°W	73	330	66-70
	40°N,165°W	74	260	69-75

TABLE 4

WAVE STATISTICS AT 27°30'N, 157°45'W FOR 23Z, 1 DECEMBER 1969

Largest Wave Height in One Hour Sample	24.4 meters	80 feet
Significant Wave Height	14.4 meters	49 feet
Average Wave Height	10.5 meters	34.5 feet

Predominant Wave Spectral Peak 0.05-0.062HZ (20 to 16 sec)

TABLE 5

RATIO OF ACTUAL WAVE AMPLITUDE TO TUCKER RECORDED AMPLITUDE

HERTZ	AMPLITUDE RATIO
.05	1.06
.06	1.04
.07	1.04
.08	1.06
.09	1.09
.10	1.13
.11	1.18
.12	1.24
.13	1.32
.14	1.41
.15	1.52
.16	1.64
.17	1.78
.18	1.94
.19	2.14
.20	2.35
.21	2.62
.22	2.92
.23	3.28
.24	3.70
.25	4.20
.26	4.78
.27	5.48
.28	6.31
.29	7.31
.30	8.51
.31	9.96
.32	11.71
.33	13.85
.34	16.46
.35	19.66
.36	23.61
.37	26.49
.38	34.57
.39	42.16
.40	51.69
.41	63.69
.42	78.89
.43	98.23
.44	122.9
.45	154.7
.46	195.6
.47	243.6
.48	317.6
.49	407.9
.50	526.5

TABLE 6

WIND VELOCITY

DTG	GRD PT 164	GRD PT 165	OSV PAPA
	50.9°N,145.6W	48.5N,147.5W	50°N,145°W
	KTS DIR	KTS DIR	
73102512	20.5, 227°	22.5, 220	
73102518	18.5, 216°	19.5, 208	
73102600	14.2, 207	16.7, 206	
73102606	15.5, 179	20.1, 200	+3 13,140[15,110]
73102612	9.6, 142	16.9, 213	17,080[17,090]
73102618	13.7, 201	26.0, 219	27,230[35,240]
73102700	25.0, 228	33.0, 229	31,210[31,200]
73102706	28.0, 209	35.7, 210	31,200[38,210]
73102712	25.9, 232	30.6, 226	35,220[32,200]
73102718	21.0, 233	31.6, 224	31,230[36,280]
73102800	25,0, 280	30.8, 259	36,310[30,300]
73102806	27.2 283	32.6, 273	27,280[14,230]
73102812	21.8, 240	26.2, 255	24,220[26,190]
73102818	34.3, 179	34.7, 199	37,180[41,180]
73102900	35.6, 207	38.9, 214	34,200

TABLE 7

COMPARISON OF SHIP VISUAL OBSERVATIONS WITH WAVE SPECTRAL MODEL SIGNIFICANT HEIGHTS AND DIRECTIONS

Ship DTG	Model DTG	LAT	LONG	Ship Speed	Observed Height/ Direction	SOWM Height/ Direction
75020200Z	75020200Z	37°31'N	124°38'W	26	13ft/270°	15ft/305°
75020216Z	75020212Z	37°15'N	133°17'W	26	15ft/310°	12ft/299°
75020218Z	75020212Z	37°12'N	134°30'W	26	17ft/340°	16ft/305°
75020220Z	75020300Z	37°12'N	135°30'W	25	20ft/350°	12ft/305°
75020223Z	75020300Z	37°12'N	137°36'N	26	13ft/320°	12ft/321°
75020302Z	75020300Z	37°10'N	139°00'W	26	16ft/350°	12ft/360°
75020317Z	75020312Z	36°56'N	147°11'W	27	12ft/40° (200°)	6ft/170° (15°)
75020319Z	75020400Z	36°55'N	148°20'W	26	10ft/20° (190°)	10ft/172° (15°)
75020321Z	75020400Z	36°53'N	149°20'W	27	8ft/20° (190°)	10ft/172° (15°)
75020323Z	75020400Z	36°5'N	150°24'W	27	8ft/220°	10ft/172° (15°)
75020400Z	75020400Z	36°50'N	150°56'W	26	8ft/210°	10ft/172°
75020401Z	75020400Z	36°49'N	151°30'W	26	8ft/210°	9ft/170°
75020418Z	75020500Z	36°34'N	160°40'W	21	18ft/310°	15ft/307°
75020503Z	75020500Z	36°22'N	165°20'W	26	6ft/340° (290°)	10ft/300° (320°)
75020519	75020600Z	36°05'N	174°W	26	8ft/280°	6ft/290°
75020601Z	75020600Z	36°08'N	177°W	26	12ft/295°	9ft/290°
75020603Z	75020600Z	36°07'N	178°09'W	26	12ft/290°	9ft/290°

TABLE 7 - CONTINUED

Ship DTG	Model DTG	LAT	LONG	Ship Speed	Observed Height/ Direction	SOWM Height/ Direction
75020622Z	75020700Z	35°40'N	172°00'E	26	35ft/267° (270°)	42ft/280°
75020623Z	75020700Z	35°40'N	172°00'E	9	40ft/265° (270°)	42ft/280°
75020700Z	75020700Z	35°36'N	171°50'E	8	50ft/270° (280°)	42ft/280°
75020702Z	75020700Z	35°36'N	171°35'E	8	30ft/275° (280°)	40ft/280°
75020704Z	75020700Z	35°32'N	171°13'E	8	40ft/310° (300°)	40ft/280° (270°)
75020705Z	75020700Z	35°30'N	171°03'E	8	40ft/290°	40ft/280°
75020721Z	75020800Z	34°40'N	165°58'E	28	25ft/350° (310°)	21ft/330°
75020723Z	75020800Z	34°30'N	165°00'E	31	25ft/10° (190°)	21ft/330° (200°)
75020801Z	75020800Z	34°30'N	163°45'E	31	20ft/10°	18ft/20°
75020805	75020800Z	34°34'N	161°22'E	30	18ft/220°	16ft/20° (200°)
75020806	75020812Z	34°34'N	160°44'E	31	25ft/200°	18ft/10° (180°)
75020822	75020900Z	35°32'N	151°40'E	30	20ft/130°	15ft/200°
75020900Z	75020900Z	35°25'N	150°20'E	32	14ft/180°	15ft/200°
75020902Z	75020900Z	35°25'N	149°10'E	30	10ft/150° (180°)	12ft/200°
75020907Z	75020912Z	35°10'N	146°06'E	30	10ft/320°	9ft/270°

WAVE ENERGY GROWTH (FIG1)

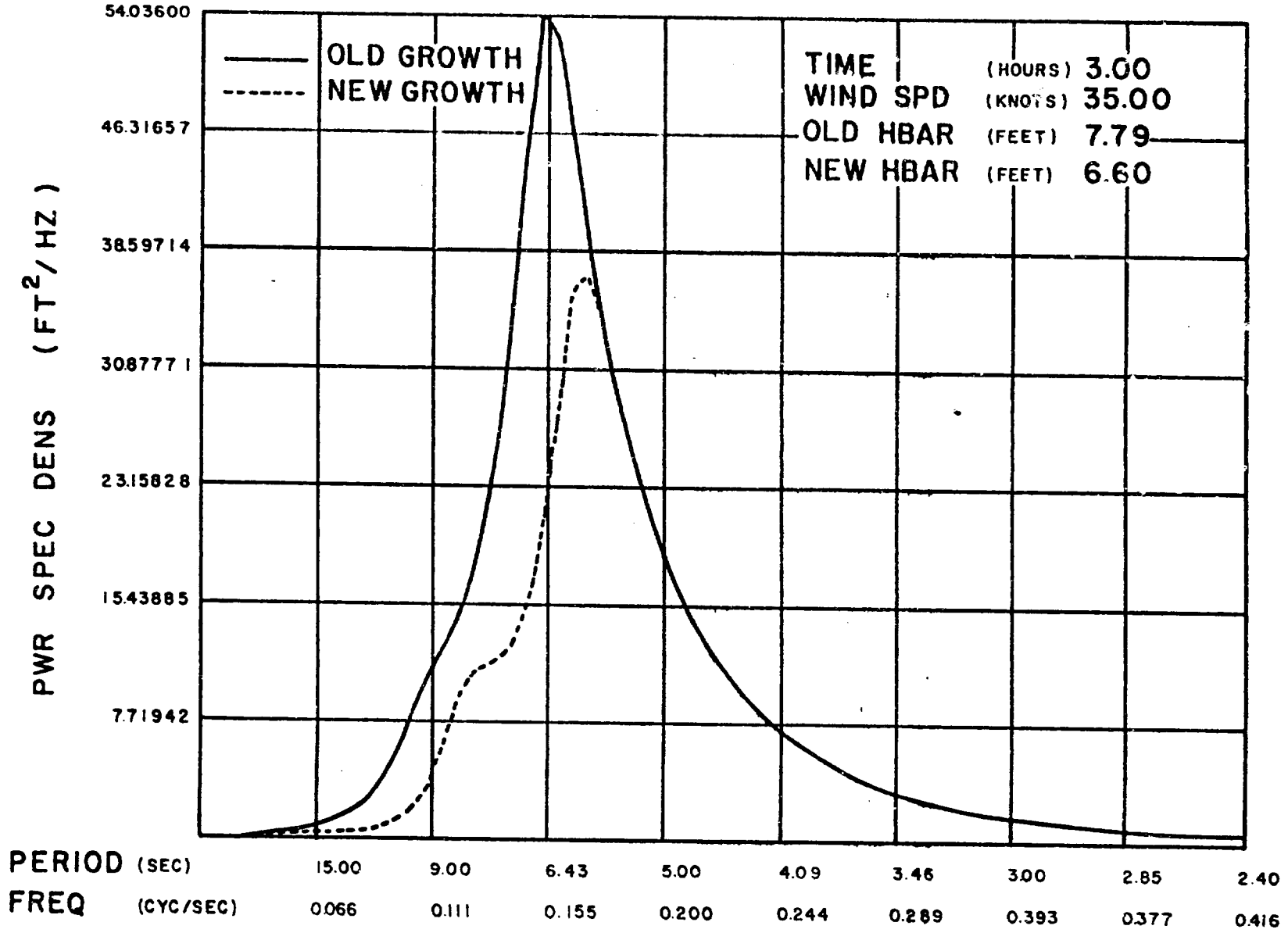

WAVE ENERGY GROWTH (FIG 2)

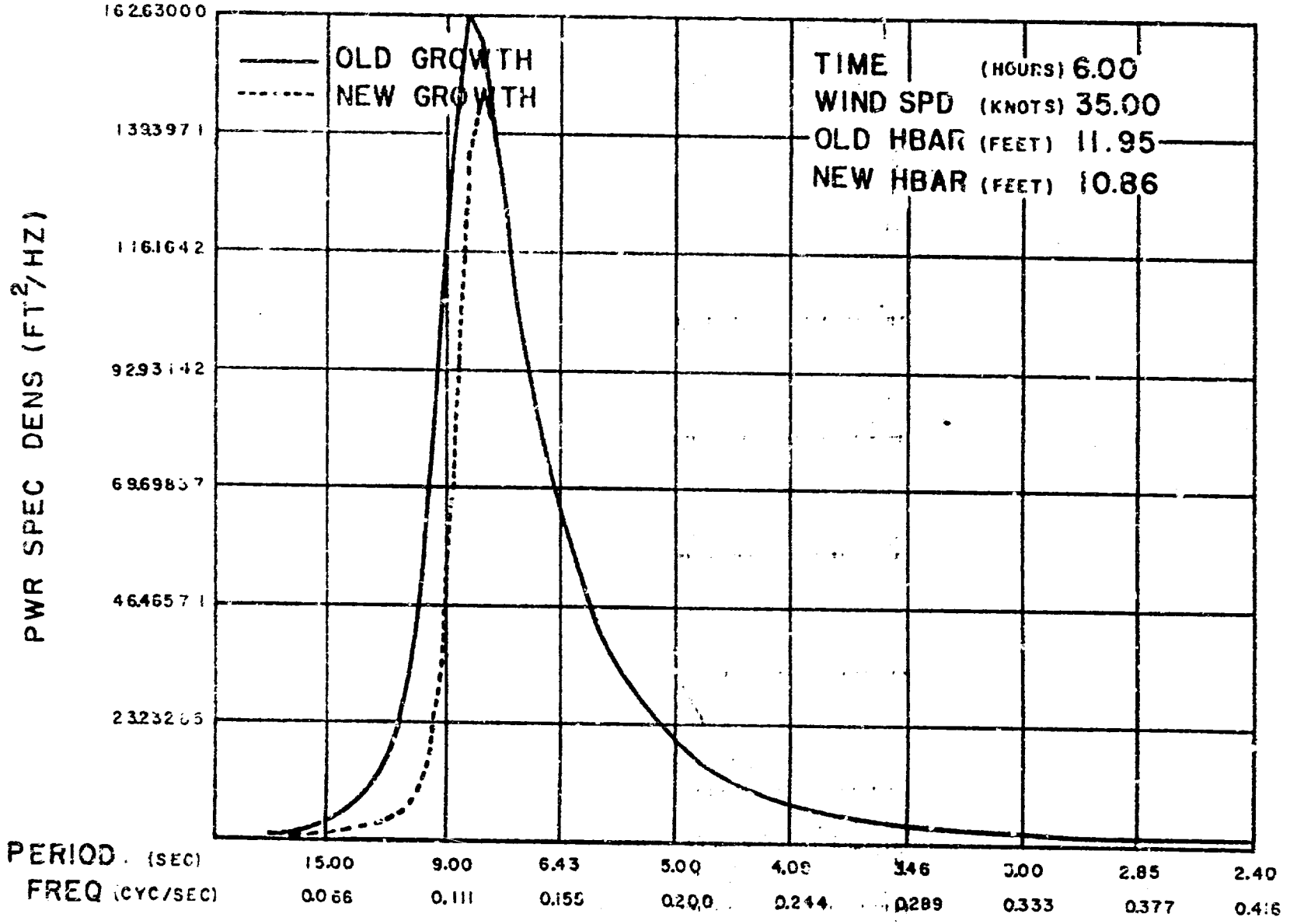

WAVE ENERGY GROWTH (FIG 3)

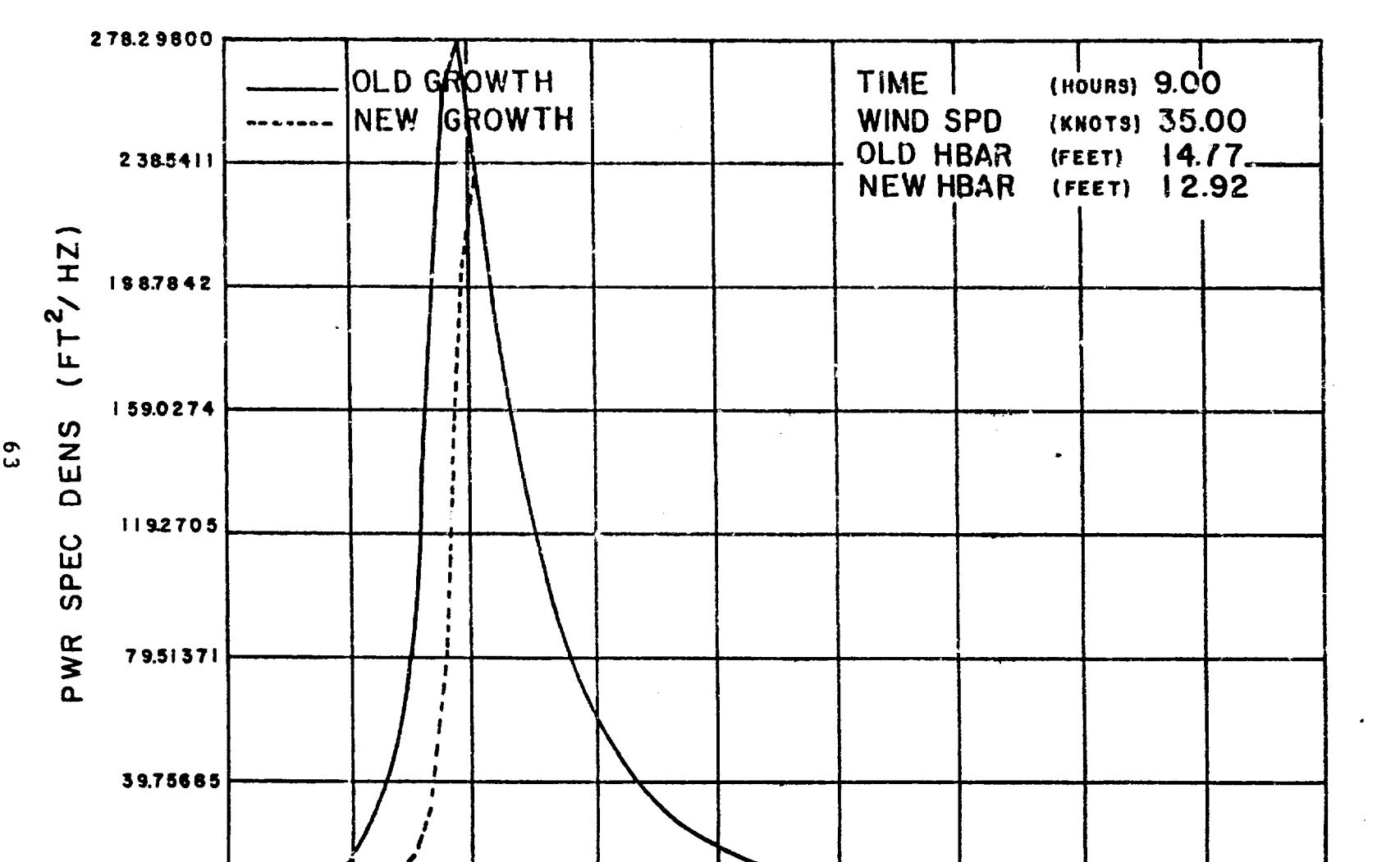

WAVE ENERGY GROWTH (FIG 4)

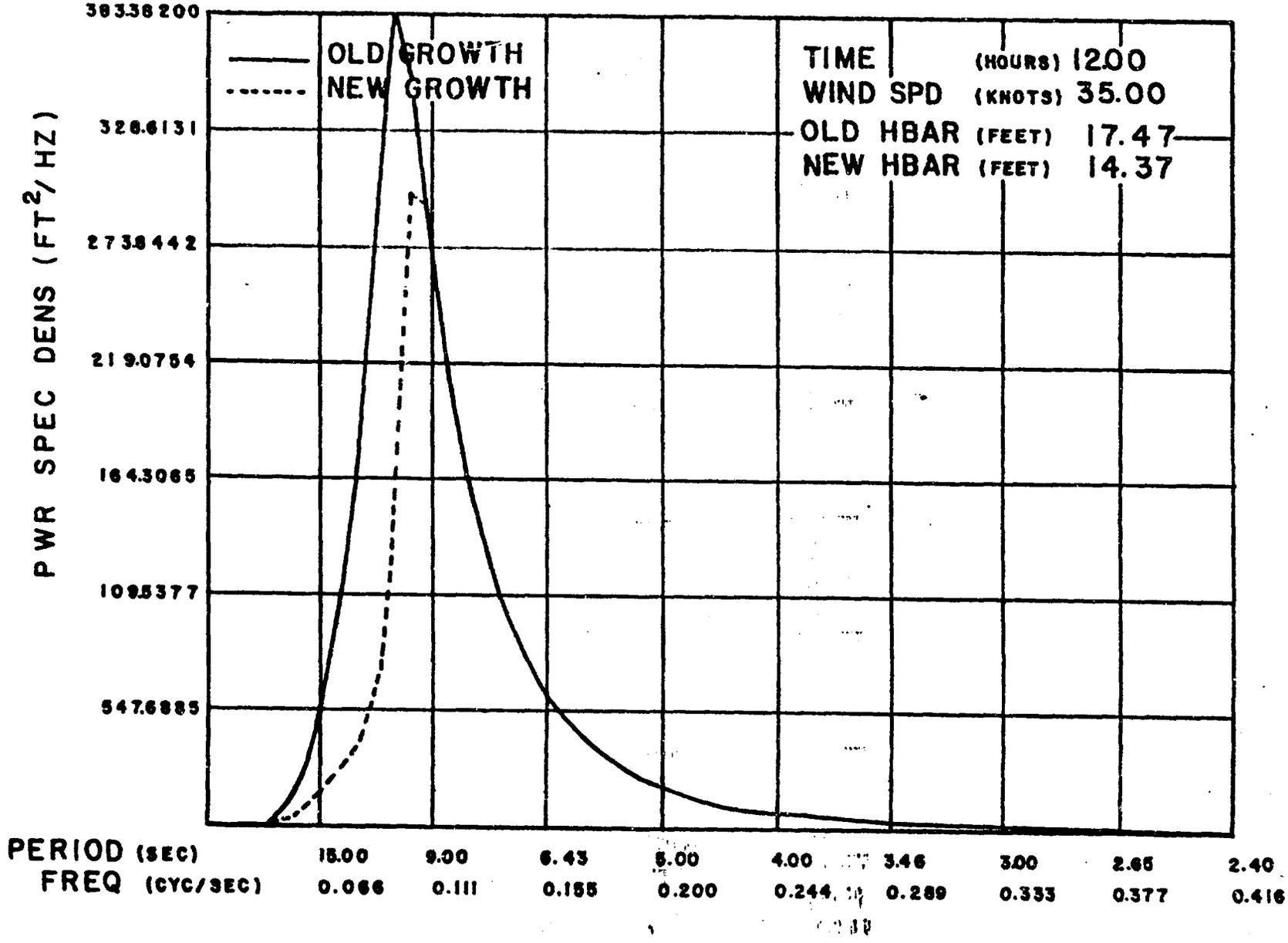

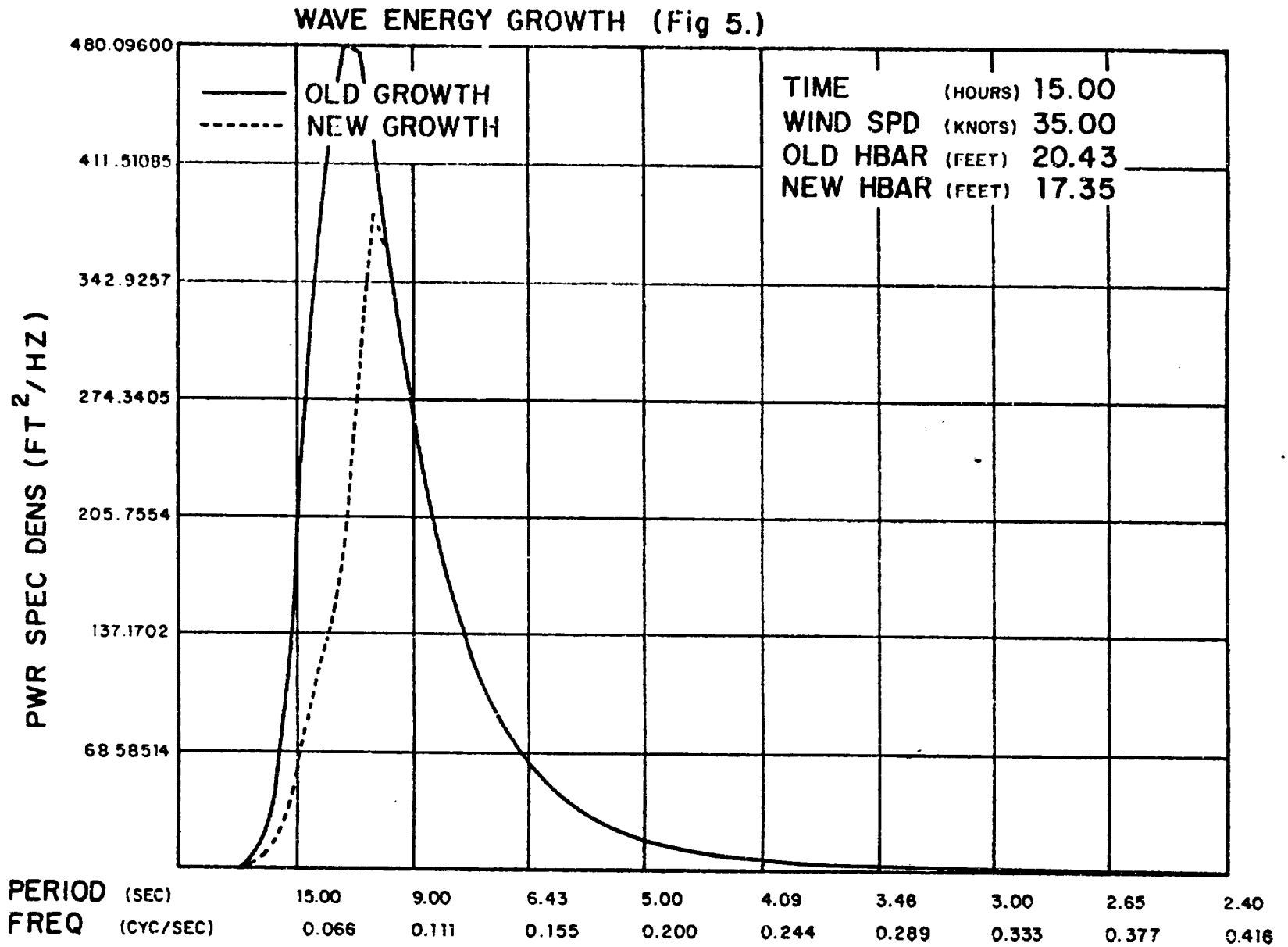
WAVE ENERGY GROWTH (Fig 5.)
480.09600
411.51085
342.9257
274.3405
205.7554
137.1702
68.58514
PWR SPEC DENS (FT²/HZ)
OLD GROWTH
NEW GROWTH
TIME (HOURS) 15.00
WIND SPD (KNOTS) 35.00
OLD HBAR (FEET) 20.43
NEW HBAR (FEET) 17.35
PERIOD (SEC) 15.00 9.00 6.43 5.00 4.09 3.46 3.00 2.65 2.40
FREQ (CYC/SEC) 0.066 0.111 0.155 0.200 0.244 0.289 0.333 0.377 0.416

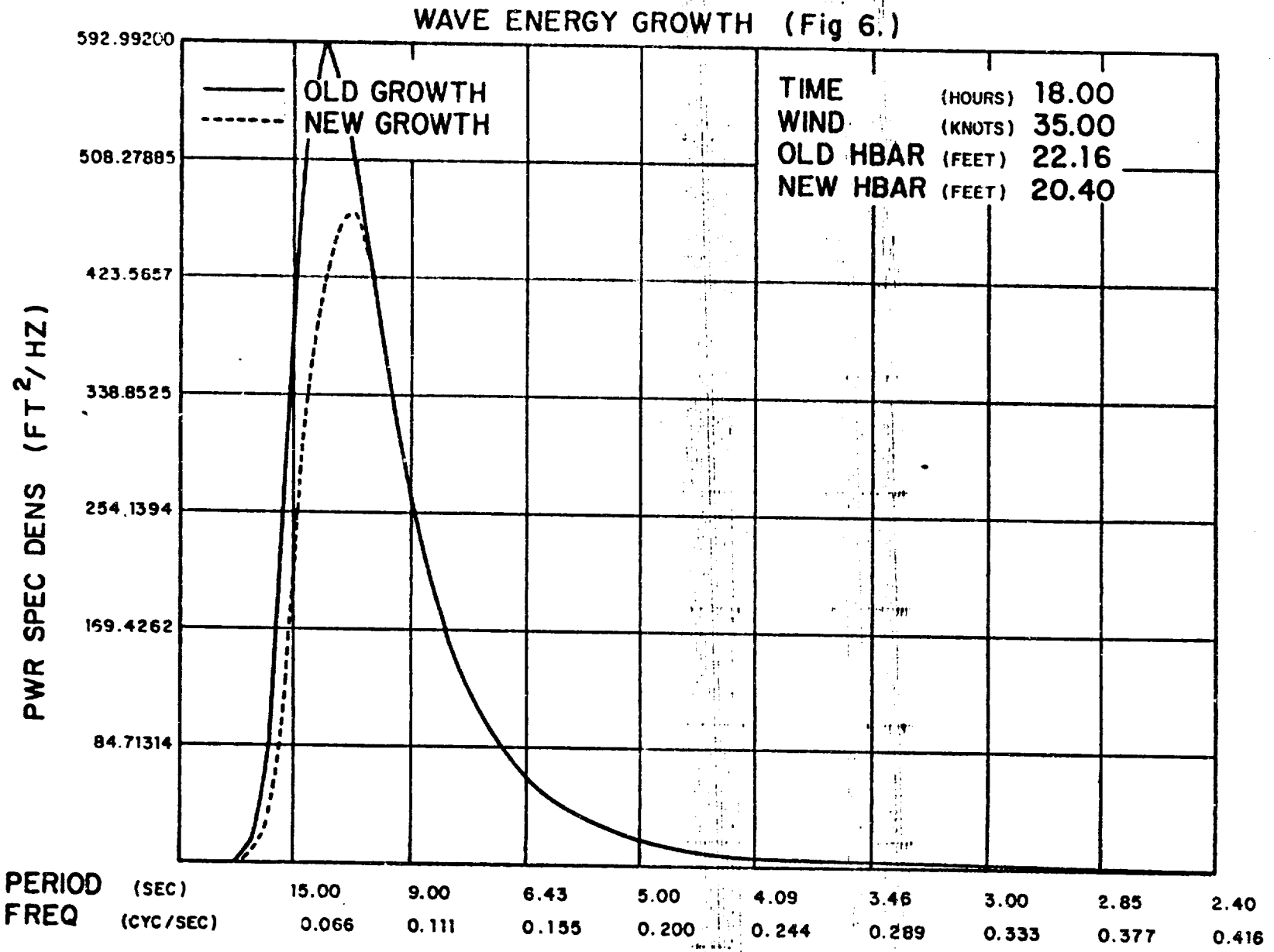
WAVE ENERGY GROWTH (Fig 6.)
592.99200
508.27885
423.5657
338.8525
254.1394
169.4262
84.71314
PWR SPEC DENS (FT²/HZ)
OLD GROWTH
NEW GROWTH
TIME (HOURS) 18.00
WIND (KNOTS) 35.00
OLD HBAR (FEET) 22.16
NEW HBAR (FEET) 20.40
PERIOD (SEC) 15.00 9.00 6.43 5.00 4.09 3.46 3.00 2.85 2.40
FREQ (CYC/SEC) 0.066 0.111 0.155 0.200 0.244 0.289 0.333 0.377 0.416

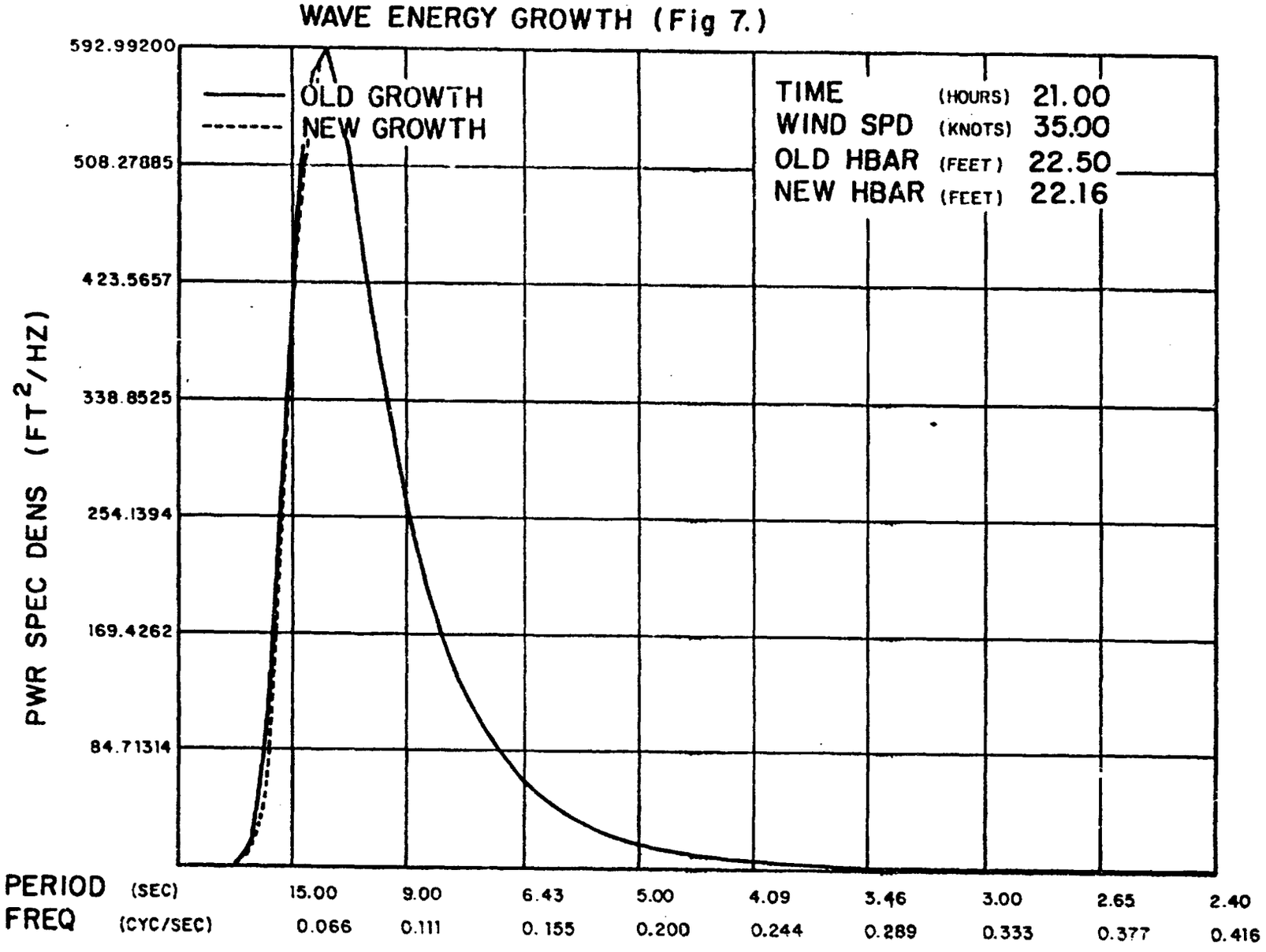
WAVE ENERGY GROWTH (Fig 7.)
592.99200
508.27885
423.5657
338.8525
254.1394
169.4262
84.71314
PWR SPEC DENS (FT²/HZ)
OLD GROWTH
NEW GROWTH
TIME (HOURS) 21.00
WIND SPD (KNOTS) 35.00
OLD HBAR (FEET) 22.50
NEW HBAR (FEET) 22.16
PERIOD (SEC) 15.00 9.00 6.43 5.00 4.09 3.46 3.00 2.65 2.40
FREQ (CYC/SEC) 0.066 0.111 0.155 0.200 0.244 0.289 0.333 0.377 0.416

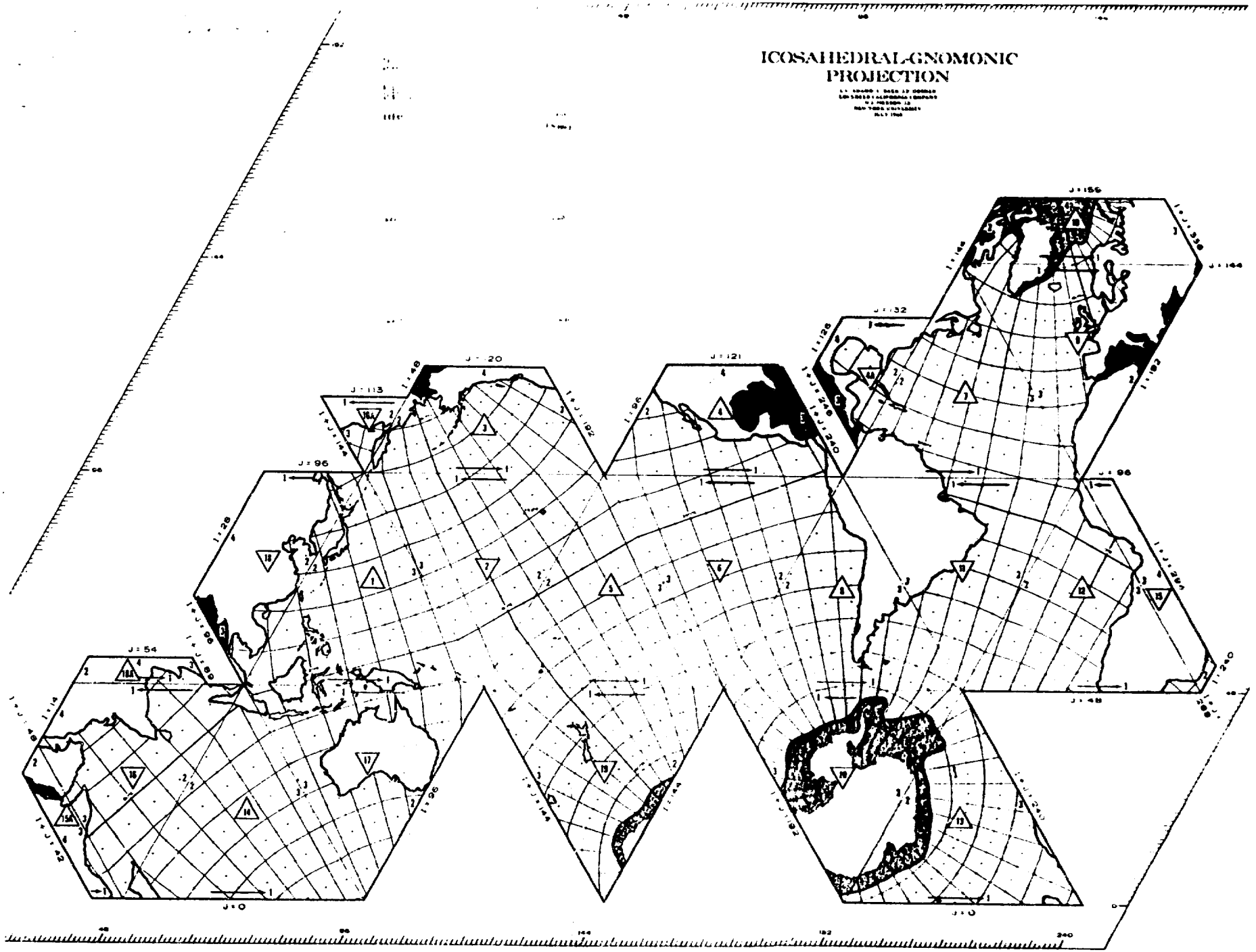

MAP OF THE WORLD OCEAN FOR WAVE STUDIES

FIG 8

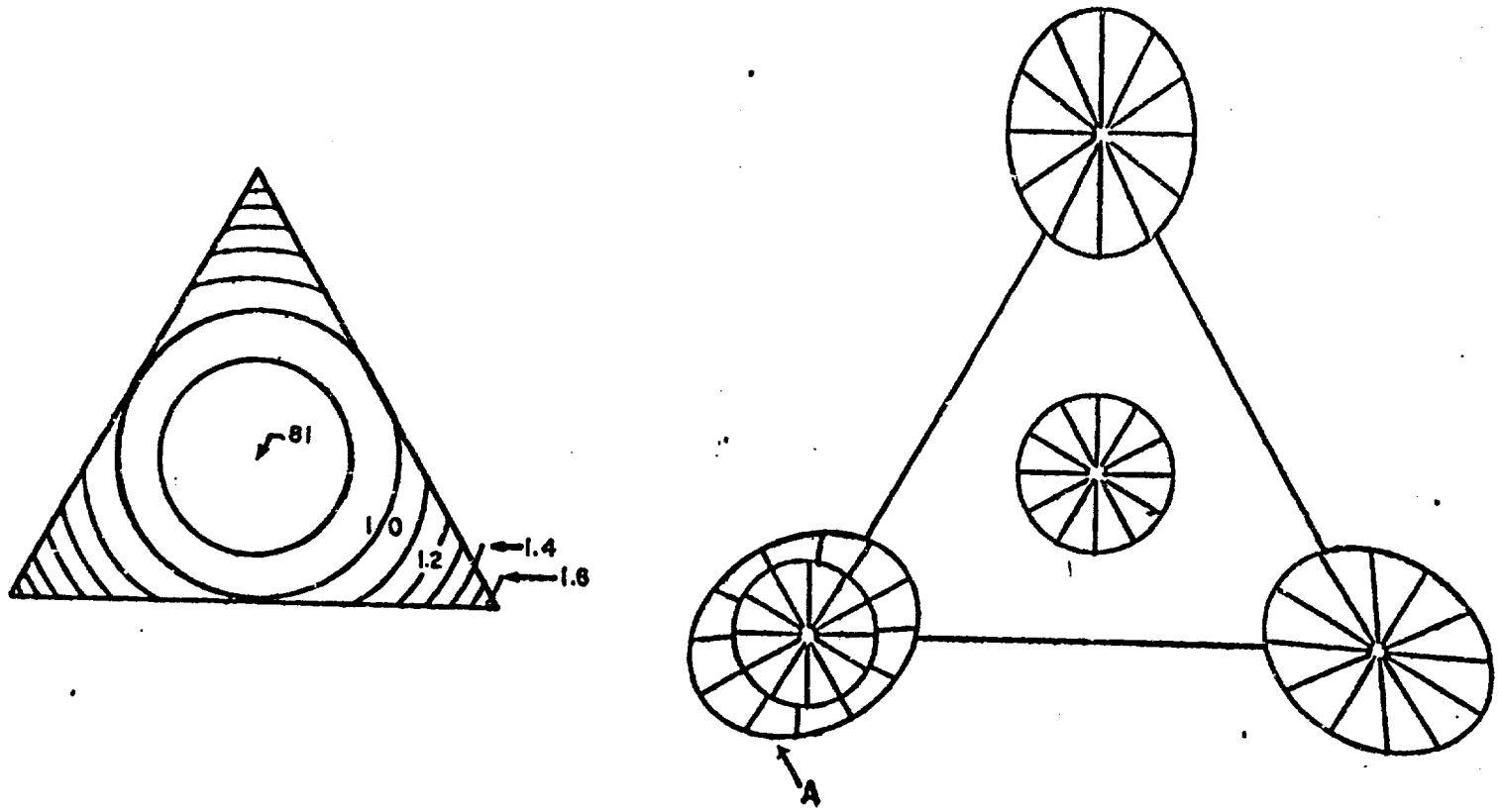

FIG. 9

Figure 9. Distortion of a gnomonic projection on the face of an icosahedron. On the left are shown the contours of areal distortion relative to 1.00 at the midpoint of the sides. On the right are shown distortions of scales and directions at the vertices relative to the tangent point. At "A", a region on the Earth is superposed on the same region in the projection. (Lockheed, 1966)

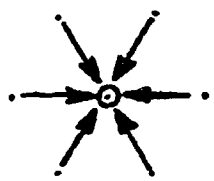

USE DIRECTLY.

PRIMARY

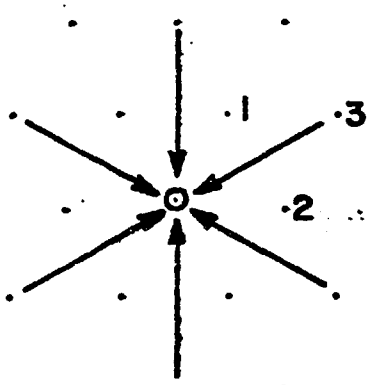

USE LOCATIONS AND 2 ALTERNATELY TO GET EQUIVALENT OF PATH FROM LOCATION 3.

SECONDARY

FIG. 10

Directions to Nearest Neighbors (Lockheed, 1966)

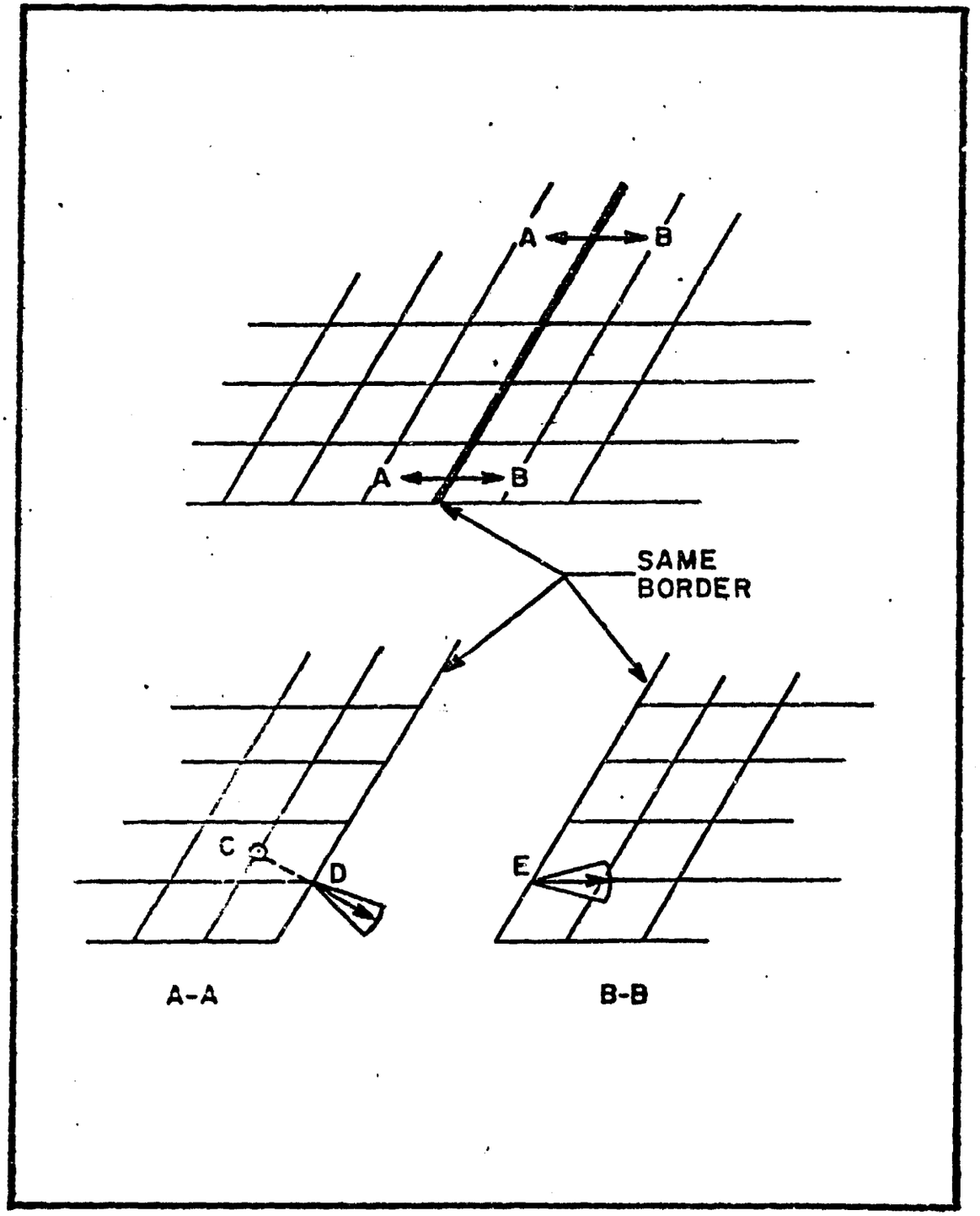

FIG. 11

Bridging Subprojections. The two subprojections are shown separated along their common border. The incoming energy at E in the direction shown is propagation from the interpolated point C and refracted as it crosses the border. D and E represent the same points but have their energy stored in the coordinates of subprojection A-A and B-B respectively. (Lockheed, 1967)

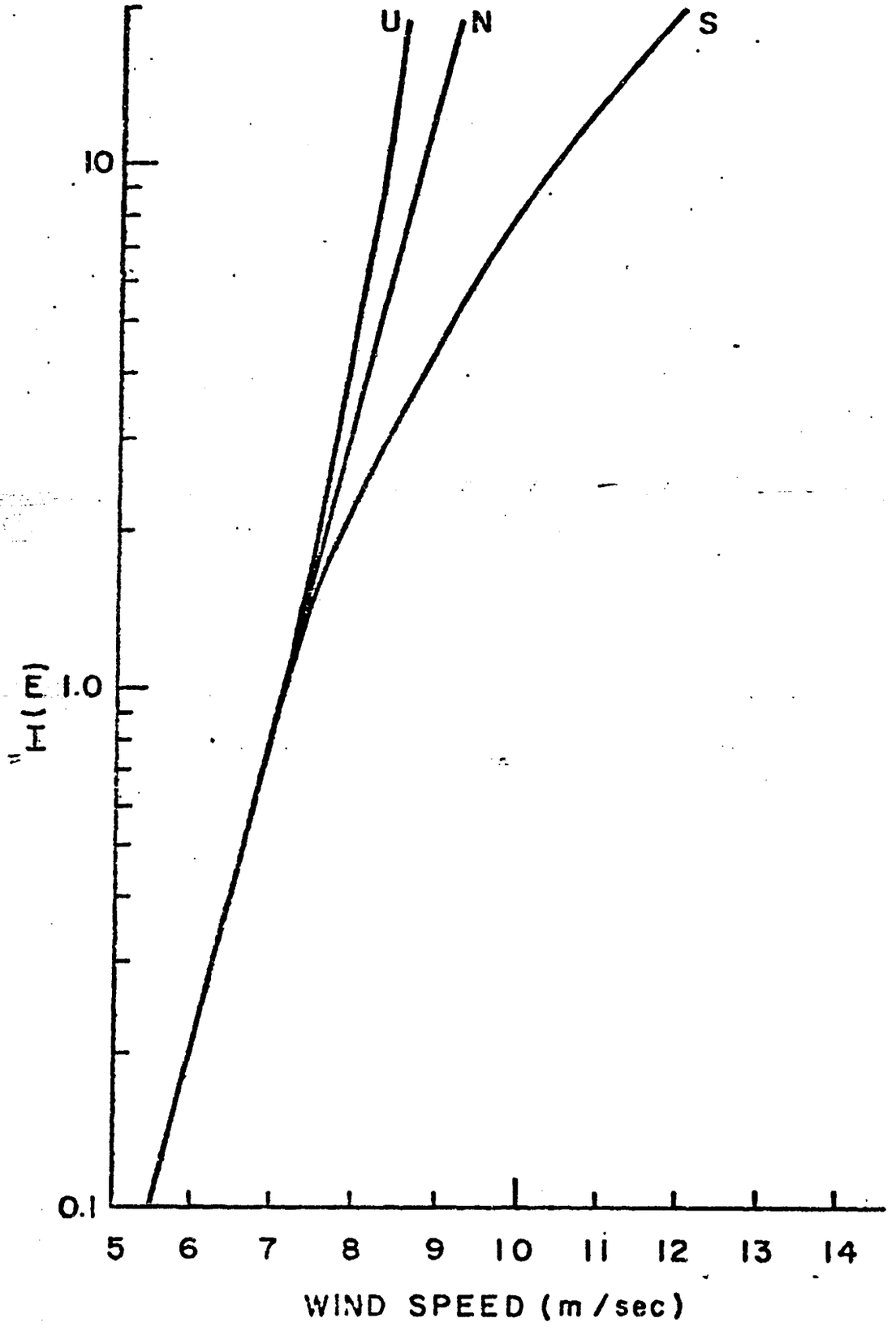

FIG. 12

Theoretical wind profiles in the marine surface boundary layer for a surface stress of 1 dyne/cm^2 and neutral (N), unstable (U), and stable (S) stratification. (Cardone, 1969)

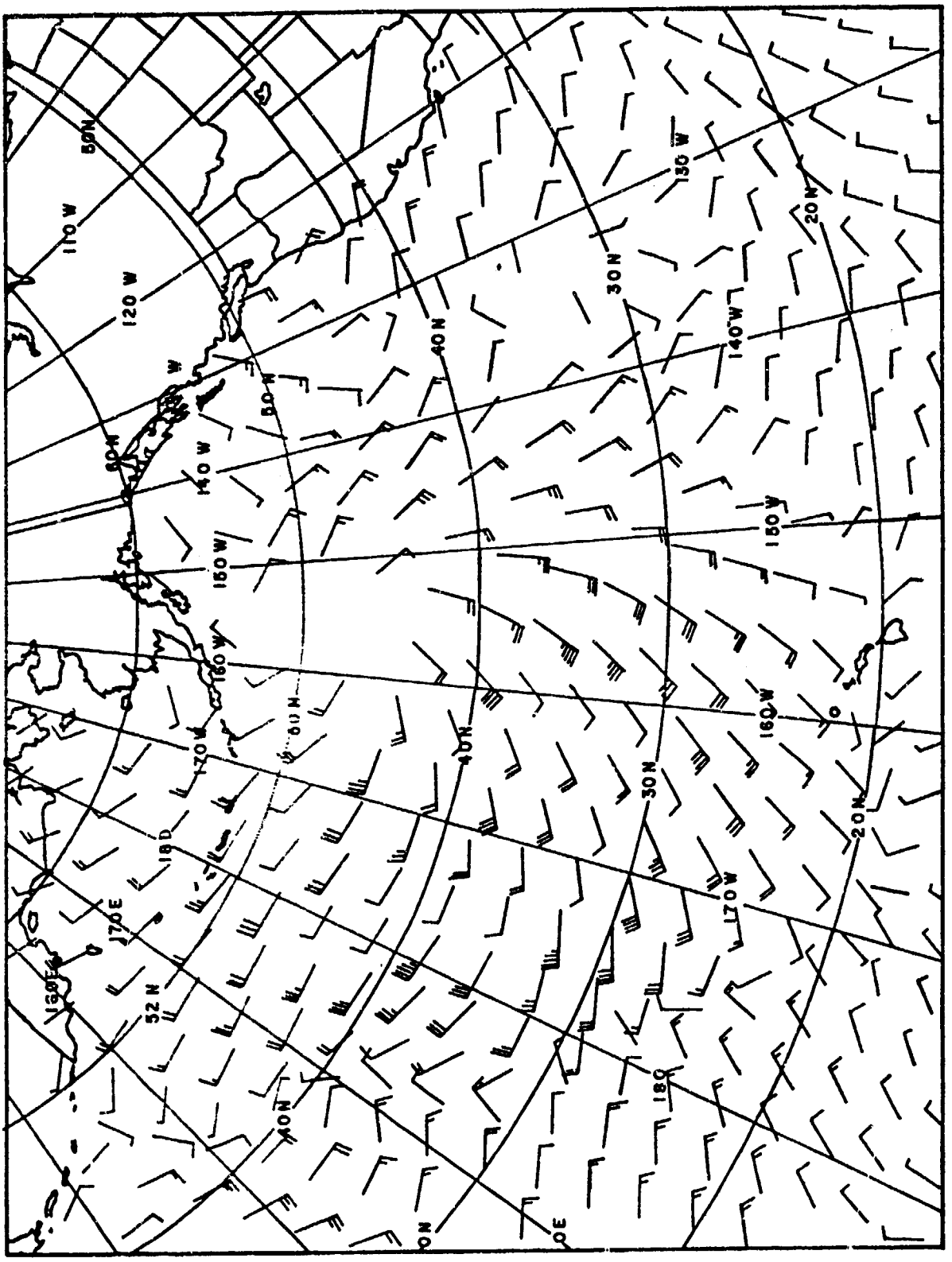

FIG 13
30 NOV 69 18Z WIND FIELD

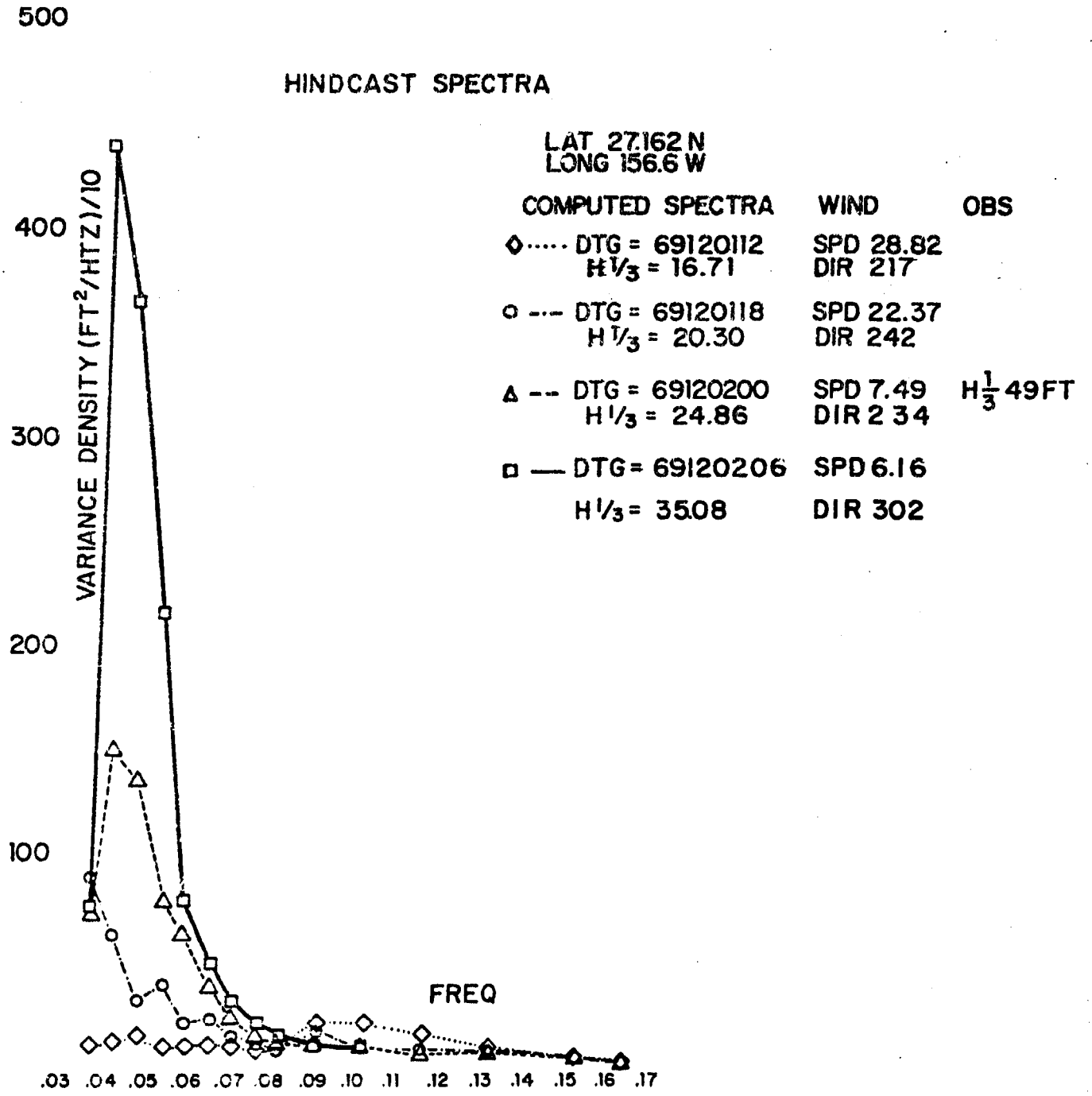
500
HINDCAST SPECTRA
LAT 27.162 N
LONG 156.6 W
COMPUTED SPECTRA
WIND
OBS
◇····· DTG = 69120112
H 1/3 = 16.71
SPD 28.82
DIR 217
o --- DTG = 69120118
H 1/3 = 20.30
SPD 22.37
DIR 242
△ -- DTG = 69120200
H 1/3 = 24.86
SPD 7.49
DIR 234
H 1/3 49FT
□ — DTG = 69120206
H 1/3 = 35.08
SPD 6.16
DIR 302
400
300
200
100
VARIANCE DENSITY (FT²/HTZ)/10
FREQ
.03 .04 .05 .06 .07 .08 .09 .10 .11 .12 .13 .14 .15 .16 .17

FIG. 14

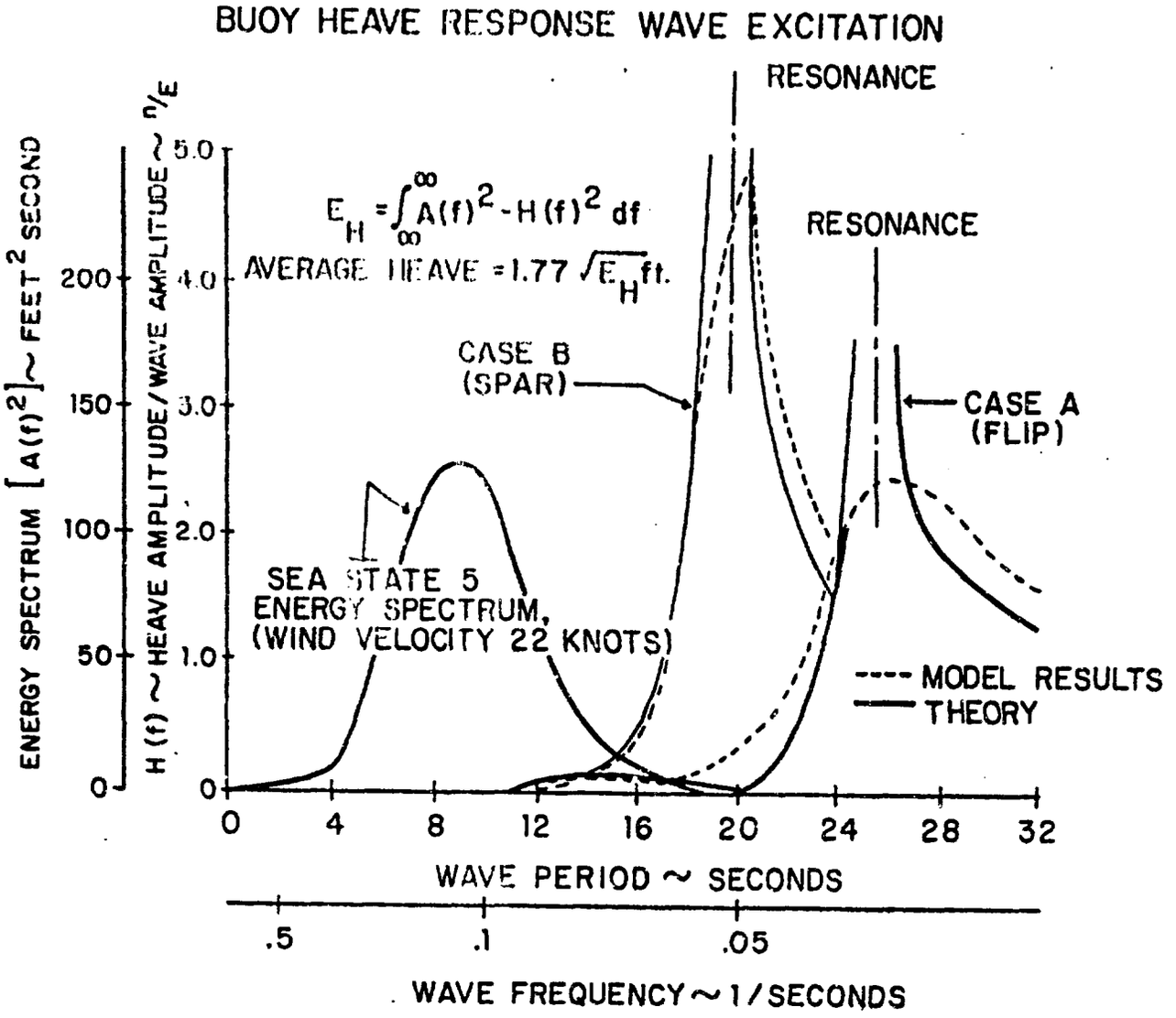

Figure 15

(after KERR, 1964)

DTG= 69120200 TAU= 0

TIME STEP 1 SUBPROJECTION 2 GRID PT 57 LAT 27.162 LONG (EAST) 203.396
WIND SPEED 7.49 WIND DIR 233.6 USTR .26

FREQ / DIR	.164	.153	.133	.117	.103	.092	.083	.076	.072	.067	.061	.056	.050	.044	.039		(MET DIR)
1	0.000	0.000	0.000	0.000	0.000	0.000	0.000	0.000	0.000	0.000	0.000	0.000	0.000	0.000	0.000	.001	126.77
2	0.000	0.000	0.000	0.000	0.000	.001	0.000	0.000	0.000	0.000	0.000	0.000	0.000	0.000	0.000	.001	96.77
3	0.000	0.000	0.000	0.000	0.000	0.000	0.000	0.000	0.000	0.000	0.000	0.000	0.000	0.000	0.000	0.000	66.77
4	0.000	0.000	0.000	0.000	0.001	0.000	0.000	0.000	0.000	0.000	0.000	0.000	0.000	0.000	0.000	0.000	36.77
5	0.000	0.000	0.000	0.000	0.000	0.000	0.000	0.000	0.000	0.000	0.000	0.000	0.000	0.000	0.000	0.000	6.77
6	0.000	0.000	0.000	.007	.005	.039	.032	.058	.026	.200	.196	.519	.997	1.669	.348	4.097	336.77
7	0.000	.011	.033	.097	.233	.659	.585	.765	1.147	1.638	2.846	3.917	6.685	6.845	3.817	29.277	306.77
8	.011	.254	.315	.450	.411	.395	0.000	.004	.193	.306	.535	0.000	0.000	0.000	0.000	2.874	276.77
9	.026	.264	.283	.245	.108	0.000	0.000	0.000	0.000	0.000	0.000	0.000	0.000	0.000	0.000	.929	246.77
10	.028	.293	.364	.417	.102	.030	0.000	0.000	0.000	0.000	0.000	0.000	0.000	0.000	0.000	1.235	216.77
11	.011	.175	0.000	0.000	0.000	0.000	0.000	0.000	0.000	0.000	0.000	0.000	0.000	0.000	0.000	.186	186.77
12	0.000	.007	.015	0.000	0.001	0.000	0.000	0.000	0.000	0.000	0.000	0.000	0.000	0.000	0.000	.022	156.77
	.079	1.035	1.011	1.216	.858	1.123	.617	.828	1.366	2.145	3.577	4.436	7.683	8.514	4.165	38.622	

$\overline{H}$ 1/3=24.8 FT

FIG. 16

SOWM TWO DIMENSIONAL WAVE SPECTRUM
FOR 27.16°N, 156.29°W

DECEMBER 2 1969 00Z

DTG= 69120212 TAU= +6

TIME STEP 1 SUBPROJECTION 2 GRID PT 57 LAT 27.162 LONG (EAST) 203.396
WIND SPEED 6.16 WIND DIR 302.1 USTAR .21

FREQ / DIR	.164	.153	.133	.117	.103	.092	.083	.078	.072	.067	.062	.056	.050	.044	.039		(MET DIR)
1	0.000	0.000	.000	.000	.000	0.000	0.000	0.000	0.000	0.000	0.000	0.000	0.000	0.000	0.000	.000	128.77
2	0.000	0.000	0.000	.000	.000	.000	0.000	.000	0.000	0.000	0.000	0.000	0.000	0.000	0.000	.001	98.77
3	0.000	0.000	0.000	0.000	0.000	0.000	0.000	0.000	0.000	0.000	0.000	0.000	0.000	0.000	0.000	0.000	68.77
4	0.000	0.000	0.000	0.000	0.000	0.000	0.000	0.000	0.000	0.000	0.000	0.000	0.000	0.000	0.000	0.000	38.77
5	.001	0.000	0.000	0.000	0.000	0.000	0.000	0.000	0.000	0.000	0.000	0.000	0.000	0.000	0.000	.001	8.77
6	.005	0.000	.000	.006	.007	.030	.035	.162	.027	.222	.345	0.679	11.605	2.248	1.632	23.051	338.77
7	.010	.005	.022	.086	.579	.852	.767	1.005	1.473	2.178	3.648	5.434	8.732	2.294	2.692	69.702	308.77
8	.008	.261	.326	.488	.403	.467	.022	.011	.267	.351	.448	0.000	0.000	0.000	0.000	3.047	278.77
9	.002	.238	.240	.197	.091	0.000	0.000	0.000	0.000	0.000	0.000	0.000	0.000	0.000	0.000	.759	248.77
10	0.000	.043	.116	.105	0.000	0.000	0.000	0.000	0.000	0.000	0.000	0.000	0.000	0.000	0.000	.264	218.77
11	0.000	0.000	0.000	0.000	0.000	0.000	0.000	0.000	0.000	0.000	0.000	0.000	0.000	0.000	0.000	0.000	188.77
12	0.000	.001	.002	0.000	0.000	0.000	0.000	0.000	0.000	0.000	0.000	0.000	0.000	0.000	0.000	.003	158.77
****	.026	.547	.707	.673	1.080	1.350	.824	1.178	1.767	2.751	4.443	12.103	20.419	4.542	4.324	76.918	

$\bar{H}$ 1/3=35.2 FT

FIGURE 17

SOWM Two Dimensional Wave Spectrum for 27.16°N, 156.20°W
December 2 1969 06Z

DTG = 69120212 TAU = -6

TIME STEP 1 SUBPROJECTION 3 GRID PT 38 LAT 39,380 LONG (EAST) 161,000
WIND SPEED 24,85 WIND DIR 287,7 USTAR 1,00

FREQ	,164	,153	,133	,117	,103	,092	,085	,078	,072	,067	,060	,050	,044	,039		(MET DIR
DIR																
1	,431	,317	,441	,845	1,091	1,780	1,429	2,017	2,820	4,165	6,248	8,617	9,021	6,586	1,059	346,822	307,98
2	,473	,432	,557	,968	1,110	1,903	1,552	2,161	3,039	4,559	6,638	8,528	8,623	6,009	1,382	367,928	277,98
3	,309	,481	,616	1,061	1,210	2,006	1,511	2,018	2,961	4,070	5,448	7,411	3,105	,259	0,000	332,468	247,98
4	,141	,401	,490	,895	1,057	1,813	1,327	1,790	2,394	3,070	4,038	4,595	2,896	0,000	0,000	224,910	217,98
5	,004	,008	,047	,201	,377	,089	,085	,977	1,379	1,636	1,695	1,539	0,000	1,024	0,000	10,561	187,98
6	0,000	,000	,002	,011	,098	,269	,238	,310	,314	,350	,288	,416	,252	0,000	,016	2,565	157,98
7	0,000	0,000	0,000	,001	,016	,056	,031	,034	,038	,037	,036	,032	,002	0,000	0,000	,261	127,98
8	0,000	0,000	0,000	,000	,005	,006	,004	,005	,007	,001	0,000	0,000	0,000	0,000	0,000	,028	97,98
9	0,000	0,000	0,000	,000	,001	,008	,002	,000	0,000	,001	0,000	0,000	0,000	0,000	0,000	,012	67,98
10	0,000	0,000	0,000	0,000	,000	,008	,000	,001	,001	0,000	0,000	0,000	0,000	0,000	0,000	,017	37,98
11	,021	,000	,000	,002	,014	,035	,027	,036	,010	0,000	0,000	0,000	0,000	0,000	0,000	,149	7,98
12	,239	,007	,065	,095	,258	,735	,074	1,033	1,146	,347	1,497	2,085	1,377	,526	,141	10,266	337,98
****	1,610	1,648	2,226	4,081	5,203	9,428	7,487	10,390	14,107	18,436	25,868	33,283	25,277	14,404	2,597	173,997	

H 1/3=52.8 FT

78

FIGURE 18

SOWM Two Dimensional Wave Spectrum for 39.38°N, 161.00°W
December 2 1969 06Z

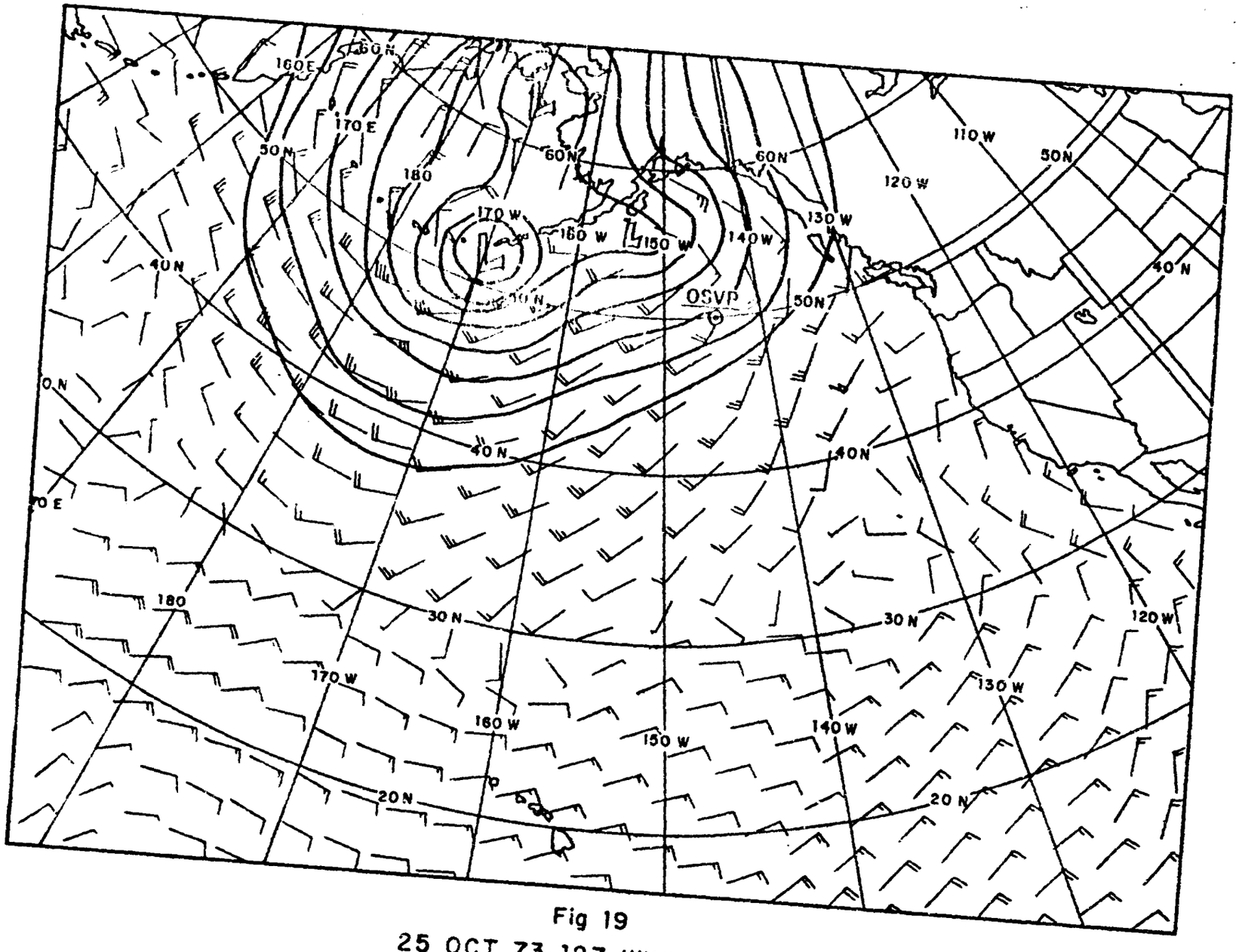

Fig 19

25 OCT 73 12Z WIND FIELD

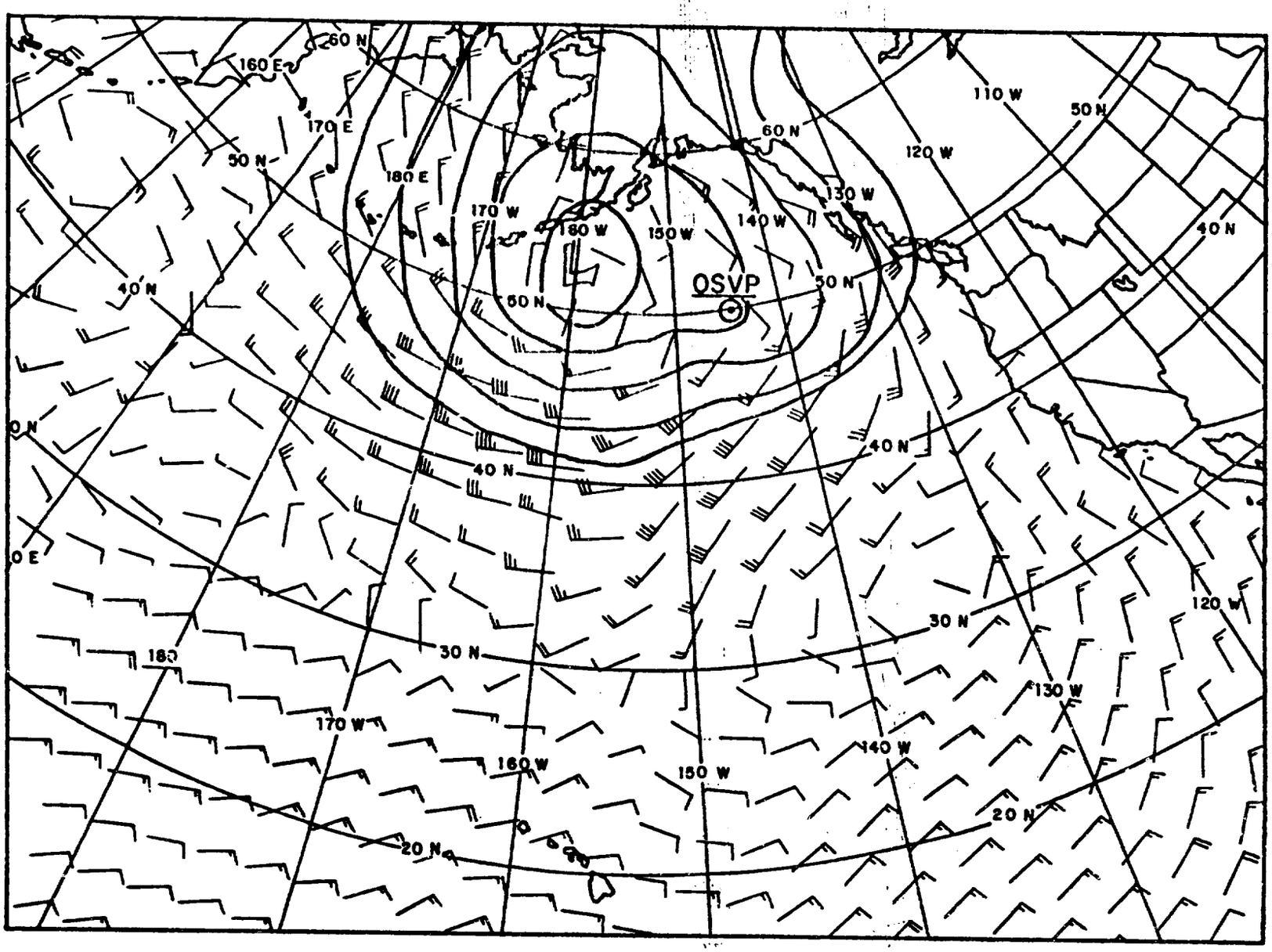

Fig 20

26 OCT 73 12Z WIND FIELD

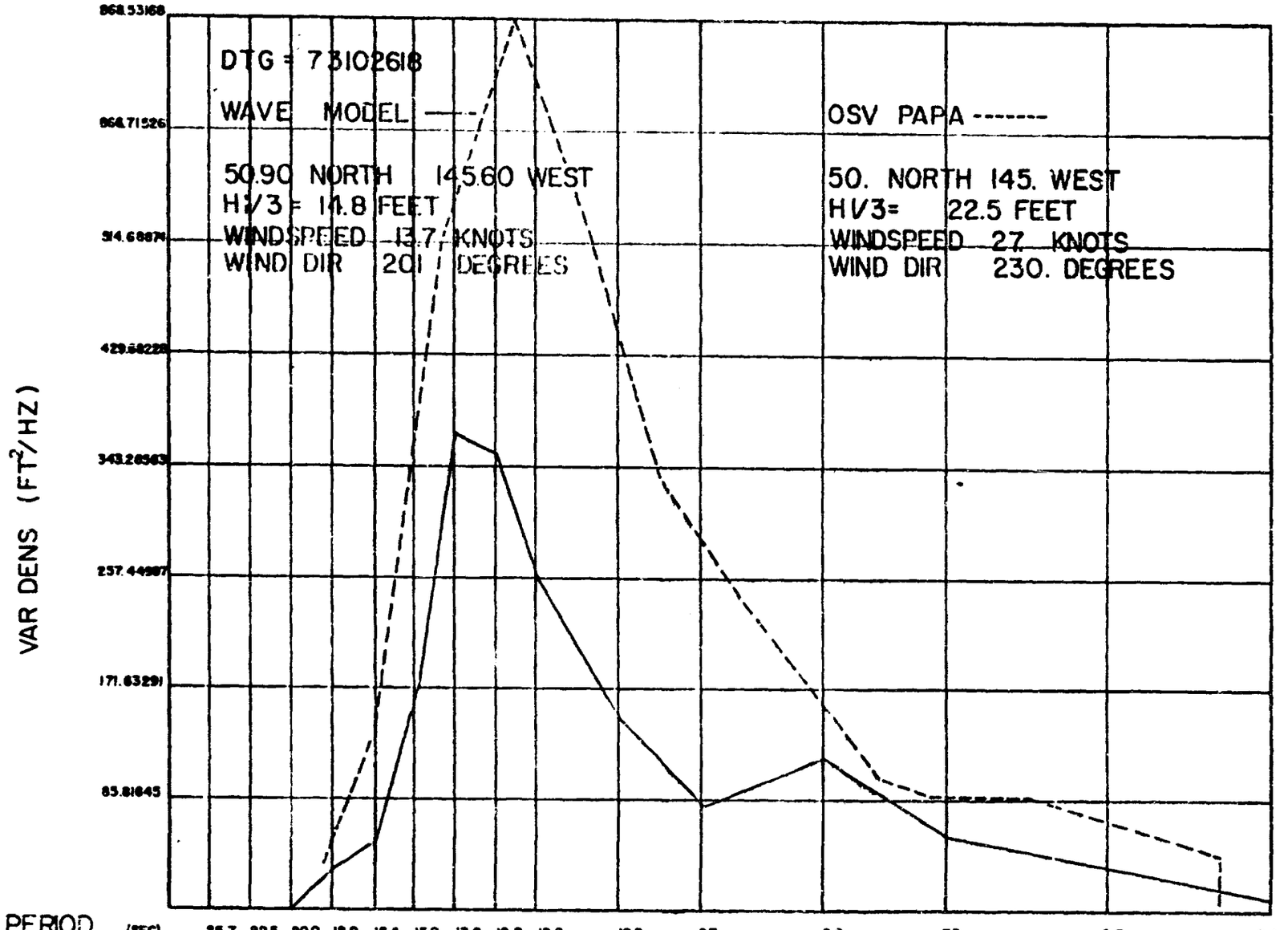
DTG = 73102618
WAVE MODEL ----
50.90 NORTH 145.60 WEST
H1/3 = 14.8 FEET
WINDSPEED 13.7 KNOTS
WIND DIR 201 DEGREES
OSV PAPA -------
50. NORTH 145. WEST
H1/3= 22.5 FEET
WINDSPEED 27. KNOTS
WIND DIR 230. DEGREES
VAR DENS (FT²/HZ)
868.53168
686.71526
514.68874
429.68228
343.26563
257.44987
171.63291
85.81645
PERIOD (SEC) 25.7 22.5 20.0 18.0 16.4 15.0 13.8 12.9 12.0 10.9 9.7 8.6 7.5 8.5 8.1
FREQ (CYC/SEC) 0.039 0.044 0.050 0.056 0.061 0.067 0.072 0.078 0.083 0.092 0.103 0.117 0.133 0.153 0.164

FIG. 21

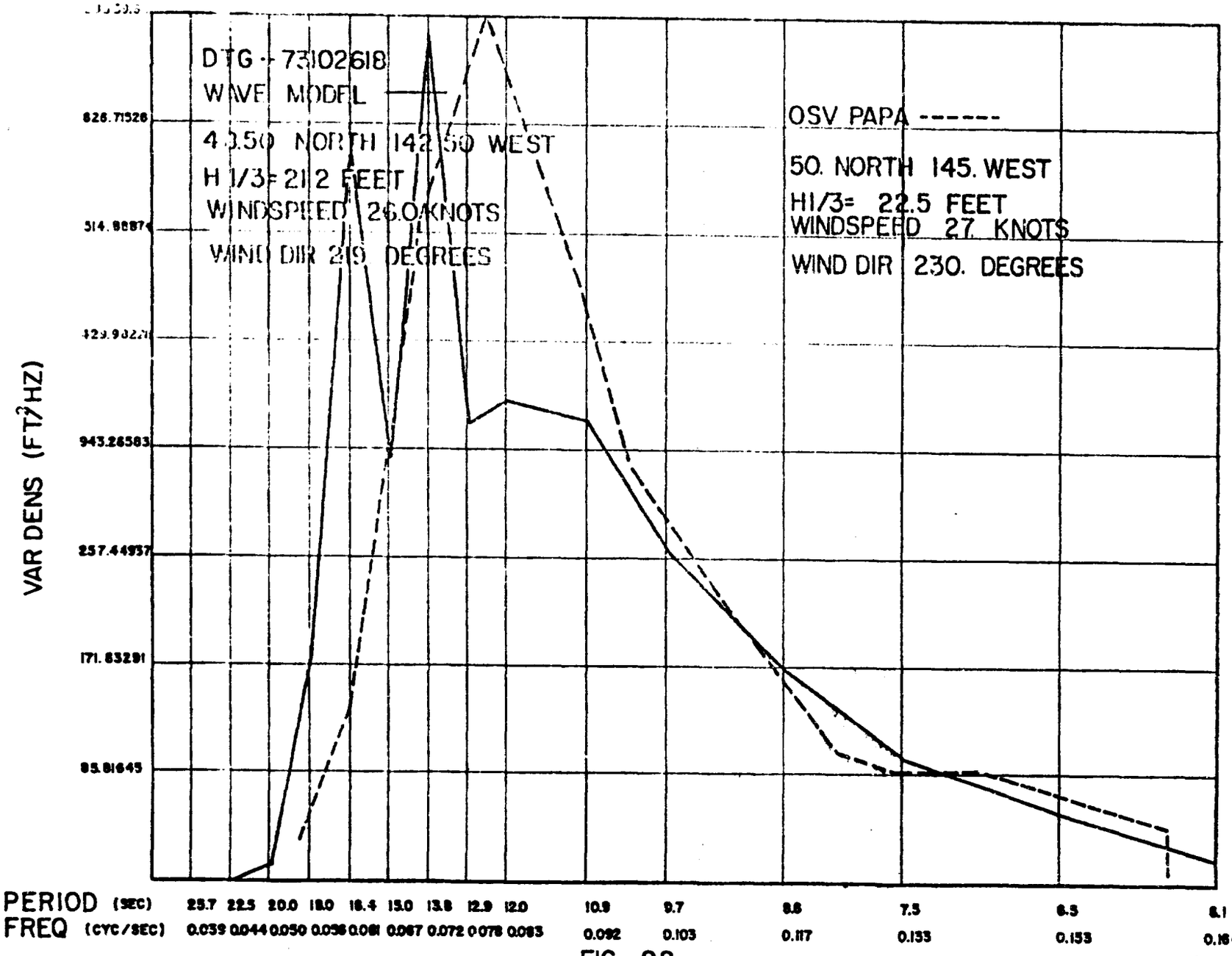
DTG - 73102618
WAVE MODEL
43.50 NORTH 142.50 WEST
H 1/3= 21.2 FEET
WINDSPEED 26.0 KNOTS
WIND DIR 219 DEGREES
OSV PAPA ------
50. NORTH 145. WEST
H1/3= 22.5 FEET
WINDSPEED 27. KNOTS
WIND DIR 230. DEGREES
826.71526
514.98874
429.90274
343.26583
257.44937
171.63291
85.81645
VAR DENS (FT²/HZ)
PERIOD (SEC) 25.7 22.5 20.0 18.0 16.4 15.0 13.8 12.9 12.0 10.9 9.7 8.8 7.5 6.5 6.1
FREQ (CYC/SEC) 0.039 0.044 0.050 0.056 0.061 0.067 0.072 0.078 0.083 0.092 0.103 0.117 0.133 0.153 0.164

FIG. 22

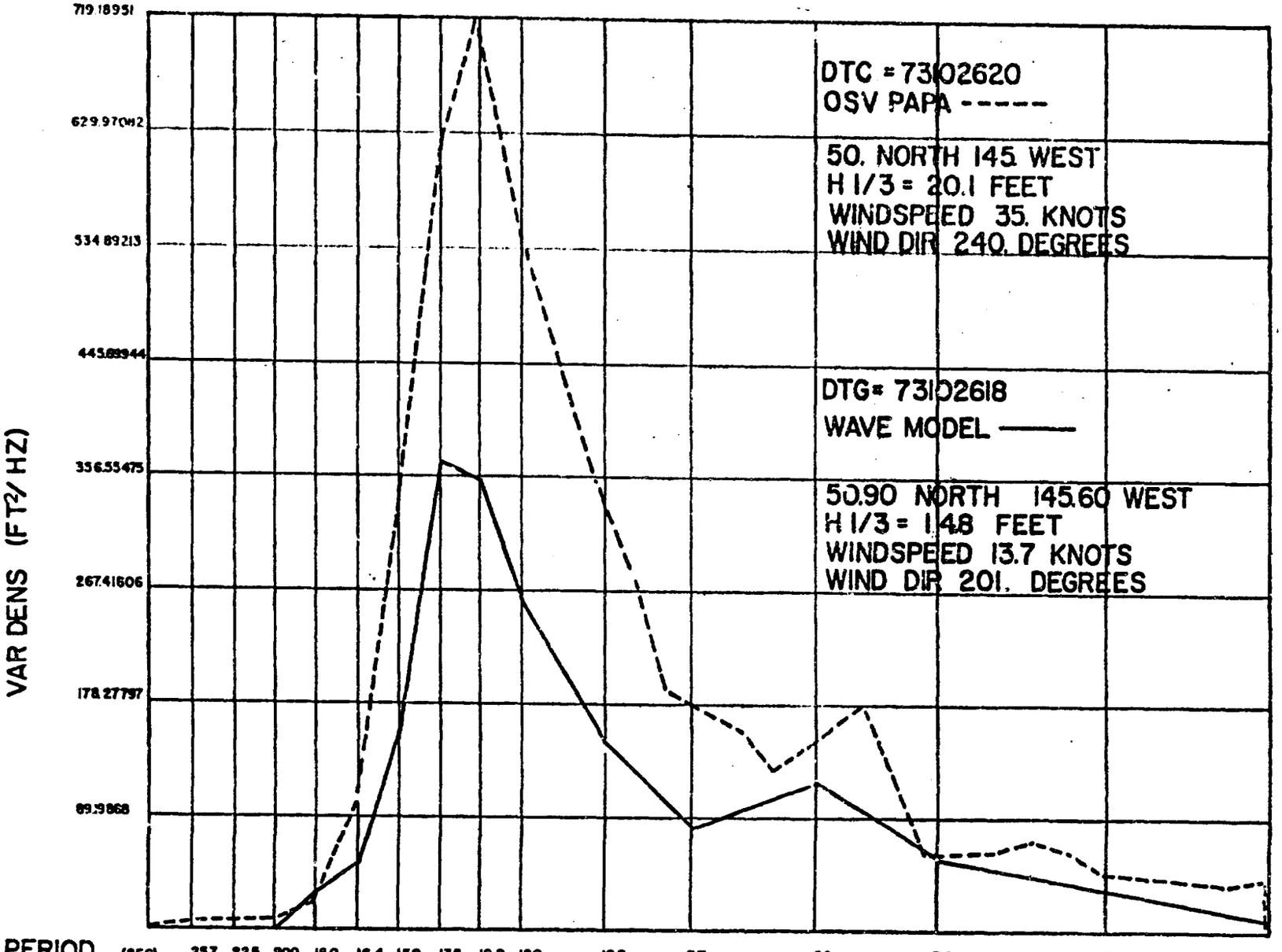
719.18951
629.97042
534.89213
445.68944
356.55475
267.41606
178.27797
89.19868
VAR DENS (FT²/ HZ)
DTC = 73102620
OSV PAPA -----
50. NORTH 145. WEST
H 1/3 = 20.1 FEET
WINDSPEED 35. KNOTS
WIND DIR 240. DEGREES
DTG= 73102618
WAVE MODEL ——
50.90 NORTH 145.60 WEST
H 1/3 = 1.48 FEET
WINDSPEED 13.7 KNOTS
WIND DIR 201. DEGREES
PERIOD (SEC) 25.7 22.5 20.0 18.0 16.4 15.0 13.8 12.9 12.0 10.9 9.7 8.6 7.8 6.5 6.1
FREQ (CYC/SEC) 0.039 0.044 0.050 0.056 0.061 0.067 0.072 0.078 0.083 0.092 0.103 0.117 0.133 0.153 0.164

FIG. 23

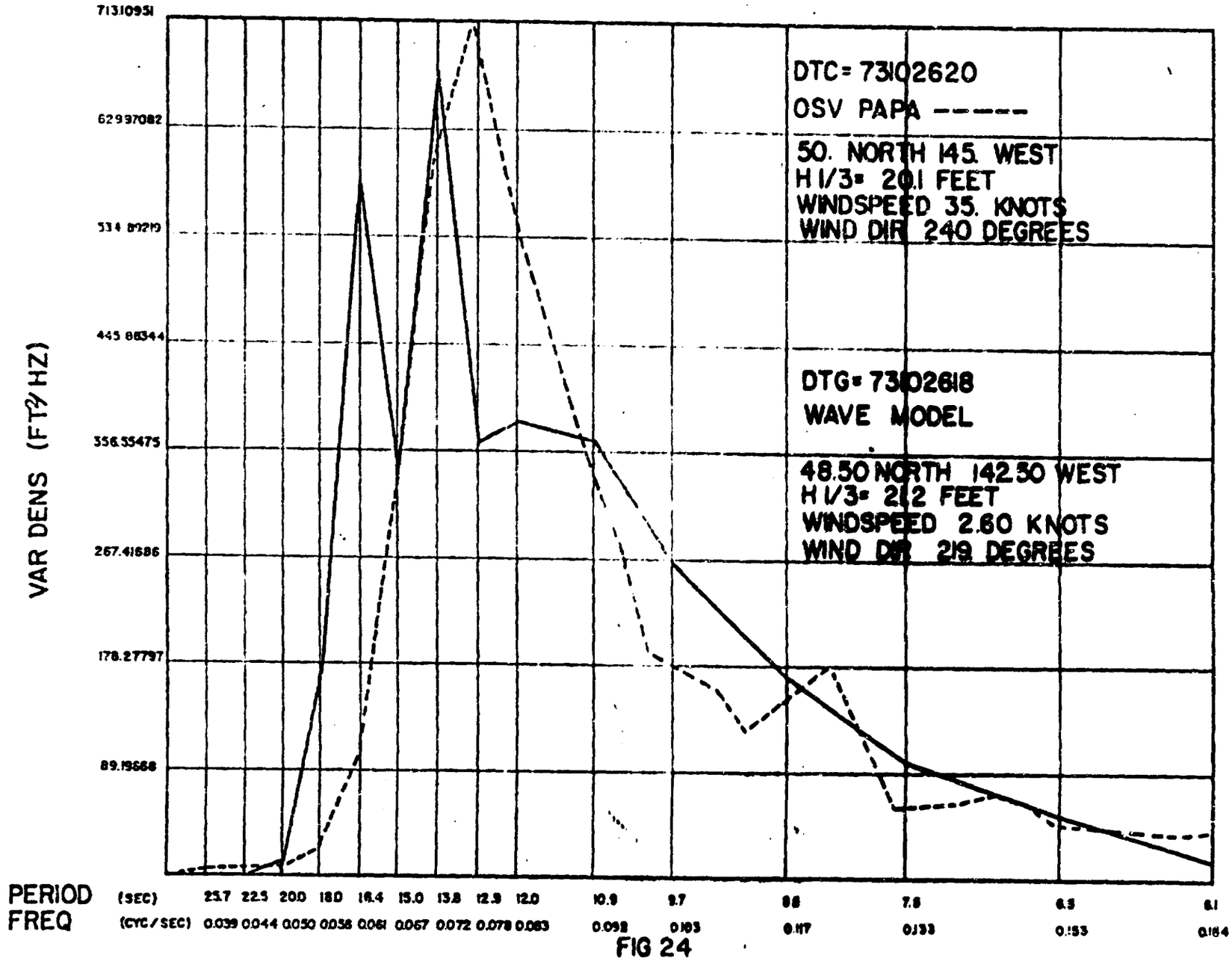
71310951
62937082
534 89219
445 88344
356.55475
267.41686
178.27797
89.19868
VAR DENS (FT²/HZ)
DTC= 73102620
OSV PAPA ------
50. NORTH 145. WEST
H 1/3= 20.1 FEET
WINDSPEED 35. KNOTS
WIND DIR 240 DEGREES
DTG= 73102618
WAVE MODEL
48.50 NORTH 142.50 WEST
H 1/3= 21.2 FEET
WINDSPEED 2.60 KNOTS
WIND DIR 219 DEGREES
PERIOD (SEC) 25.7 22.5 20.0 18.0 16.4 15.0 13.8 12.9 12.0 10.9 9.7 8.8 7.8 6.3 6.1
FREQ (CYC/SEC) 0.039 0.044 0.050 0.056 0.061 0.067 0.072 0.078 0.083 0.092 0.103 0.117 0.133 0.153 0.164

FIG 24

WAVE ENERGY GROWTH (FIG 25)

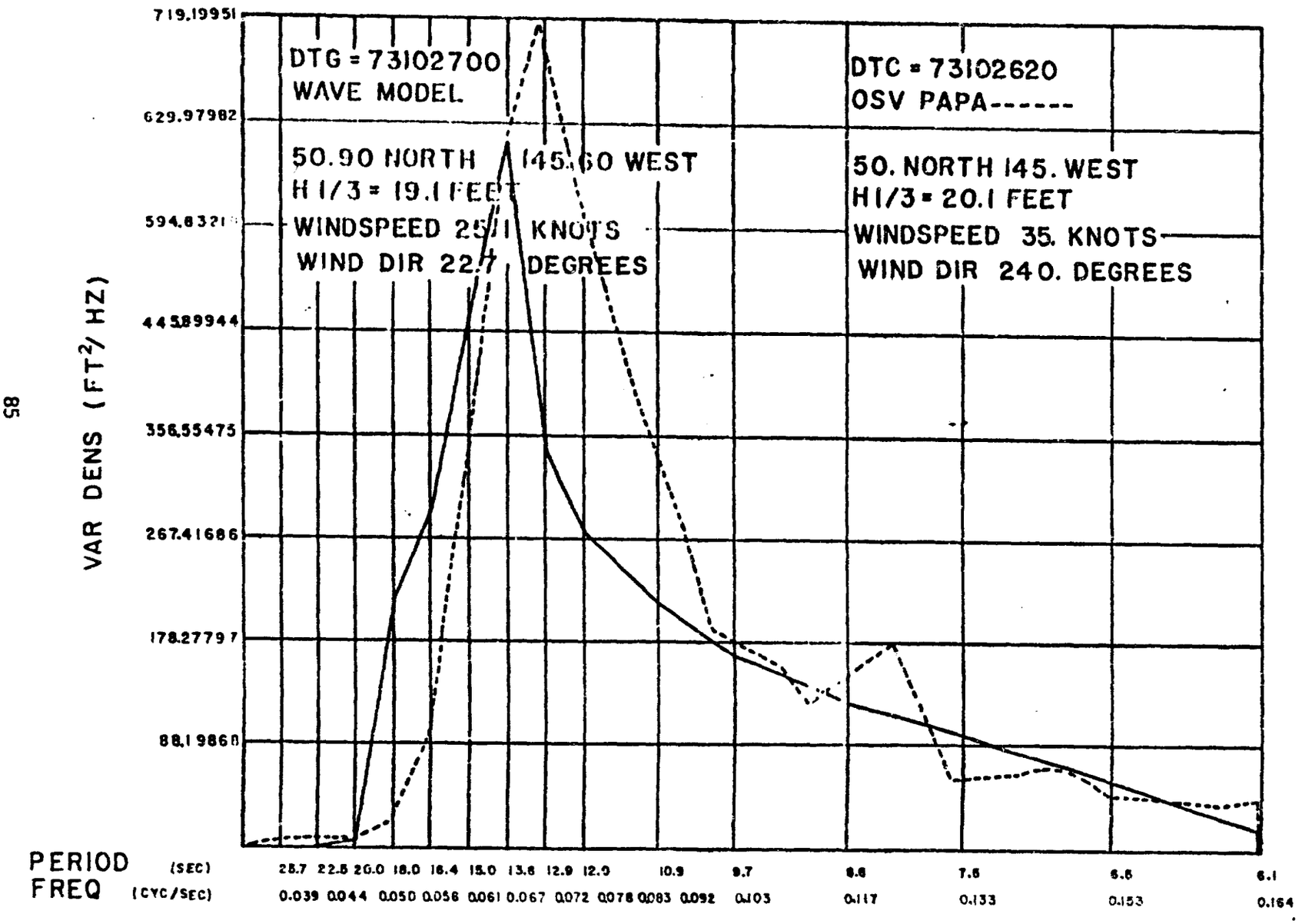

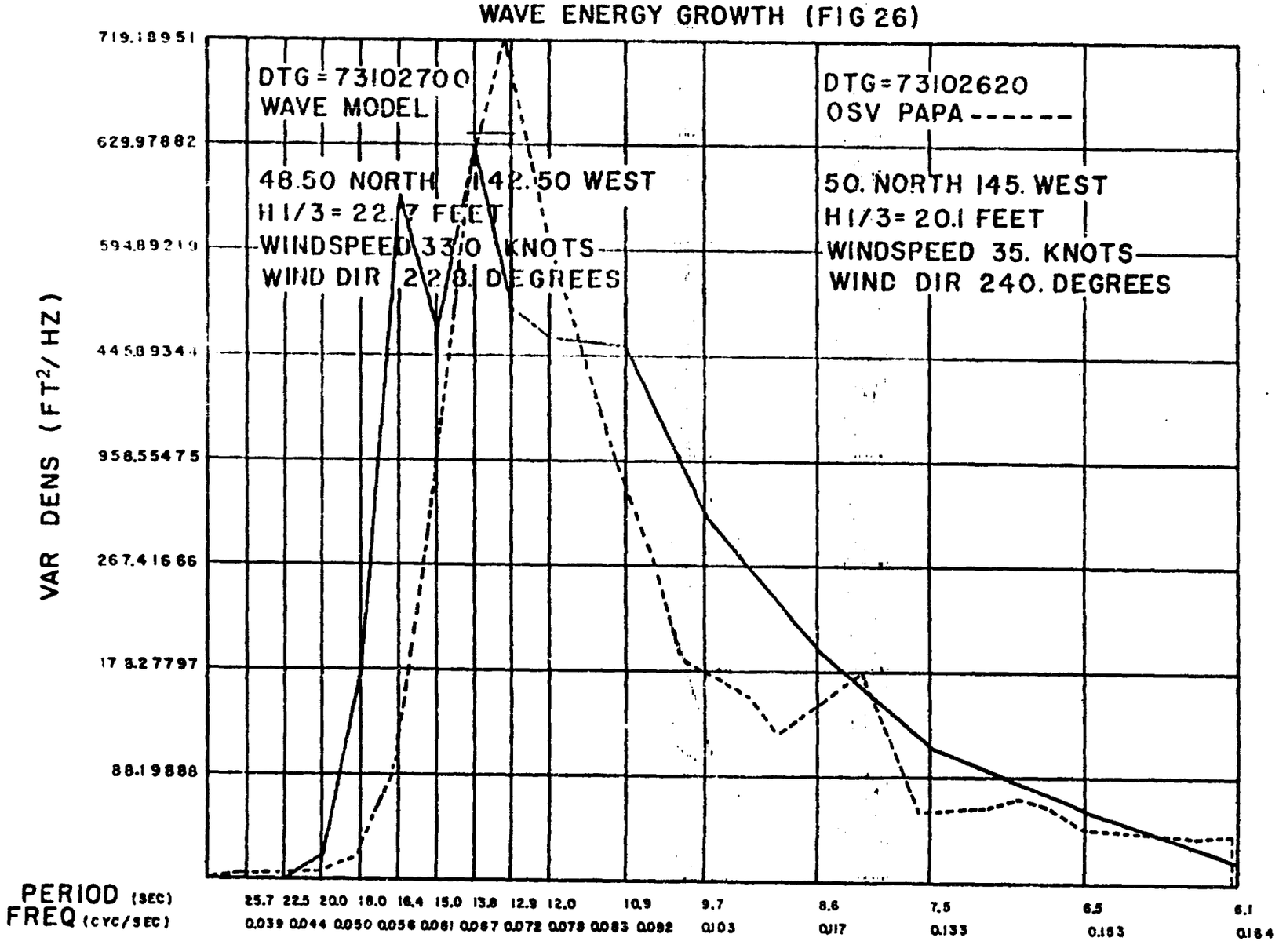
WAVE ENERGY GROWTH (FIG 26)
719.18951
629.97882
594.89219
445.89344
958.55475
267.41666
178.27797
88.19888
VAR DENS (FT²/HZ)
DTG=73102700
WAVE MODEL
48.50 NORTH 142.50 WEST
HI/3= 22.7 FEET
WINDSPEED 33.0 KNOTS
WIND DIR 228. DEGREES
DTG=73102620
OSV PAPA------
50. NORTH 145. WEST
HI/3= 20.1 FEET
WINDSPEED 35. KNOTS
WIND DIR 240. DEGREES
PERIOD (SEC)
FREQ (CYC/SEC)
25.7 22.5 20.0 18.0 16.4 15.0 13.8 12.9 12.0 10.9 9.7 8.6 7.5 6.5 6.1
0.039 0.044 0.050 0.056 0.061 0.067 0.072 0.078 0.083 0.092 0.103 0.117 0.133 0.153 0.164

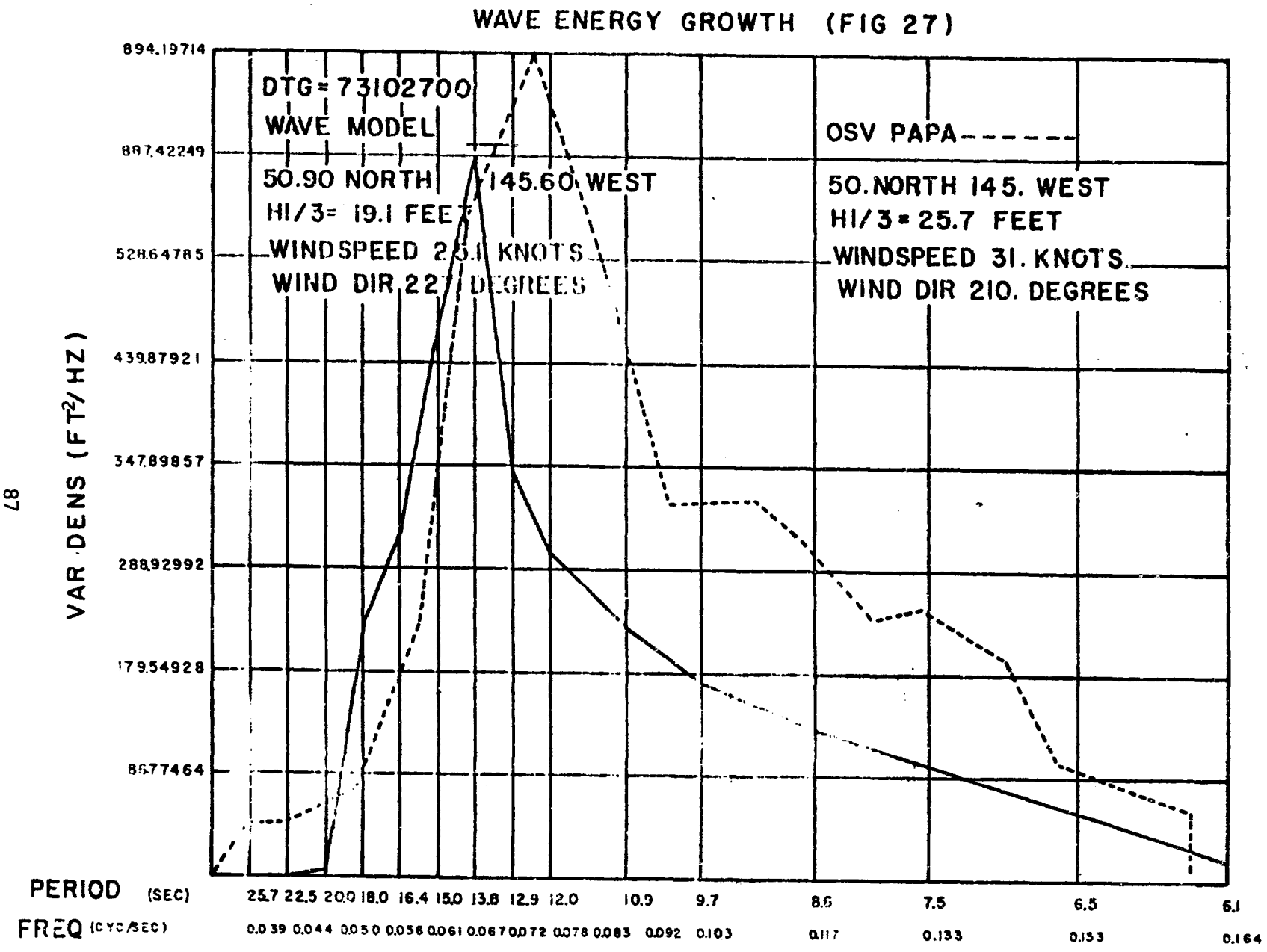
WAVE ENERGY GROWTH (FIG 27)
894.19714
887.42249
528.64785
439.87921
347.89857
288.92992
179.54928
86.77464
VAR DENS (FT²/HZ)
DTG=73102700
WAVE MODEL
50.90 NORTH 145.60 WEST
HI/3= 19.1 FEET
WINDSPEED 25.1 KNOTS
WIND DIR 227 DEGREES
OSV PAPA------
50. NORTH 145. WEST
HI/3 = 25.7 FEET
WINDSPEED 31. KNOTS
WIND DIR 210. DEGREES
PERIOD (SEC) 25.7 22.5 20.0 18.0 16.4 15.0 13.8 12.9 12.0 10.9 9.7 8.6 7.5 6.5 6.1
FREQ (CYC/SEC) 0.039 0.044 0.050 0.056 0.061 0.067 0.072 0.078 0.083 0.092 0.103 0.117 0.133 0.153 0.164

WAVE ENERGY GROWTH (FIG 28)

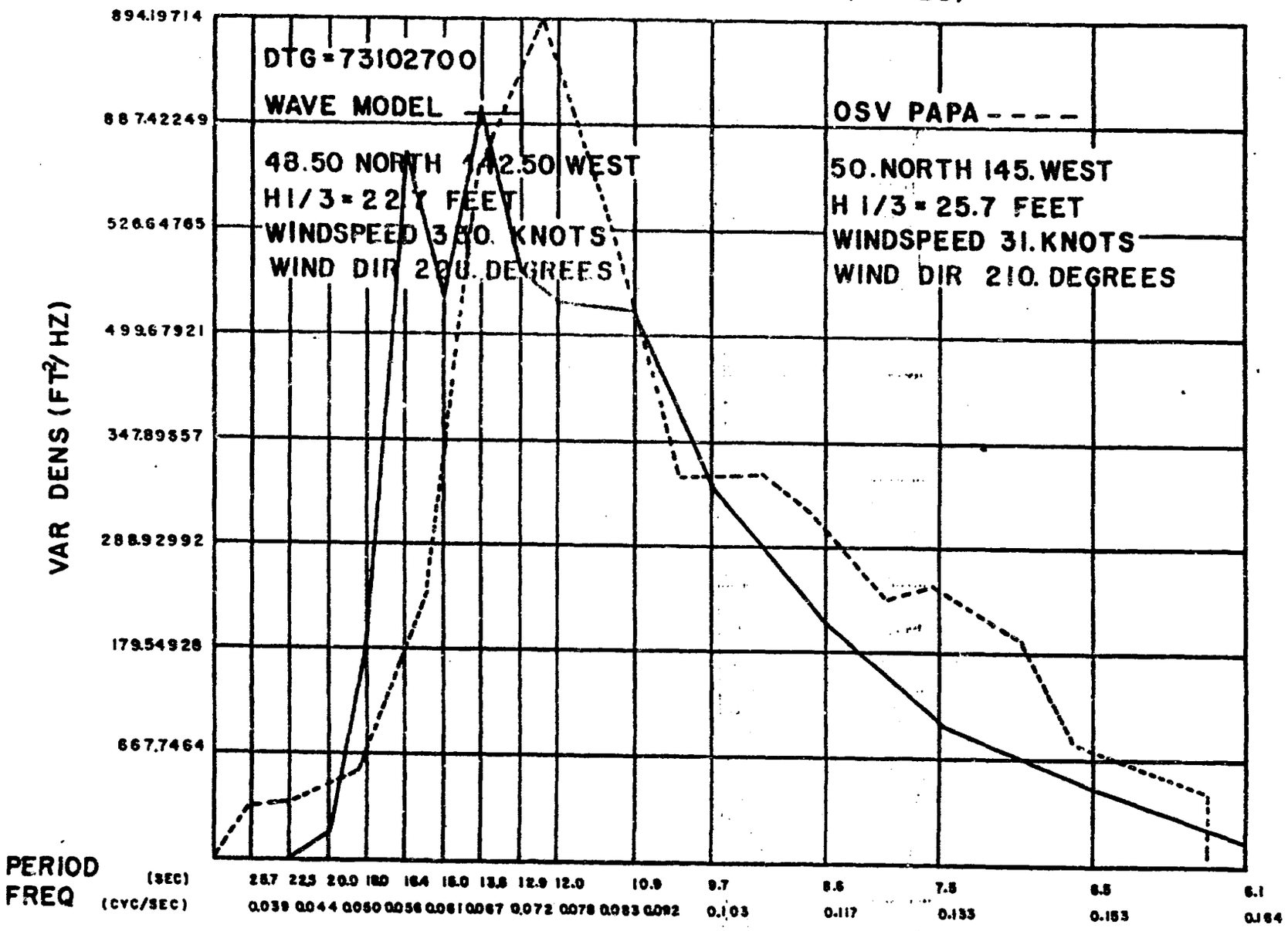

DTG= 731027/ TAU= -6

TIME STEP 1 SUBPROJECTION 3 GRID PT 154 LAT 50.887 LONG (EAST) 214.354
WIND SPEED 13.74 WIND DIR 201.0 USTAR .49

FREQ / DIR.	.164	.153	.133	.117	.103	.092	.083	.076	.072	.067	.061	.056	.050	.044	.039		(MET DI
1	0.000	0.000	0.000	0.000	0.000	0.000	0.000	0.000	0.000	0.000	0.000	0.000	0.000	0.000	0.000	0.000	319.52
2	0.000	0.000	0.000	.016	.014	0.000	.001	0.000	.106	0.000	0.000	0.000	0.000	0.000	0.000	.131	289.52
3	.060	.002	.025	.103	.375	.793	.655	1.046	1.391	.760	.250	.023	.002	0.000	0.000	5.540	259.52
4	.224	.032	.133	.479	.044	.537	.203	.255	.101	.060	0.000	.021	0.000	0.000	0.000	2.099	229.52
5	.332	.297	.432	.656	.269	.244	.553	.615	.130	.043	.034	.125	.005	.000	0.000	3.704	199.52
6	.212	.236	.294	.444	.037	.017	.016	.046	.006	.001	.000	.005	.001	0.000	0.000	1.692	169.52
7	.048	.140	.051	.176	.136	.013	.005	0.000	0.000	0.000	0.000	0.000	0.000	0.000	0.000	.600	139.52
8	0.000	0.000	.005	.009	.013	.017	.000	.001	.003	0.000	0.000	0.000	0.000	0.000	0.000	.047	109.52
9	0.000	0.000	0.000	.000	.001	0.000	0.000	0.000	0.000	0.000	0.000	0.000	0.000	0.000	0.000	.001	79.52
10	0.000	0.000	0.000	0.000	.000	.010	0.000	0.000	0.000	0.000	0.000	0.000	0.000	0.000	0.000	.010	49.52
11	0.000	0.000	0.000	0.000	0.000	0.000	0.000	0.000	0.000	0.000	0.000	0.000	0.000	0.000	0.000	0.000	19.52
12	0.000	0.000	0.000	0.000	0.000	0.000	0.000	0.000	0.000	0.000	0.000	0.000	0.000	0.000	0.000	0.000	349.52
****	.681	.707	.947	1.930	.867	2.626	1.434	1.961	2.837	.994	.282	.174	.007	.000	0.000	13.785	

$\overline{H}$ 1/3=14.8 FT

TIME STEP 1 SUBPROJECTION 3 GRID PT 155 LAT 48.474 LONG (EAST) 217.473
WIND SPEED 26.03 WIND DIR 219.3 USTAR 1.05

FREQ / DIP	.164	.153	.133	.117	.103	.092	.083	.076	.072	.067	.061	.056	.050	.044	.039		(MET DI
1	.032	0.000	0.000	0.000	0.000	0.000	0.000	0.000	0.000	0.000	0.000	0.000	0.000	0.000	0.000	.002	321.81
2	.143	.002	.013	.014	.067	.060	.064	.013	.317	0.000	.032	0.000	0.000	0.000	0.000	.734	291.81
3	.237	.297	.331	.650	.664	1.099	.803	.951	1.052	.521	0.000	.003	.000	0.000	0.000	6.729	261.81
4	.451	.361	.429	.766	.772	1.034	.350	.377	.278	.266	1.936	.139	.058	.001	0.000	7.938	231.81
5	.441	.311	.441	.775	.517	1.184	.613	.399	1.589	1.061	1.253	.023	.015	.001	0.000	8.918	201.81
6	.263	.229	.291	.460	.453	.593	.275	.281	.483	.023	.053	.024	.001	0.000	0.000	3.432	171.81
7	.126	.044	.061	.123	.101	.062	.007	.004	.002	0.000	.002	0.000	0.000	0.000	0.000	.433	141.81
8	0.000	0.000	.003	.002	.006	.029	.001	0.000	0.000	0.000	.001	0.000	0.000	0.000	0.000	.042	111.81
9	0.000	0.000	0.000	0.000	.000	.017	.001	0.000	0.000	0.000	0.000	0.000	0.000	0.000	0.000	.017	81.81
10	0.000	0.000	0.000	0.000	0.000	0.000	0.000	.000	0.000	0.000	0.000	0.000	0.000	0.000	0.000	.000	51.81
11	0.000	0.000	0.000	0.000	0.000	0.000	0.000	0.000	0.000	0.000	0.000	0.000	0.000	0.000	0.000	0.000	21.81
12	0.000	0.000	0.000	0.000	0.000	0.000	0.000	0.000	0.000	0.000	0.000	0.000	0.000	0.000	0.000	0.000	351.81
****	1.033	1.194	1.616	2.769	2.920	4.067	2.118	2.025	3.721	1.867	3.247	.989	.074	.002	0.000	28.246	

$\overline{H}$ 1/3=21.3 FT

FIG. 29
SOWM Two Dimensional Wave Spectra
For 50°.89N, 145°.25W and 48°.47N, 142°.53W
October 26 1973 18Z

TIME STEP 1 SUBPROJECTION 3 GRID PT 164 LAT 50.887 LONG (EAST) 214.354
WIND SPEED 25.11 WIND DIR 227.3 USTAR 1.02

FREQ / DIR	.164	.153	.133	.117	.103	.092	.083	.078	.072	.067	.061	.056	.050	.044	.039		(MET DIR
1	.011	.006	.003	0.000	0.000	0.000	0.000	0.000	0.000	0.000	0.000	0.000	0.000	0.000	0.000	.027	319.52
2	.179	.107	.053	.015	.061	0.000	.002	0.000	.003	0.000	0.000	0.000	0.000	0.000	0.000	.557	289.52
3	.365	.249	.322	.190	.478	.915	.705	.962	1.203	.634	.239	.019	.002	0.000	0.000	6.384	259.52
4	.483	.327	.415	.655	.585	.523	.179	.168	.145	.089	.002	.048	.002	0.000	0.000	3.653	229.52
5	.385	.296	.435	.676	.454	.857	.611	.732	1.607	1.489	1.154	1.107	.018	.000	0.000	3.791	199.52
6	.195	.224	.283	.444	.127	.019	.013	.029	.328	.376	.211	.010	.007	.000	0.000	2.276	169.52
7	.014	.041	.043	.093	.092	.020	.006	.003	.002	0.000	.002	0.000	0.000	0.000	0.000	.321	139.52
8	0.000	0.000	.001	.001	.006	0.000	.000	.001	.007	.013	.006	0.000	0.000	0.000	0.000	.038	109.52
9	0.000	0.000	0.000	0.000	.001	0.000	0.000	0.000	.002	0.000	0.000	0.000	0.000	0.000	0.000	.003	79.52
10	0.000	0.000	0.000	0.000	.000	.006	0.000	0.000	0.000	0.000	0.000	0.000	0.000	0.000	0.000	.006	49.52
11	0.000	0.000	0.000	0.000	0.000	0.000	0.000	0.000	0.000	0.000	0.000	0.000	0.000	0.000	0.000	0.000	19.52
12	0.000	0.000	0.000	0.000	0.000	0.000	0.000	0.000	0.000	0.000	0.000	0.000	0.000	0.000	0.000	0.000	349.52
****	1.632	1.258	1.605	2.078	1.827	2.339	1.517	1.915	3.370	2.082	1.614	1.184	.029	.001	0.000	22.975	

$\bar{H}$ 1/3=19.2 FT

06

TIME STEP 1 SUBPROJECTION 3 GRID PT 155 LAT 48.474 LONG (EAST) 217.473
WIND SPEED 32.99 WIND DIR 228.5 USTAR 1.40

FREQ / DIR	.164	.153	.133	.117	.103	.092	.083	.078	.072	.067	.061	.056	.050	.044	.039		(MET DIR)
1	.013	.012	.022	.032	.024	.027	.000	0.000	0.000	0.000	0.000	0.000	0.000	0.000	0.000	.131	321.81
2	.218	.153	.191	.282	.232	.245	.091	0.000	.332	0.000	.038	0.000	0.000	0.000	0.000	1.692	291.81
3	.373	.330	.393	.602	.718	1.166	.825	.946	.824	.371	.014	.004	.000	.000		6.627	261.81
4	.463	.332	.491	.922	1.033	1.550	.638	.143	.310	.917	1.074	.089	.061	.001	0.000	8.619	231.81
5	.401	.310	.442	.794	.674	1.313	.788	1.366	1.505	1.212	1.237	.907	.042	.001	.000	11.191	201.81
6	.245	.222	.233	.464	.463	.601	.295	.234	.492	.079	.073	0.000	.005	0.000	0.000	3.464	171.81
7	.122	.023	.045	.079	.083	.089	.047	.039	.005	0.000	.004	0.000	0.000	0.000	0.000	.366	141.81
8	0.000	0.000	0.000	.001	.007	.034	.001	0.000	.003	0.000	.002	0.000	0.000	0.000	0.000	.048	111.81
9	0.000	0.000	0.000	.001	.009	.016	.003	.004	0.000	.001	0.000	0.000	0.000	0.000	0.000	.041	81.81
10	0.000	0.000	0.000	0.000	0.000	0.000	0.000	0.000	0.000	0.000	0.000	0.000	0.000	0.000	0.000	0.000	51.81
11	0.000	0.000	0.000	0.000	0.000	0.000	0.000	0.000	0.000	0.000	0.000	0.000	0.000	0.000	0.000	0.000	21.81
12	0.000	0.000	0.000	0.000	0.000	0.000	0.000	0.000	0.000	0.000	0.000	0.000	0.000	0.000	0.000	0.000	351.81
****	1.735	1.383	1.877	3.257	3.435	5.044	2.564	2.696	3.470	2.579	3.239	1.010	.112	.003	.000	32.378	

$\bar{H}$ 1/3=22.8 FT

FIG. 30
SOWM Two Dimensional Wave Spectra
For 50°.89N, 145°.25W and 48°.47N, 142°.53W
October 27 1973 00Z

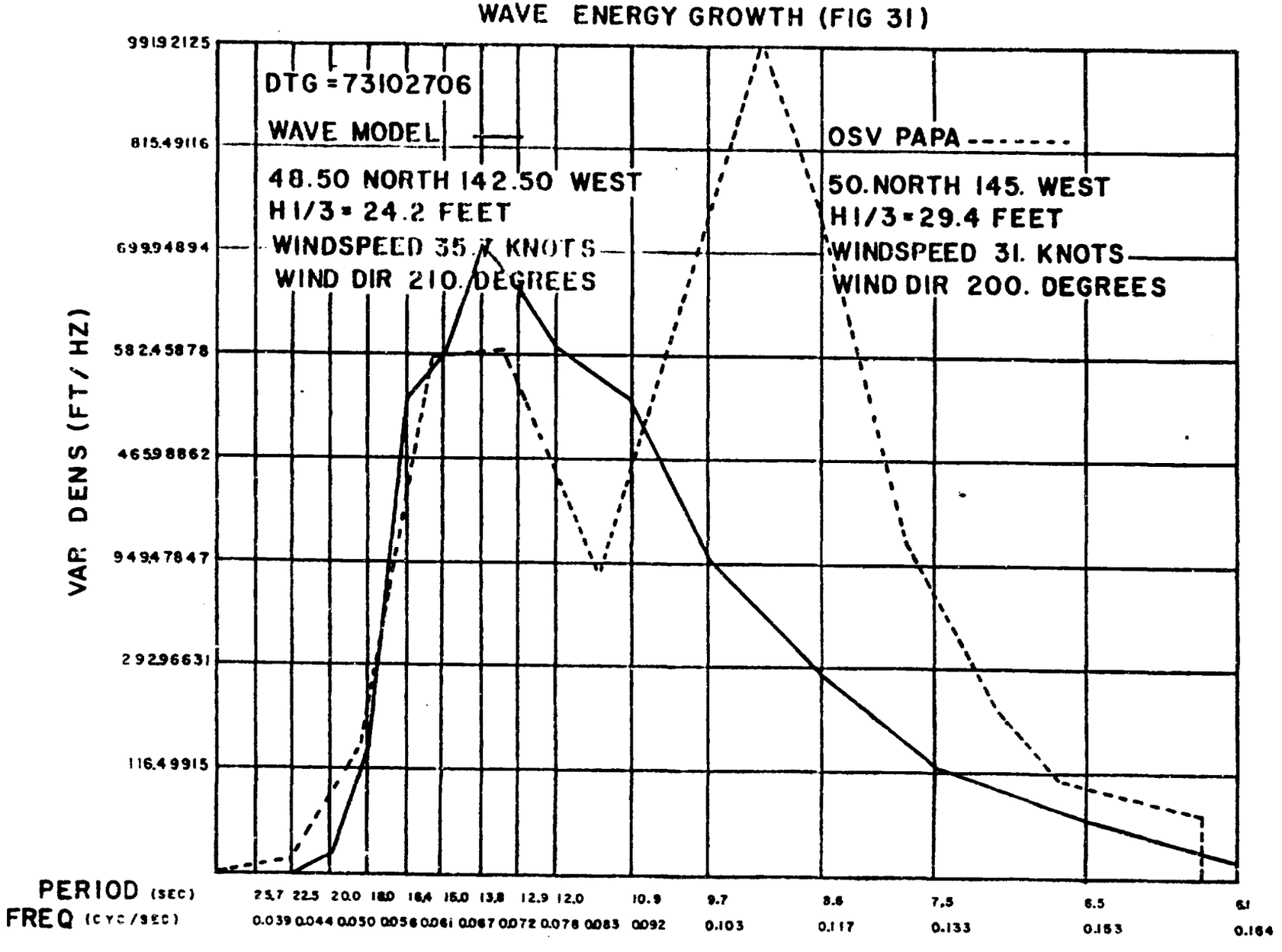
WAVE ENERGY GROWTH (FIG 31)
DTG = 73102706
WAVE MODEL
48.50 NORTH 142.50 WEST
H1/3 = 24.2 FEET
WINDSPEED 35.7 KNOTS
WIND DIR 210. DEGREES
OSV PAPA
50. NORTH 145. WEST
H1/3 = 29.4 FEET
WINDSPEED 31. KNOTS
WIND DIR 200. DEGREES
VAR DENS (FT/HZ)
99192125
815.49116
699.94894
582.45878
465.98862
349.47847
292.96631
116.49915
PERIOD (SEC)
FREQ (CYC/SEC)
25.7 22.5 20.0 18.0 16.4 15.0 13.8 12.9 12.0 10.9 9.7 8.6 7.5 6.5 6.1
0.039 0.044 0.050 0.056 0.061 0.067 0.072 0.078 0.083 0.092 0.103 0.117 0.133 0.153 0.164

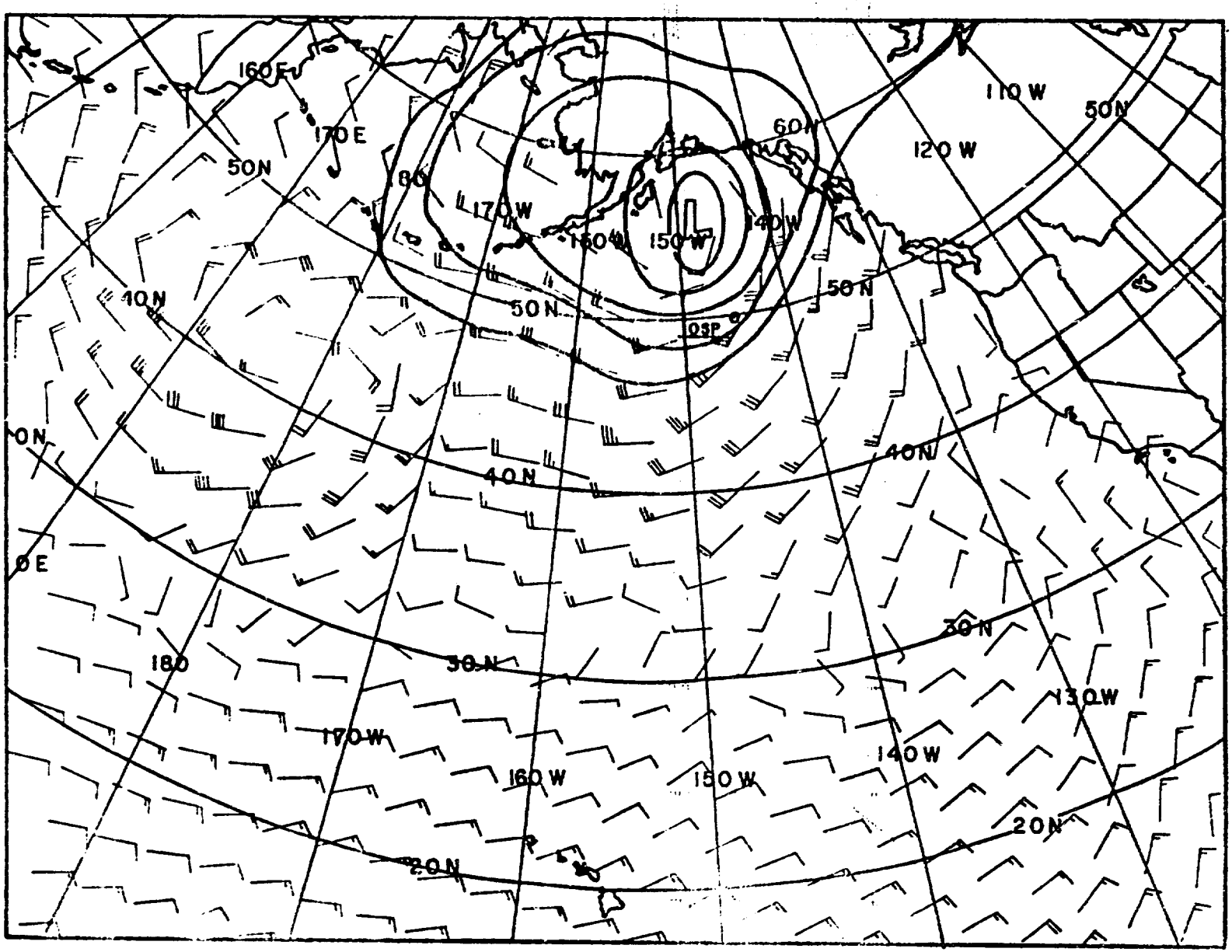

FIGURE 32

27 OCT 73 12Z WIND FIELD

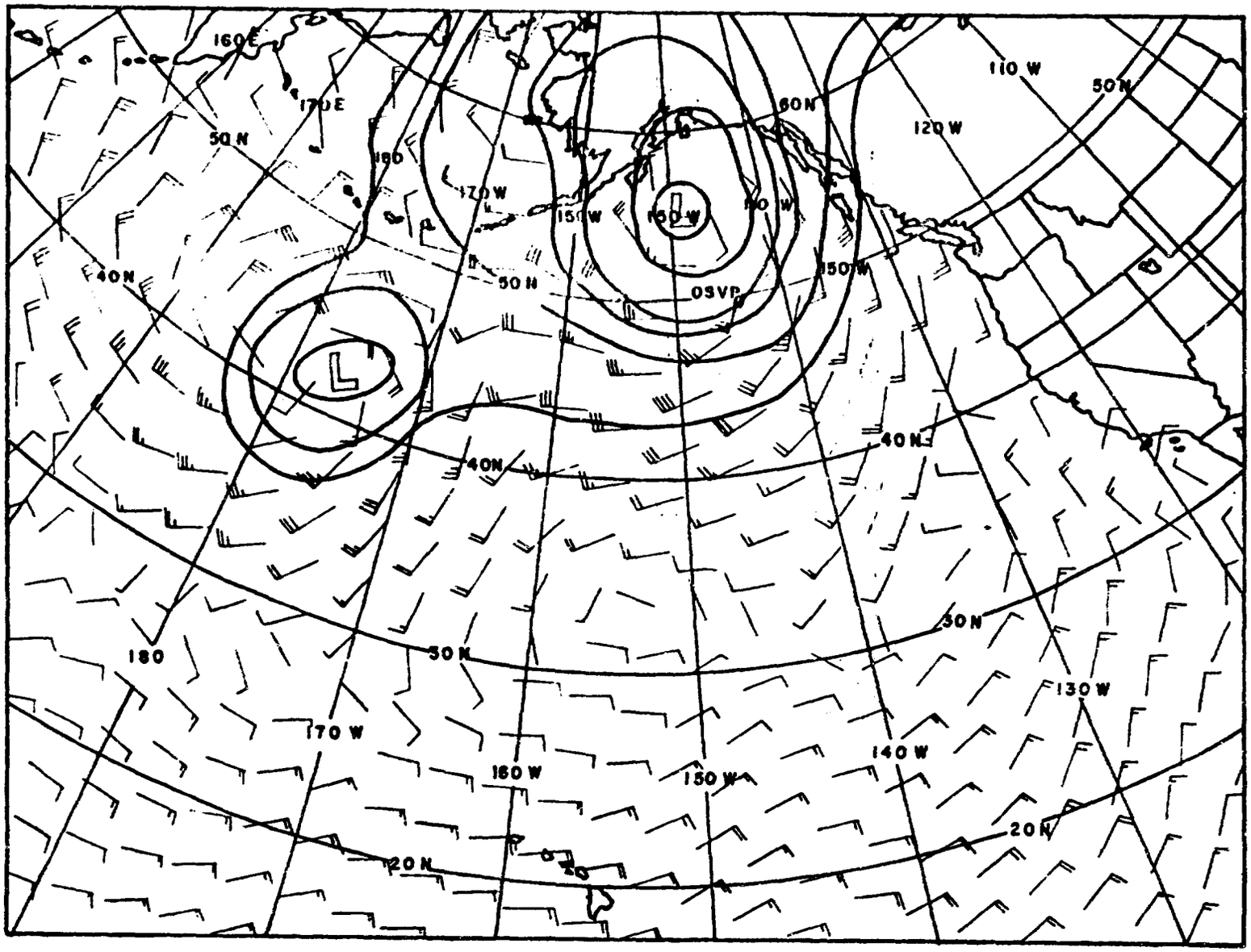

FIGURE 33
27 OCT 73 18 Z WIND FIELD

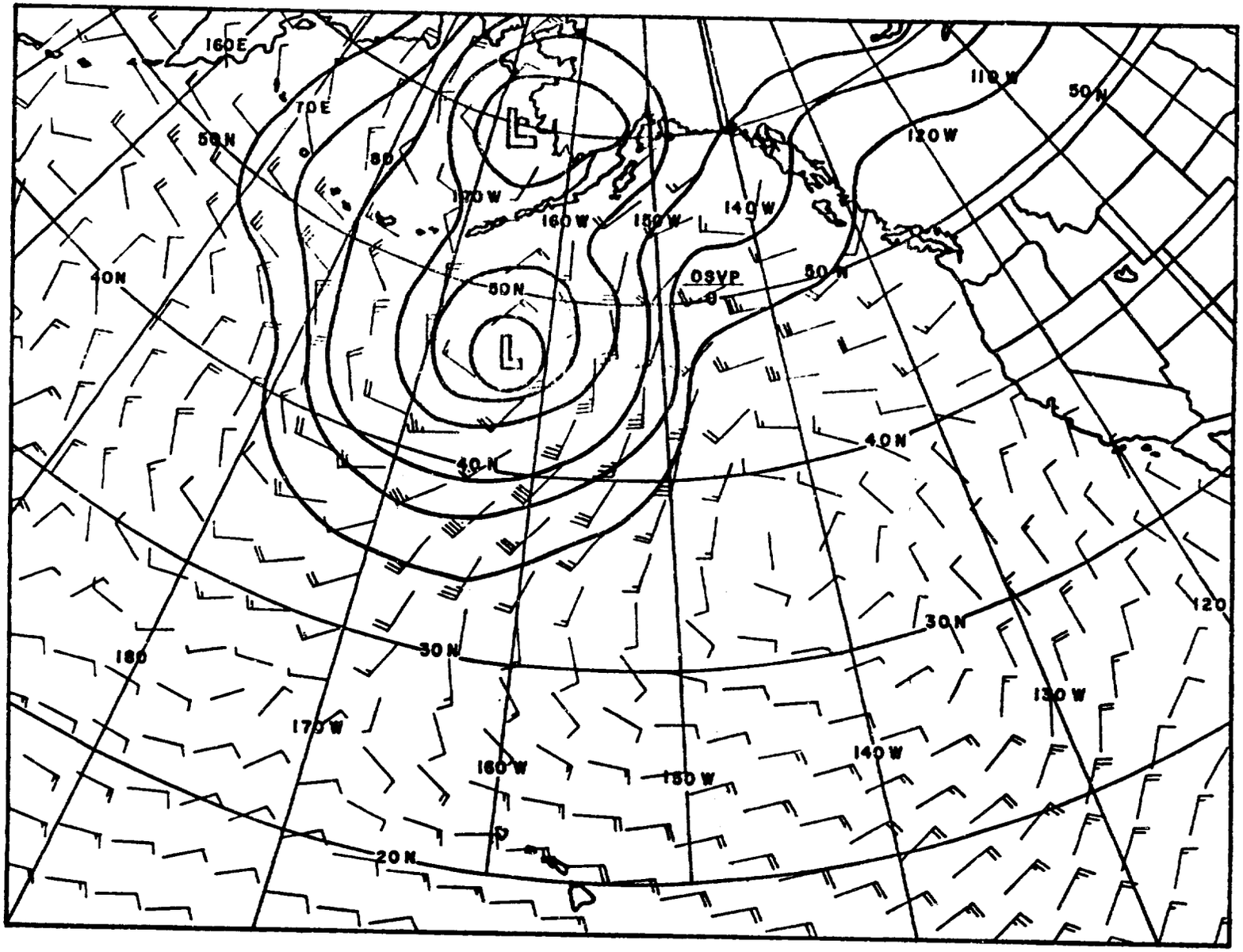

FIGURE 34

28 OCT 73 12 Z WIND FIELD

WAVE ENERGY GROWTH (FIG 35)

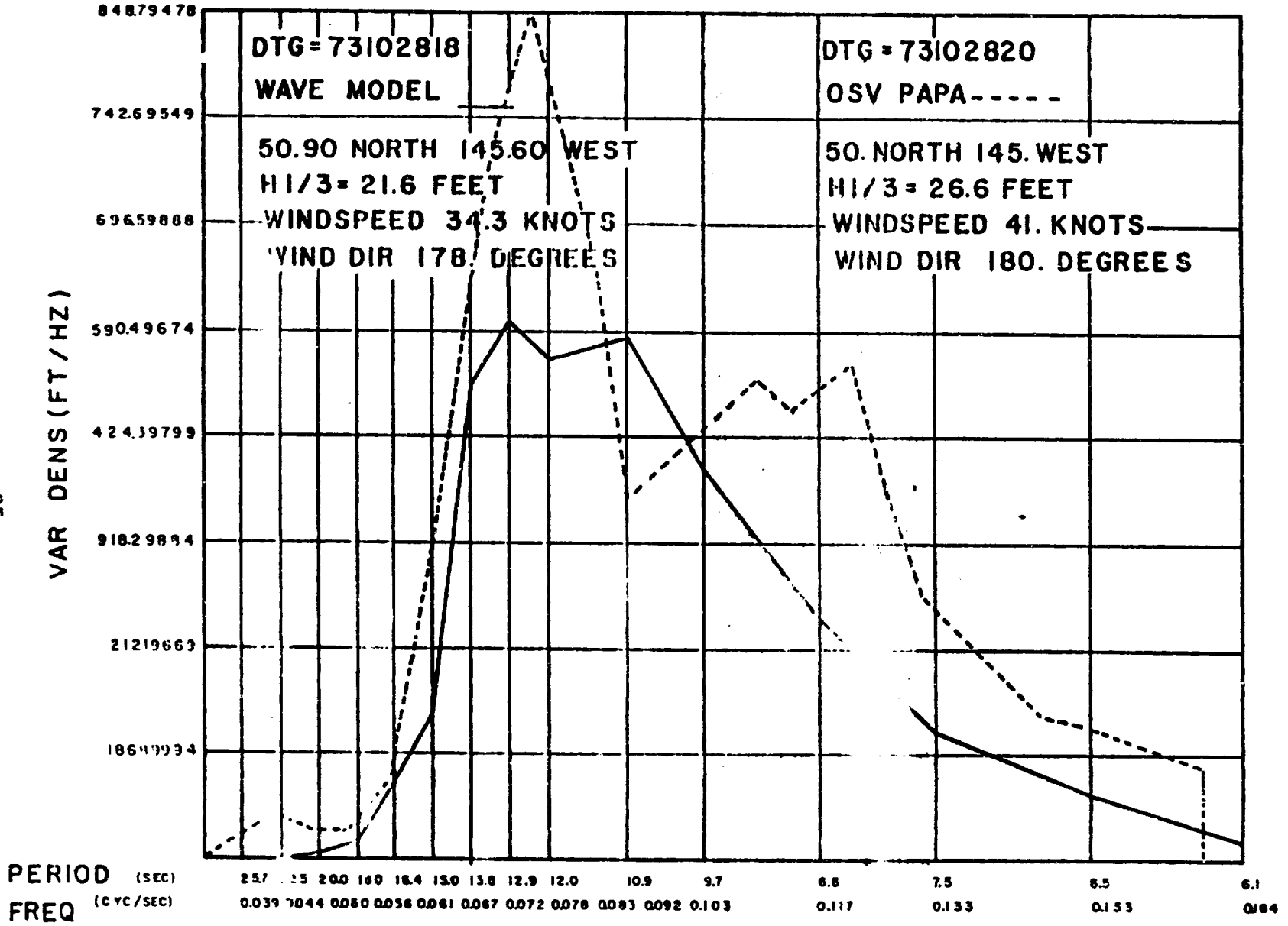

WAVE ENERGY GROWTH (FIG 36)

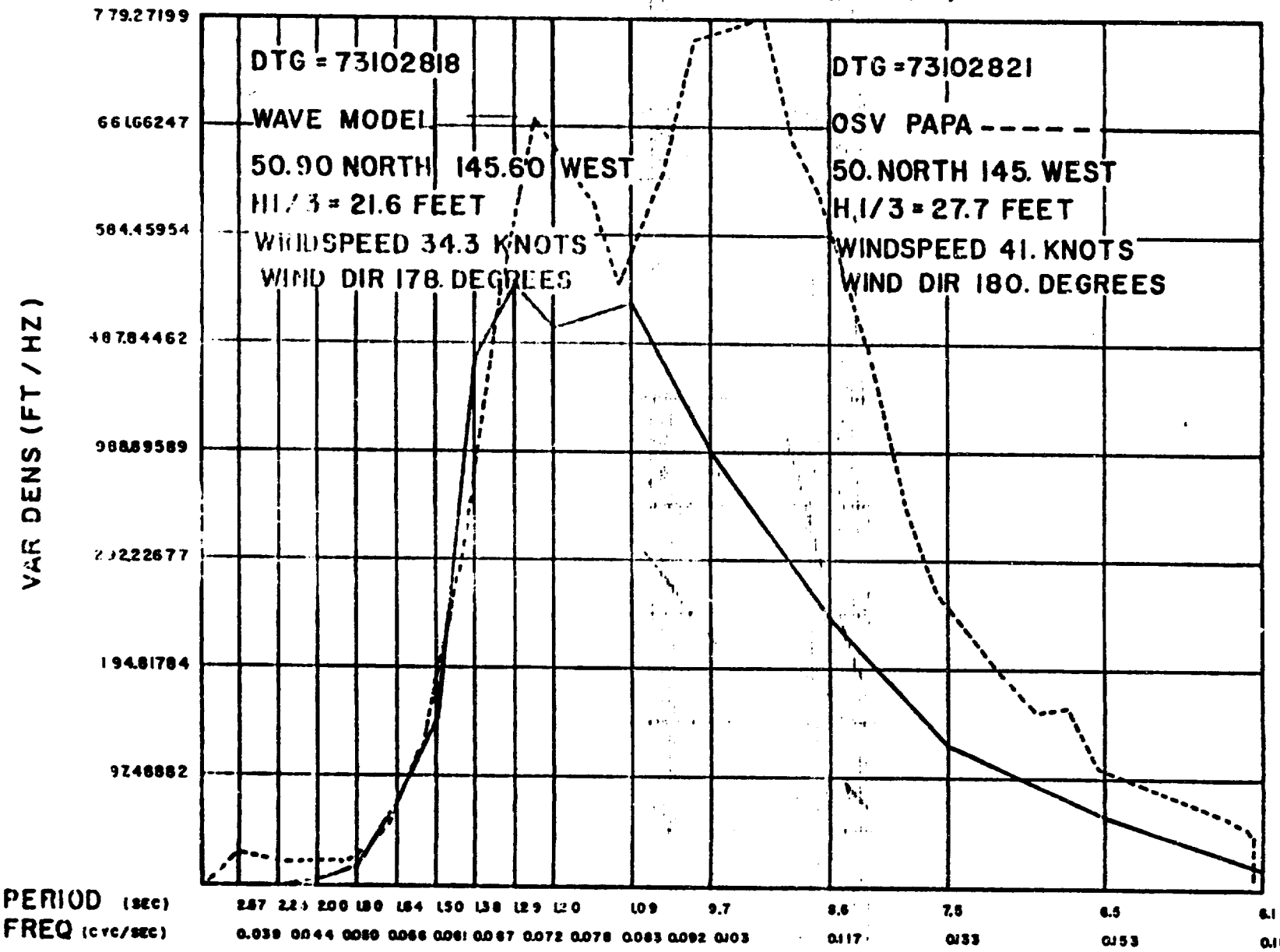

WAVE ENERGY GROWTH (FIG 37)

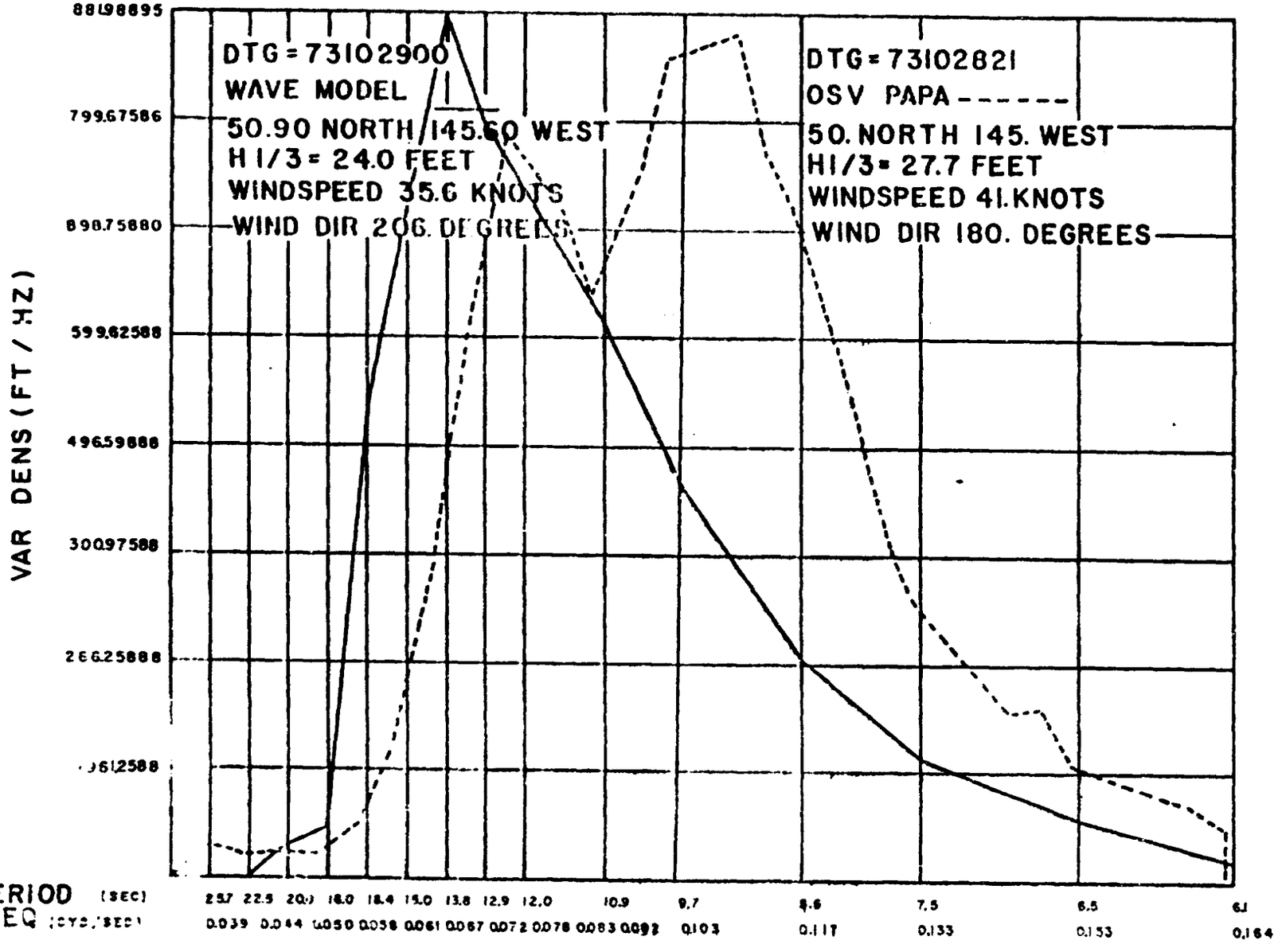

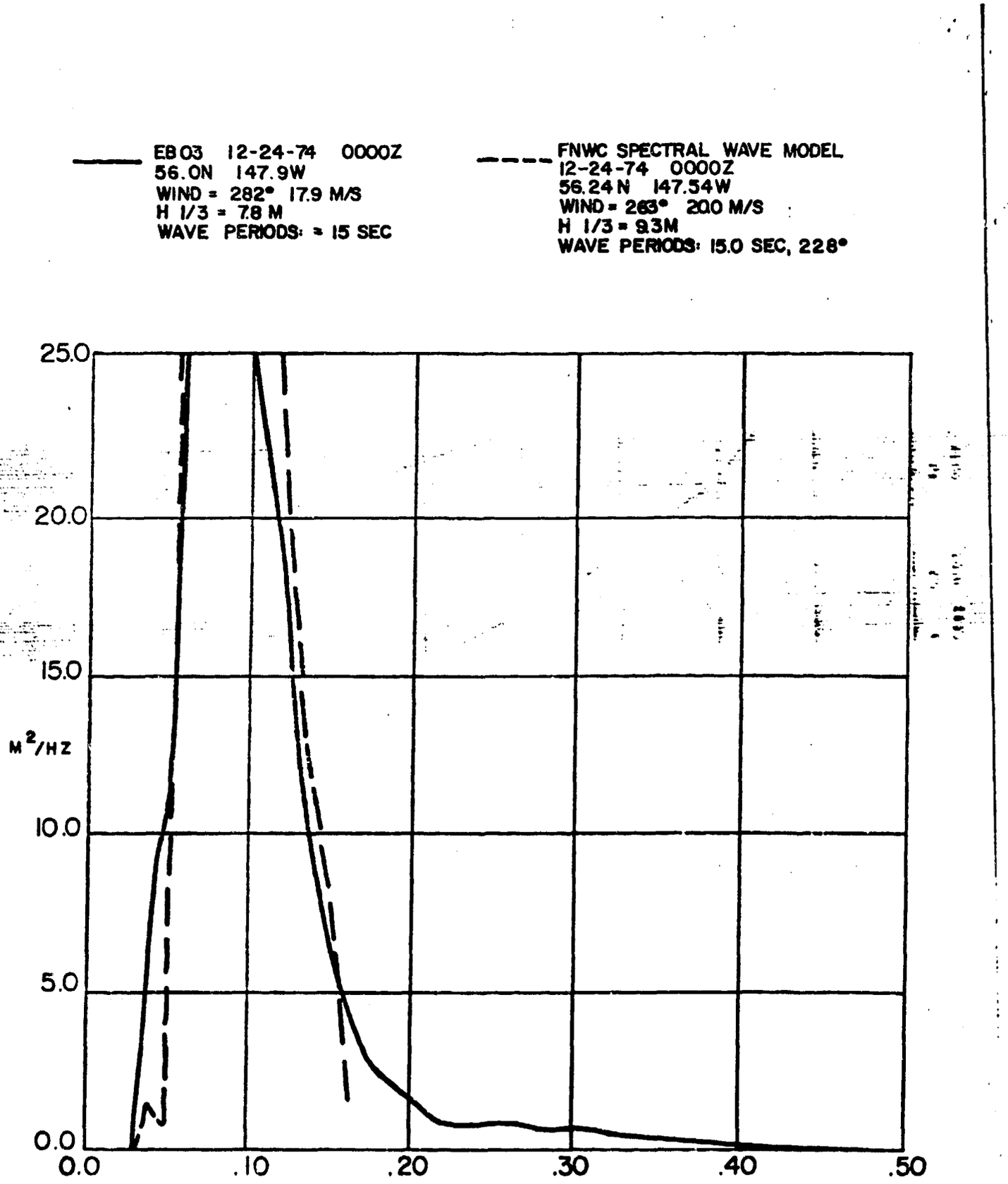

FIGURE 38
(After ODSI, 1975)

——— EB03 12-26-74 0000Z
56.0N 147.9W
WIND 331° 6.0 M/S
H 1/3 = 3.1 M
WAVE PERIODS: 10.0 SEC

_____ FNWC SPECTRAL WAVE MODEL
12-26-74 0000 Z
56.24N 147.54 W
WIND 287° 9.6 M/S
H 1/3 = 4.1 M
WAVE PERIODS: 10.9 SEC, 258°

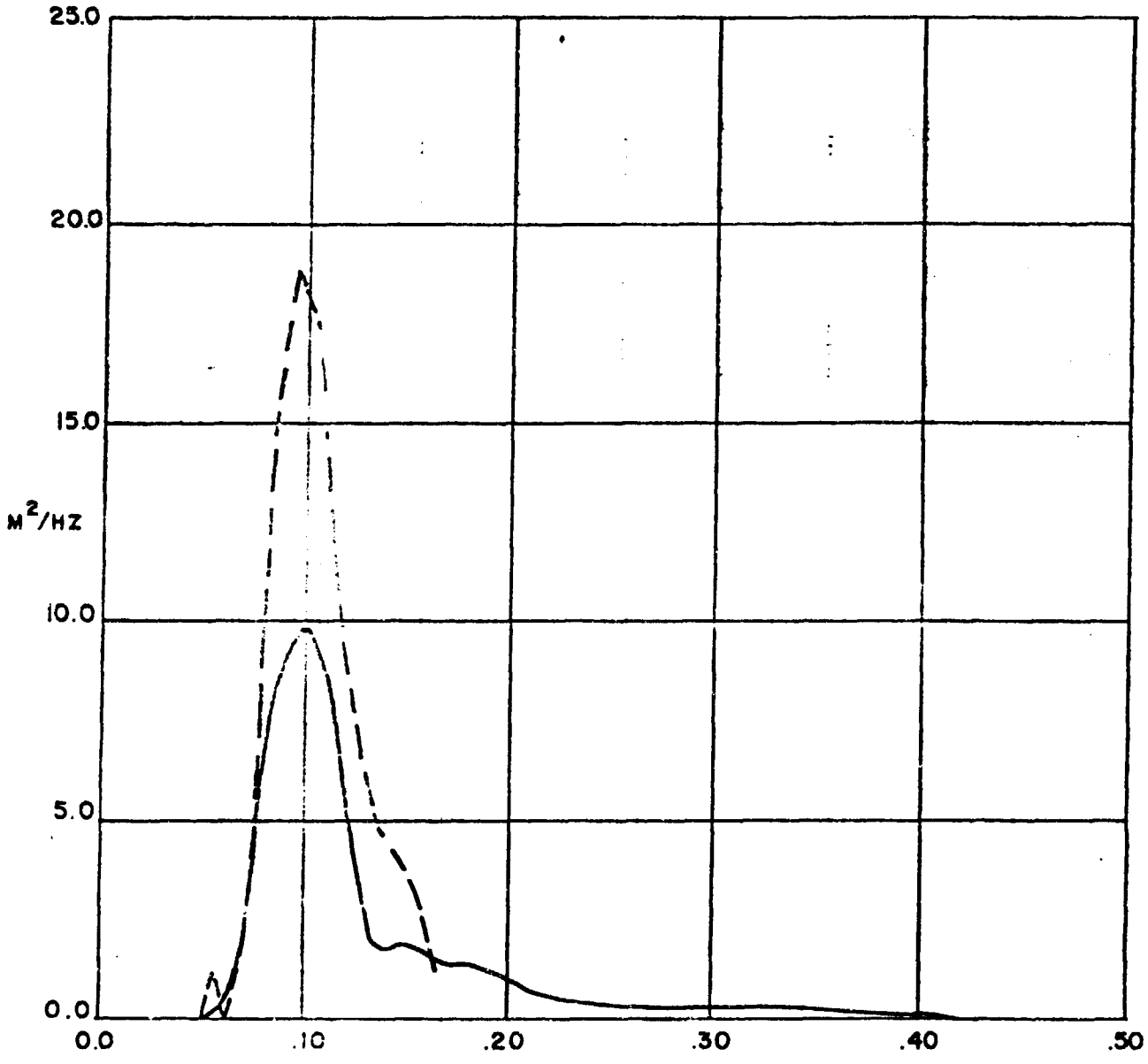

FIGURE 39

(After ODSI, 1975)

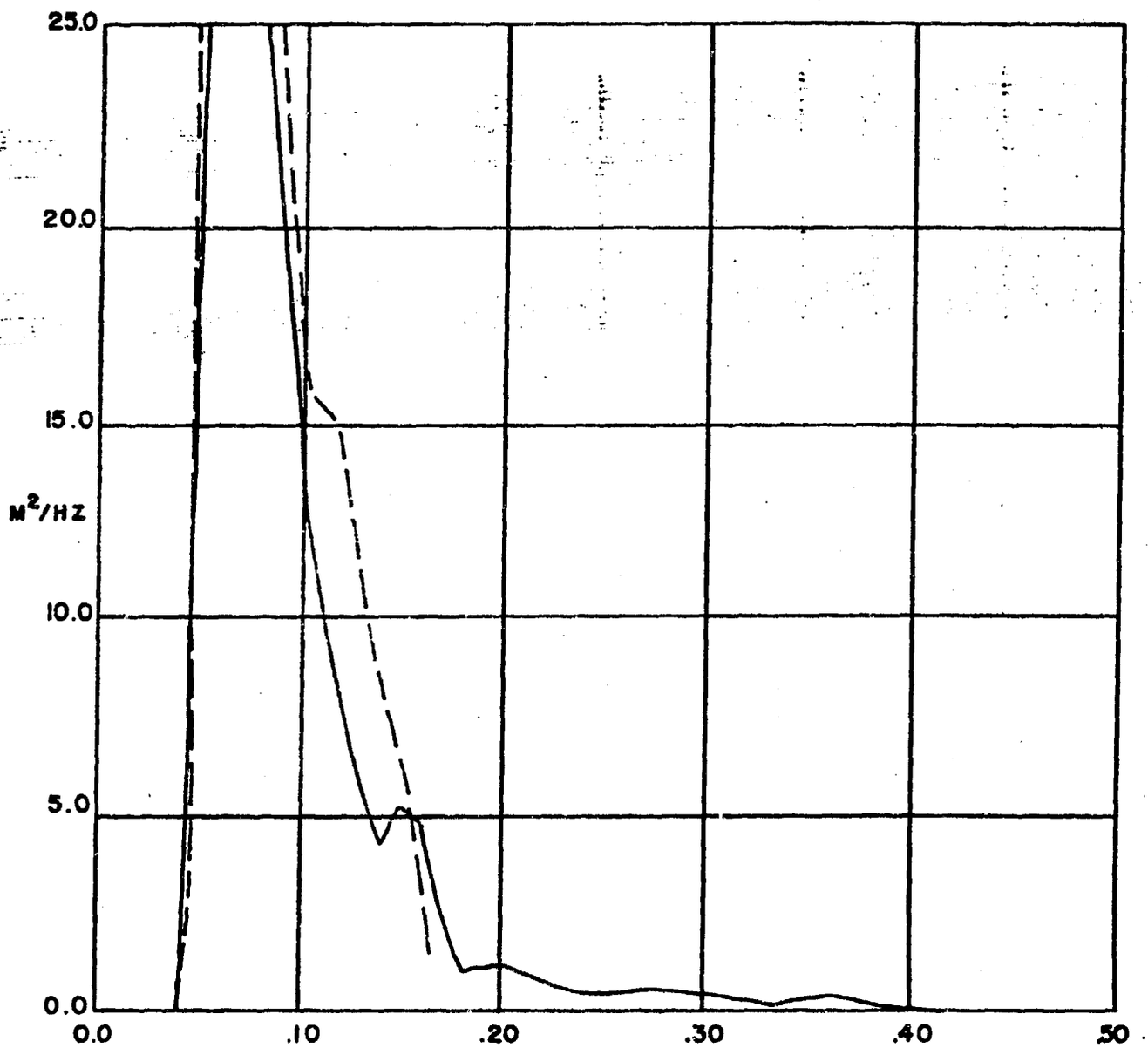

FIGURE 40
(After ODSI, 1975)

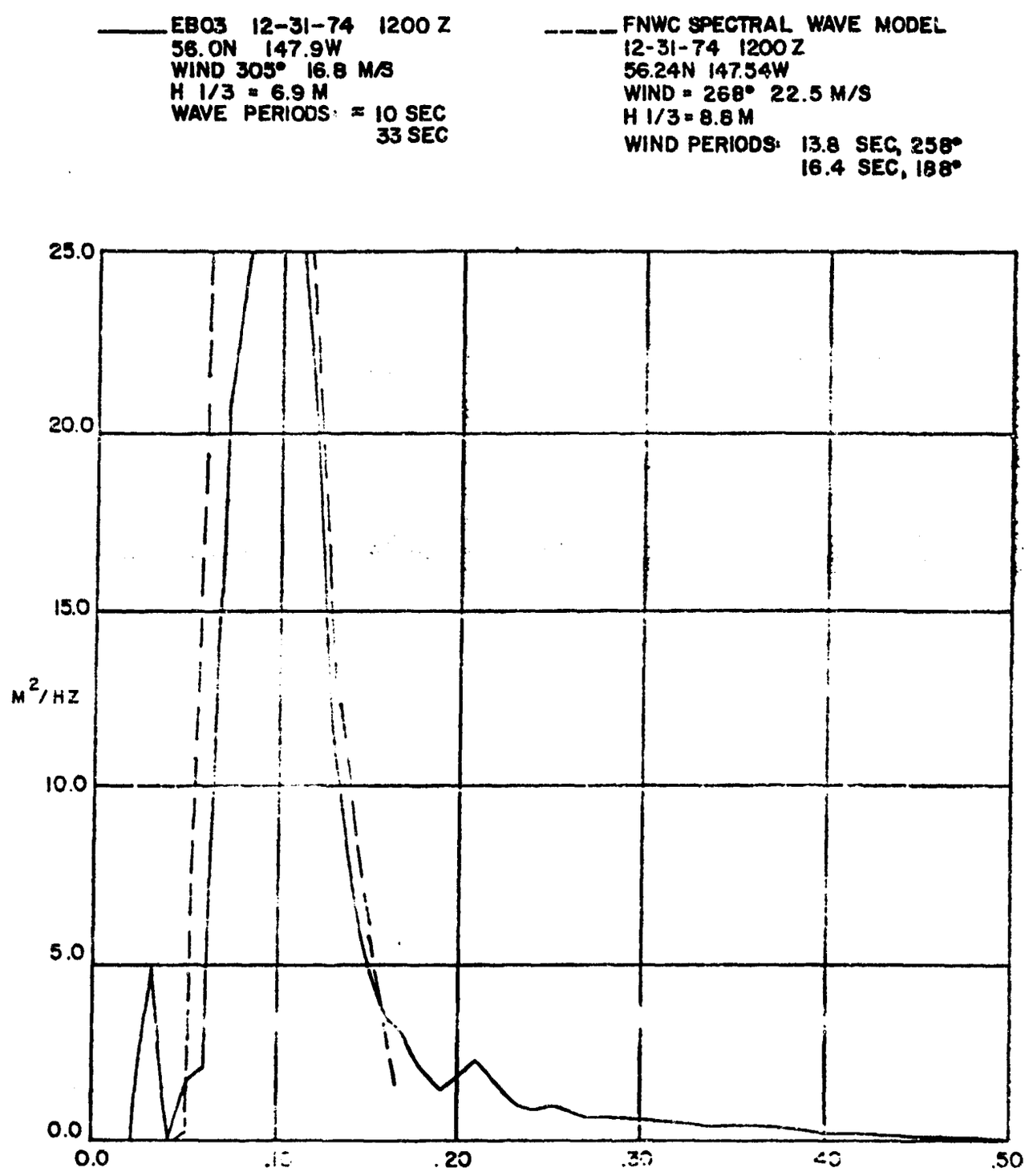

FIGURE 41

(After ODSI, 1975)

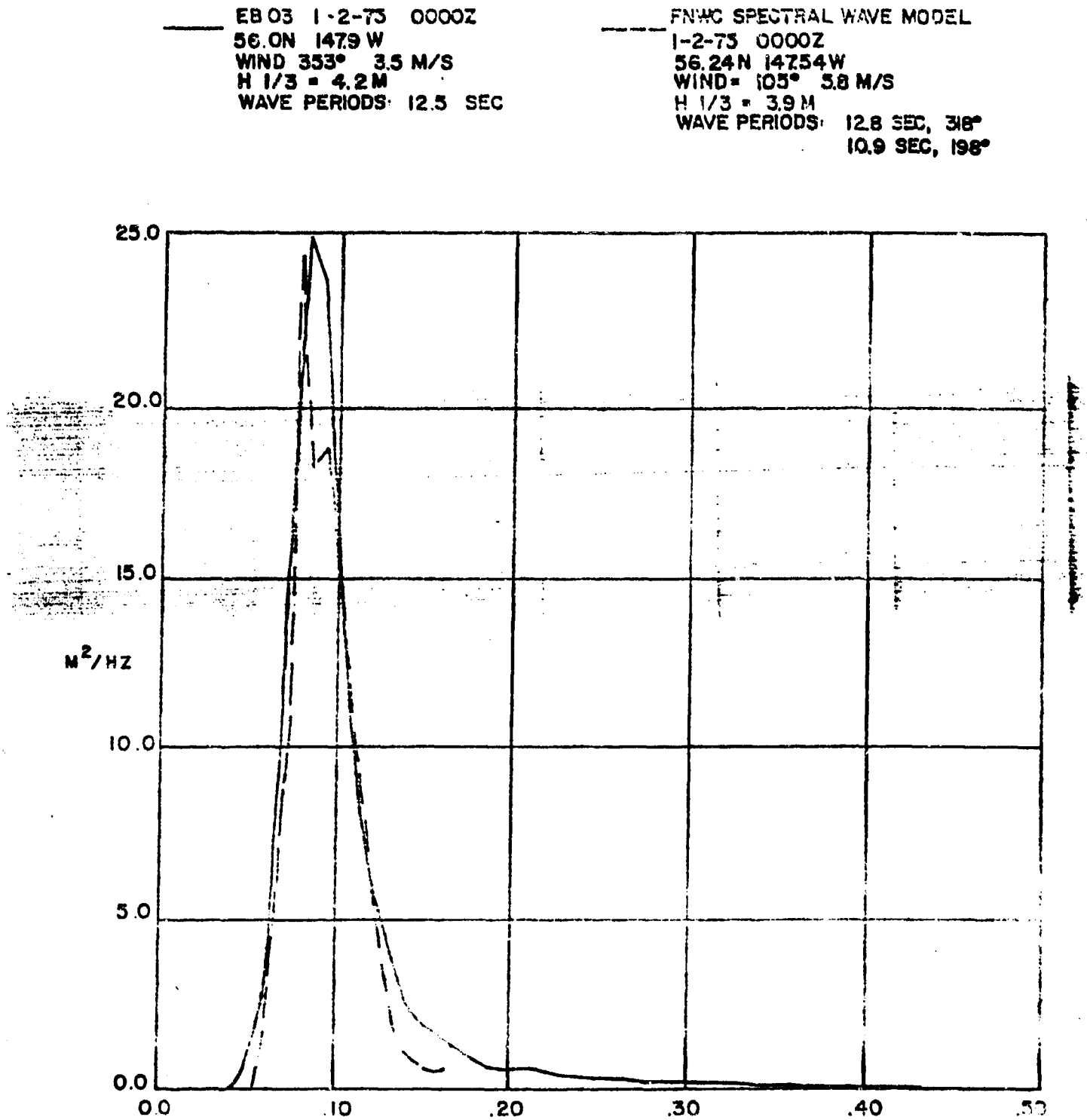

FIGURE 42

(After ODSI, 1975)

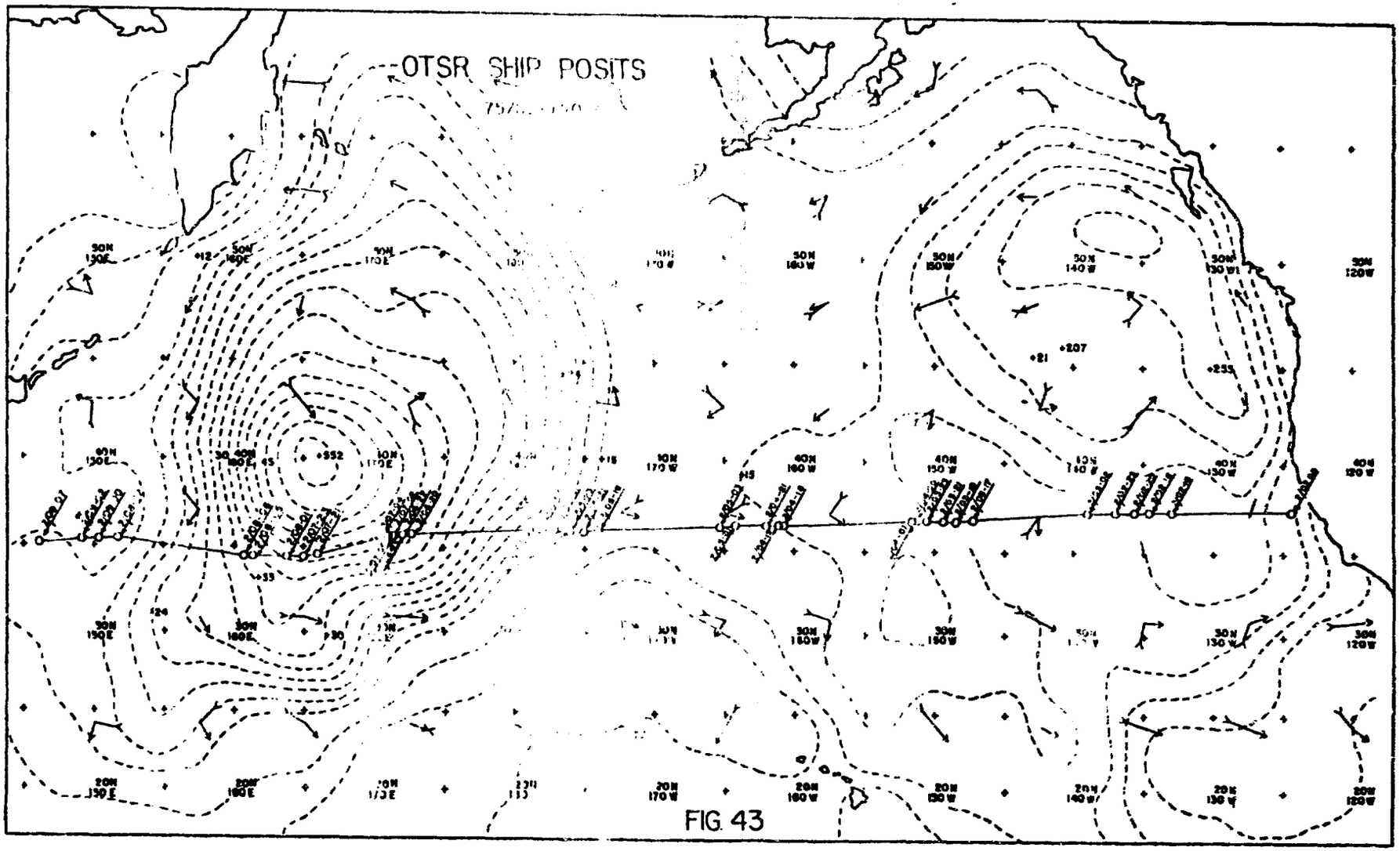

FIG 43

SHIP ROUTE
February 2 1975 00Z - February 9 1975 07Z

UNCLASSIFIED

SECURITY CLASSIFICATION OF THIS PAGE (When Data Entered)

REPORT DOCUMENTATION PAGE		READ INSTRUCTIONS BEFORE COMPLETING FORM
1. REPORT NUMBER Technical Note 75-3	2. GOVT ACCESSION NO. AD-A099	3. RECIPIENT'S CATALOG NUMBER 334
4. TITLE (and Subtitle) An Evaluation of a Hemispheric Operational Wave Spectral Model		5. TYPE OF REPORT & PERIOD COVERED Final Report 6. PERFORMING ORG. REPORT NUMBER
7. AUTHOR(s) Sheldon M. Lazanoff Norman M. Stevenson		8. CONTRACT OR GRANT NUMBER(s)
9. PERFORMING ORGANIZATION NAME AND ADDRESS Fleet Numerical Weather Central Monterey, California 93940		10. PROGRAM ELEMENT, PROJECT, TASK AREA & WORK UNIT NUMBERS
11. CONTROLLING OFFICE NAME AND ADDRESS Fleet Numerical Weather Central Monterey, California 93940		12. REPORT DATE July 1975 13. NUMBER OF PAGES 103
14. MONITORING AGENCY NAME & ADDRESS(if different from Controlling Office)		15. SECURITY CLASS. (of this report) Unclassified 15a. DECLASSIFICATION/DOWNGRADING SCHEDULE

16. DISTRIBUTION STATEMENT (of this Report)

Approved for public release; distribution unlimited

17. DISTRIBUTION STATEMENT (of the abstract entered in Block 20, if different from Report)

18. SUPPLEMENTARY NOTES

19. KEY WORDS (Continue on reverse side if necessary and identify by block number)

spectral ocean wave model
wave spectra
icosahedral gnomonic model
wind velocity
fictional wind velocity
wave growth
wave propagation
wave dissipation
forecasting
analyses

20. ABSTRACT (Continue on reverse side if necessary and identify by block number)

Through the cooperative efforts of the Naval Oceanographic Office and Fleet Numerical Weather Central personnel, the open ocean Icosahedral-Gnomonic wave spectral computer model ~~developed by Professor Willard Pierson~~ has been placed in real time operational use at FNWC under the title Spectral Ocean Wave Model (SOWM). The model computes semi-daily on-time analyses and forecasts to seventy-two hours. A gnomonic projection ~~allows~~ great circles to be

next page

DD FORM 1 JAN 73 1473 EDITION OF 1 NOV 65 IS OBSOLETE
S/N 0102-014-6601

UNCLASSIFIED

SECURITY CLASSIFICATION OF THIS PAGE (When Data Entered)

represented by straight lines within the icosahedral triangles, thus minimizing propagation errors.